Exact constructions of square-root Helmholtz operator symbols: The focusing quadratic profile

Louis Fishman*, Maarten V. de Hoop† and Mattheus J.N. van Stralen‡

*Naval Research Laboratory, Code 7181, Stennis Space Center, MS 39529

†Center for Wave Phenomena, Colorado School of Mines, Golden, CO 80401

‡Plasma Optical Fibre B.V., Zwaanstraat 1, 5651 CA Eindhoven, The Netherlands

ABSTRACT

Operator symbols play a pivotal role in both the exact, well-posed, one-way reformulation of solving the (elliptic) Helmholtz equation and the construction of the generalized Bremmer coupling series. The inverse square-root and square-root Helmholtz operator symbols are the initial quantities of interest in both formulations, in addition to providing the theoretical framework for the development and implementation of the 'parabolic equation' (PE) method in wave propagation modeling. Exact, standard (left) and Weyl symbol constructions are presented for both the inverse square-root and square-root Helmholtz operators in the case of the focusing quadratic profile in one transverse spatial dimension, extending (and, ultimately, unifying) the previously published corresponding results for the defocusing quadratic case [J. Math. Phys. **33** (5), 1887-1914 (1992)]. Both (i) spectral (modal) summation representations and (ii) contour-integral representations, exploiting the underlying periodicity of the associated, quantum mechanical, harmonic oscillator problem, are derived, and, ultimately, related through the propagating and nonpropagating contributions to the operator symbol. High- and low-frequency, asymptotic operator symbol expansions are given along with the exact symbol representations for the corresponding operator rational approximations which provide the basis for the practical computational realization of the PE method. Moreover, while the focusing quadratic profile is, in some respects, nonphysical, the corresponding Helmholtz operator symbols, nevertheless, establish canonical symbol features for more general profiles containing locally-quadratic wells.

Key words: one-way wave equations, pseudodifferential operators, normal modes

1. Introduction

The global nature of wave propagation problems, as modeled by the elliptic scalar Helmholtz equation, renders the computational solution quite difficult in extended inhomogeneous environments (1, 2). The development and application of the 'parabolic equation' (PE) method (3, 4, 5, 6, 7) has successfully addressed this issue for appropriately, weakly range-dependent environments, where, for the most part, one-way (forward) wave fields are computed and back-scattered energy is neglected. In recent years, the PE method has been extended to fully-coupled, two-way, elliptic wave propagation through two complementary approaches: (i) the exact, well-posed, one-way reformulation of elliptic wave propagation problems (1, 2, 8) and (ii) the construction and application of the generalized Bremmer coupling series (9, 10, 11). Both methods of extension are based on ideas and constructions from wave field decomposition, invariant imbedding (reflection and transmission operators), and the closely related Dirichlet-to-Neumann (DtN) operators, and make use of micro-local analysis (pseudodifferential and Fourier integral operators and path integrals). While the current focus in the direct and inverse analysis of the above two approaches is primarily on the properties and singularity structure of the scattering (reflection and transmission) and DtN operator symbols (1, 12, 13), the inverse square-root and square-root Helmholtz operator symbols are the initial quantities of

interest in both formulations. In many respects, however, despite the detailed treatment of the fully-coupled, two-way, elliptic formulations in the above-referenced literature, the original PE method provides the most straightforward introduction to the Helmholtz operator symbols.

Starting from the two-dimensional, space-frequency domain, scalar Helmholtz equation, the formally exact wave equation for propagation in a transversely inhomogeneous half-space supplemented with appropriate right-traveling-wave radiation and initial-value conditions is given by (1, 2)

$$(\mathrm{i}/\bar{k})\,\partial_x w^+ + \boldsymbol{B}\,w^+ = 0\ , \tag{1}$$

where w^+ is the one-way wave function, $\bar{k}$ is a reference or average wave number (proportional to frequency), and

$$\boldsymbol{B} = \boldsymbol{B}(z,\partial_z) = [K^2(z) + (1/\bar{k})^2\partial_z^2]^{1/2} \tag{2}$$

is the square-root Helmholtz operator, where $K(z)$ is the refractive index field. The range coordinate, x, is associated with the 'one-way' direction; z is the transverse coordinate. In the subsequent formal analysis, the transverse coordinates will also be freely denoted by q.

For a point source of the volume injection type, located at $x = 0$ and $z = z_s$, the appropriate initial-value condition or (source) decomposition is given by (1)

$$w^+(0,z) = (\mathrm{i}/2\bar{k})\,\boldsymbol{B}^{-1}\delta(z - z_s)\ , \tag{3}$$

where $\boldsymbol{B}^{-1}$ denotes the inverse or parametrix of $\boldsymbol{B}$ (i.e., the inverse square-root Helmholtz operator).

The Helmholtz operator symbols are defined in a pseudodifferential operator (operator-ordering) calculus (14, 15, 16, 17). Let $\mathcal{B} = \mathcal{B}(z,z')$ denote the *kernel* associated with operator $\boldsymbol{B}$, i.e.,

$$(\boldsymbol{B}w^+)(x,z) = \int_{\mathbb{R}} \mathrm{d}z'\,\mathcal{B}(z,z')\,w^+(x,z')\ , \tag{4}$$

and $\mathcal{B}^{-1} = \mathcal{B}^{-1}(z,z')$ denote the kernel associated with the inverse $\boldsymbol{B}^{-1}$. Then the *symbol*, for the inverse square-root Helmholtz operator, is defined as

$$h^s_{\boldsymbol{B}^{-1}}(p,q) = \int_{\mathbb{R}} \mathrm{d}u\,\exp(\mathrm{i}\bar{k}\,pu)\mathcal{B}^{-1}(q,q+u) \tag{5}$$

in the standard (left) pseudodifferential operator calculus, and as

$$\Omega_{\boldsymbol{B}^{-1}}(p,q) = \int_{\mathbb{R}} \mathrm{d}u\,\exp(\mathrm{i}\bar{k}\,pu)\mathcal{B}^{-1}\left(q - \tfrac{1}{2}u, q + \tfrac{1}{2}u\right) \tag{6}$$

in the Weyl pseudodifferential operator calculus (14, 15, 16, 17). Likewise, definitions of $h^s_{\boldsymbol{B}}$ and $\Omega_{\boldsymbol{B}}$ hold for the square-root Helmholtz operator itself.

In terms of the square-root Helmholtz operator symbols, the one-way wave equation (1) can be written as ⋆

$$(\mathrm{i}/\bar{k})\,\partial_x w^+ + \int_{\mathbb{R}} (\bar{k}/2\pi)\mathrm{d}p\,h^s_{\boldsymbol{B}}(p,z)\exp(\mathrm{i}\bar{k}\,pz)\,\widetilde{w^+}(x,p) = 0\ , \tag{7}$$

or

$$(\mathrm{i}/\bar{k})\,\partial_x w^+ + \int_{\mathbb{R}} \mathrm{d}z' \int_{\mathbb{R}} (\bar{k}/2\pi)\mathrm{d}p\,\Omega_{\boldsymbol{B}}\left(p, \tfrac{1}{2}(z+z')\right)\exp[\mathrm{i}\bar{k}\,p(z-z')]\,w^+(x,z') = 0\ , \tag{8}$$

in the standard and Weyl calculi (14, 15, 16, 17), respectively. Here, $\widetilde{w^+}(x,p)$ is the Fourier transform of the one-way wave function $w^+(x,z)$ with respect to the transverse coordinate,

$$\widetilde{w^+}(x,p) = \int_{\mathbb{R}} \mathrm{d}z'\,\exp(-\mathrm{i}\bar{k}\,pz')\,w^+(x,z')\ . \tag{9}$$

For a fixed range point, $x = x_b$ say, Eqs.(7) and (8) provide the basis for the nonreflecting boundary conditions ubiquitous in numerical wave field computations (1, 4, 10).

⋆ In Van Stralen *et al.* (10), interchange x and z, and replace $\hat{\Gamma}$ (the vertical slowness operator) by $\boldsymbol{B}$, $\hat{\gamma}$ by $h^s_{\boldsymbol{B}}$, and $\hat{W}_1$ by w^+ (and $\hat{W}_2$ by w^-).

The fundamental solution (propagator), $\mathcal{G}^+$, associated with Eq.(1) can be expressed as a lattice multivariate integral, with Hamiltonian equal to the square-root Helmholtz operator symbol (1, 2, 11, 18, 19, 20, 21),

$$\mathcal{G}^+(x,z;x',z') = H(x-x') \lim_{M\to\infty} \int_{\mathbb{R}^{2M-1}} \prod_{i=1}^{M} (\bar{k}/2\pi) \mathrm{d}p^{(i)} \prod_{j=1}^{M-1} \mathrm{d}z^{(j)}$$
$$\times \exp\left[\mathrm{i}\bar{k} \sum_{k=1}^{M} \{ p^{(k)}(z^{(k)} - z^{(k-1)}) + h^s_{\boldsymbol{B}}(p^{(k)}, z^{(k)}) M^{-1} \Delta x \} \right] , \tag{10}$$

with $z^{(0)} = z'$, $z^{(M)} = z$, $\Delta x = x - x'$, and where $H(\cdot)$ is the Heaviside function. All the integrations are taken over the interval $(-\infty, \infty)$, $M^{-1}\Delta x$ is the step size in the parameter ξ along the range direction, and $(z^{(k)}, p^{(k)})$ are the coordinates of a path (in transverse phase space) at the discrete values ξ_k of ξ as $k = 1, \cdots, M$. A similar phase-space path-integral representation is found in the Weyl calculus (1, 2, 18, 19, 20, 21). The structure of the path-integral representation in Eq.(10) straightforwardly results in the phase space, marching algorithm, which generalizes the Tappert/Hardin (6, 7) split-step FFT algorithm for the standard parabolic approximation to the one-way Helmholtz equation (1) and has been discussed and illustrated in detail in the literature (19, 20, 21).

Moreover, in the context of the inverse scattering problem, the composition equation in the pseudodifferential operator calculus connects the square-root Helmholtz operator symbol with the square of the refractive index field through (1, 14, 15, 16, 17)

$$K^2(q) - p^2 = \Omega_{\boldsymbol{B}^2}(p,q) \tag{11}$$
$$= (\bar{k}/\pi)^2 \int_{\mathbb{R}^4} \mathrm{d}s\mathrm{d}u\mathrm{d}t\mathrm{d}v \; \Omega_{\boldsymbol{B}}(s+p, u+q) \Omega_{\boldsymbol{B}}(t+p, v+q) \; \exp[2\mathrm{i}\bar{k}\,(ut - sv)]$$

in the Weyl calculus, with a similar expression in the standard calculus (14, 15, 16) (see also Appendix C). The composition equation (11) also serves as the starting point for the exact, approximate, and numerical constructions of the square-root Helmholtz operator symbols (1, 17, 22, 23).

Finally, the operator symbols in the Weyl and standard pseudodifferential operator calculi are related to one another (14, 15, 16, 17, 19), viz.,

$$h^s_{\boldsymbol{B}}(p,q) = (\bar{k}/\pi) \int_{\mathbb{R}^2} \mathrm{d}s\mathrm{d}u \, \Omega_{\boldsymbol{B}}(s,u) \exp[-2\mathrm{i}\bar{k}\,(q-u)(p-s)] , \tag{12}$$

while

$$\Omega_{\boldsymbol{B}}(p,q) = (\bar{k}/\pi) \int_{\mathbb{R}^2} \mathrm{d}s\mathrm{d}u \, h^s_{\boldsymbol{B}}(s,u) \exp[2\mathrm{i}\bar{k}\,(q-u)(p-s)] . \tag{13}$$

Recasting the formal operator equations (1) and (3), in a chosen pseudodifferential operator calculus, in terms of the appropriate operator symbols provides the explicit means to extend Fourier analysis of wave propagation in (transversely) homogeneous media to inhomogeneous environments: the analysis is carried out in the transverse Fourier (p) domain without leaving the transverse space (q) domain. The transverse space-wave number domain constitutes the transverse phase space. The transverse variable p together with the principal part of $h^s_{\boldsymbol{B}}$ form the components of the cotangent vector attached to the wave front.

Rather than focusing on the individual operator eigenvalues and eigenfunctions as is done in the traditional spectral analysis, the focus here is on the operator symbols: they contain the complete spectral information in just the appropriate manner to lead immediately to the infinitesimal propagator and initial wave field.

Operator symbols are a natural quantity to consider. For example, they provide the 'generalized slowness surface' in geophysics (11), the natural multidimensional extension of the scattering (reflection and transmission) coefficients in the one-dimensional formulation (2, 13), and the framework to quantize (semi-)classical theories in quantum physics (24). While either the Weyl or the standard pseudodifferential operator calculus provides a complete description of the propagation problem, they are, in many respects, complementary, and can be used in conjunction to advantage. For example, the symmetry inherent in the Weyl calculus can often be exploited in operator symbol constructions and analysis (particularly that involving integrated energy-flux conservation calculations and that separating the effects due to anisotropy from those due to heterogeneity), while the standard calculus naturally results in more computationally efficient algorithms (19, 20).

The brief outline presented from Eq.(5) to Eq.(13) indicates the pivotal role that both the inverse square-root and square-root Helmholtz operator symbols play in the PE method for wave propagation. The explicit construction of the one-way wave equation and initial wave field, path-integral solution representation and subsequent numerical algorithm, computational boundary conditions, and fundamental inverse relationship all depend crucially upon the analysis and subsequent properties of the relevant Helmholtz operator symbols. The extension to the scattering and DtN operator symbols in the fully-coupled, two-way, elliptic

formulations only reinforces the importance of their role (1, 2, 8, 9, 10, 11). From this perspective, the construction of exact square-root Helmholtz operator symbols is of great value in illuminating the general mathematical propagation theory, in addition to providing benchmark solutions for both asymptotic and numerical operator symbol constructions (1, 22, 23). Furthermore, the explicit construction of these nontrivial symbols, corresponding to a fractional power of the indefinite, transverse Helmholtz operator, is of mathematical interest in its own right. Since the relevant (frequency-domain) operators lie outside of the well-developed theory of elliptic pseudodifferential operators (1, 15), a new asymptotic, operator symbol characterization is required (1, 9, 12). The construction is accomplished by incorporating complex and spectral analyses in the calculus of pseudodifferential operators (see also Shubin (25)).

In view of the potentially illuminating role of exact operator symbol constructions, this paper presents the exact symbol constructions for both the inverse square-root and square-root Helmholtz operators in the case of the focusing quadratic profile in one transverse spatial dimension, extending (and, ultimately, unifying) the previously published corresponding results for the defocusing quadratic case (23). The focusing case is particularly interesting in the context of the formation of caustics. The results are given for both the Weyl and standard (left) operator symbols. While the focusing quadratic profile is, in some respects, nonphysical, the corresponding Helmholtz operator symbols, nevertheless, establish canonical features for more general profiles containing locally-quadratic wells. Section 2 derives Helmholtz operator symbol representations in the form of spectral (modal) summations following from Eqs.(5) and (6) and the standard spectral theory of the corresponding operator kernels. In Section 3, contour-integral representations, exploiting the underlying periodicity of the associated, quantum mechanical, harmonic oscillator problem, are derived for the Helmholtz operator symbols. These contour-integral representations unify the focusing and defocusing quadratic profile cases, providing the appropriate analytic continuation results and a convenient form for the subsequent asymptotic analysis. The analytic continuation results are combined with the contour-integral representations constructed in the time-Fourier domain to derive the square-root 'Helmholtz' operator symbols in the time-Laplace domain in Section 4. The application of standard asymptotic methods to these contour-integral representations then results in both the high- and low-frequency expansions of the Helmholtz operator symbols in Section 5. The high-frequency asymptotic results are of particular interest in view of the fractional, transverse Helmholtz operators falling outside the scope of elliptic pseudodifferential operator theory. In Section 6, the spectral (modal) summation and contour-integral representations are related through an explicit consideration of the propagating and nonpropagating contributions to the Helmholtz operator symbols, and the multiresolution and generalized screen properties of the one-way propagation process are revealed through the structure of the Weyl and standard operator symbols, respectively. The exact symbol representations for the well-known, operator rational approximations of the square-root Helmholtz operator (1, 3, 4, 5, 6, 10, 23), which provide the basis for the practical computational realization of the PE method, are presented in Section 7 in both the spectral (modal) summation and contour-integral forms for the focusing quadratic profile. These constructions extend (and, ultimately, unify) the previously published corresponding results for the defocusing quadratic case (23). Numerical realizations of the exact and approximate Helmholtz operator symbols are presented in Section 8, while the results derived in the preceding sections are applied to illustrate several points pertinent to direct and inverse wave propagation modeling in multidimensional, extended inhomogeneous environments in the concluding discussion presented in Section 9. Appendices A-C provide the necessary mathematical detail.

2. Spectral (modal) summation operator symbol representations

A spectral (*modal*) summation symbol representation for the inverse square-root Helmholtz operator follows, in principle, from Eqs.(5) and (6) and the standard spectral theory for the corresponding operator kernel $\mathcal{B}^{-1}(z,z')$. In the usual manner (4, 11), $\mathcal{B}^{-1}(z,z')$ is represented by a convergent, complex Dunford integral in terms of the associated $\boldsymbol{B}^2$ operator resolvent – which is simply proportional to the Green's function for the corresponding, effective one-dimensional (range-transformed) Helmholtz equation. The Green's function is constructed in terms of the usual bilinear product and corresponding Wronskian of the appropriate solutions of the homogeneous equation. Whenever – for a specific profile – the effective one-dimensional Helmholtz equation can be solved in closed form, the associated operator resolvent can be explicitly constructed, the operator spectrum identified, and the Dunford integral representation subsequently evaluated to yield a modal summation representation for the kernel $\mathcal{B}^{-1}(z,z')$. Application of Eq.(5) and/or Eq.(6) then results in the spectral (modal) summation representation for the inverse square-root Helmholtz operator symbol. The corresponding symbol representation for the square-root Helmholtz operator then follows from composition with the symbol for the $\boldsymbol{B}^2$ operator (4, 11, 23).

The focusing quadratic profile in one transverse spatial dimension is defined through

$$K^2(z) = K_0^2 - \omega^2 z^2 \ , \tag{14}$$

with $K_0, \omega \in \mathbb{R}_+$. The profile in Eq.(14) is (i) a model for waveguiding structures in classical physics applications (26), (ii) the

well-known harmonic oscillator model in quantum mechanics (27), and (iii) a much-studied, exactly soluble problem in operator spectral theory (28).

A. The Schwartz kernel

The above-outlined, general, spectral (modal) summation representation construction for the inverse square-root Helmholtz operator kernel has been presented before. For a concise review of the general spectral theory and the detailed calculations for the focusing quadratic profile case, see Van Stralen (4); the final result † is given by

$$\mathcal{B}^{-1}(z,z') = \frac{\bar{k}}{\pi^{1/2}} \sum_{n=0}^{\infty} \frac{1}{n!} \frac{1}{[-(2n+1-Y)]^{1/2}} \, 2^{-n} \Theta_n(z,z') \; ,$$

which expression, for later convenience, is rewritten in the form

$$\mathcal{B}^{-1}(z,z') = -\exp\left(\tfrac{3}{4}\pi \mathrm{i}\right) \frac{\bar{k}}{\pi^{1/2}} \sum_{n=0}^{\infty} \frac{1}{n!} \frac{1}{[\mathrm{i}\,(2n+1-Y)]^{1/2}} \, 2^{-n} \Theta_n(z,z') \; , \tag{15}$$

with

$$\Theta_n(z,z') = \phi_n\left((\omega\bar{k})^{1/2} z\right) \phi_n\left((\omega\bar{k})^{1/2} z'\right) \; , \tag{16}$$

$$\phi_n(\zeta) = \exp\left(-\tfrac{1}{2}\zeta^2\right) H_n(\zeta) \; , \tag{17}$$

where H_n is the Hermite polynomial (29), while

$$Y = K_0^2/\varepsilon \; , \tag{18}$$

$$\varepsilon = \omega/\bar{k} \; . \tag{19}$$

With the *effective refractive index* associated with mode n given by $[-\varepsilon\,(2n+1-Y)]^{1/2}$, the number of *propagating* modes, L, is obtained from the estimate

$$2L - 1 < Y < 2L + 1 \; .$$

In Eq.(15), the *principal value* of the square-root function is taken, consistent with the right-traveling wave condition, enforcing the radiation condition at infinity to be satisfied in the usual manner (1, 4, 24). The series representation is understood in the distributional sense (4, 30).

B. The standard (left) symbol

For the spectral (modal) summation representations, it is technically easier to first construct the standard Helmholtz operator symbols and subsequently deduce the corresponding Weyl forms using Eq.(13). Thus, substituting Eq.(15) into Eq.(5), interchanging the order of integration and summation, and applying the Hermite, Fourier transform (29),

$$\int_{\mathbb{R}} \mathrm{d}\zeta \, \exp(\mathrm{i}\zeta\varrho)\phi_n(\zeta) = (2\pi)^{1/2} \mathrm{i}^n \phi_n(\varrho) \; , \tag{20}$$

yield the desired expression for the standard, inverse square-root Helmholtz operator symbol

$$h^{s}_{\boldsymbol{B}^{-1}}(p,q) = -\exp\left(\tfrac{3}{4}\pi \mathrm{i}\right) \left(\frac{2}{\varepsilon}\right)^{1/2} \sum_{n=0}^{\infty} \frac{1}{n!} \frac{1}{[\mathrm{i}\,(2n+1-Y)]^{1/2}} \left(\frac{\mathrm{i}}{2}\right)^{n} \Psi_n(p,q) \; , \tag{21}$$

where

$$\Psi_n(p,q) = \exp(-\mathrm{i}\bar{k}\,pq)\, \phi_n\left((\omega\bar{k})^{1/2} q\right) \phi_n\left((\bar{k}/\omega)^{1/2} p\right) \; , \tag{22}$$

see also Van Stralen (4, (4.118)). In the transformation from the kernel to the standard symbol, note the occurrence of the Gabor wavelet, $\pi^{-1/4} \exp(\mathrm{i}\zeta\varrho)\, \phi_0(\zeta)$, for $n = 0$. Application of the 'large n' asymptotic expansions for both the Hermite polynomials and the gamma function (29), $n!$, establishes the conditional convergence of the series in Eq.(21).

† In Van Stralen (4, (4.114)), replace k_0 by $\bar{k}$, a by K_0^2, b by $4\omega^2$, $\frac{1}{2}k_0^{-1}b^{1/2}$ by ε, while $c_0\mathcal{A}_{-1/2}$ should be identified with $\mathcal{B}^{-1}$; in the notation of this paper, the spectrum of the operator (cf. Eq.(2)) $K^2(z) + (1/\bar{k}^2)\partial_z^2$ follows as $c_0^2\lambda^{(n)} = -\varepsilon\,(2n+1-Y)$, $n = 0, 1, 2, \ldots$.

The standard symbol for the square-root Helmholtz operator follows, in principle, on composing $h^s_{\boldsymbol{B}^2}(p,q)$ with $h^s_{\boldsymbol{B}^{-1}}(p,q)$ with the aid of the standard integral composition
equation (14, 15, 16), i.e.,

$$h^s_{\boldsymbol{B}}(p,q) = \frac{\bar{k}}{2\pi}\int_{\mathbb{R}^2} \mathrm{d}u\mathrm{d}s\; h^s_{\boldsymbol{B}^{-1}}(p-s,q)h^s_{\boldsymbol{B}^2}(p,q-u)\;\exp(-\mathrm{i}\bar{k}\,su)\;. \tag{23}$$

Applying this composition equation in its differential counterpart form, with $h^s_{\boldsymbol{B}^2} = K_0^2 - \omega^2 q^2 - p^2$ (cf. Eq.(14)), yields

$$h^s_{\boldsymbol{B}}(p,q) = (K_0^2 - \omega^2 q^2 - p^2)\, h^s_{\boldsymbol{B}^{-1}}(p,q) + \varepsilon^2[2\mathrm{i}\bar{k}q\,(\partial_p h^s_{\boldsymbol{B}^{-1}})(p,q) + (\partial_p^2 h^s_{\boldsymbol{B}^{-1}})(p,q)]\;. \tag{24}$$

Substituting Eq.(21) into Eq.(24) then results in the *formal* series

$$h^s_{\boldsymbol{B}}(p,q) = (2\varepsilon)^{1/2}\sum_{n=0}^{\infty}\frac{1}{n!}\,[-(2n+1-Y)]^{1/2}\;\left(\frac{\mathrm{i}}{2}\right)^n\Psi_n(p,q)\;,$$

which, by the same above-referenced asymptotic expansions, is divergent, reflecting the nonvalidity of the interchange of the summation and differentiation operations in the composition calculation (4, 31).

A proper expression for $h^s_{\boldsymbol{B}}$, essentially maintaining the modal decomposition form in Eq.(21), can, however, be derived in the following manner. Partitioning the series in Eq.(21) gives

$$\begin{aligned} h^s_{\boldsymbol{B}^{-1}}(p,q) = -\exp\left(\tfrac{3}{4}\pi\mathrm{i}\right)\left(\frac{2}{\varepsilon}\right)^{1/2}\Bigg\{&\sum_{n=0}^{N-1}\frac{1}{n!}\,\frac{1}{[\mathrm{i}\,(2n+1-Y)]^{1/2}}\;\left(\frac{\mathrm{i}}{2}\right)^n\Psi_n(p,q)\\ &+\sum_{n=N}^{\infty}\frac{1}{n!}\,\frac{1}{[\mathrm{i}\,(2n+1-Y)]^{1/2}}\;\left(\frac{\mathrm{i}}{2}\right)^n\Psi_n(p,q)\Bigg\}\;, \end{aligned} \tag{25}$$

where N is a positive integer with

$$N > L+1\;.$$

The infinite series in Eq.(25) contains only nonpropagating modes. In the second term in (25), for $n \geq N$, application of the identity (Magnus *et al.* (29, p.6))

$$\frac{\pi^{1/2}}{(2n+1-Y)^{1/2}} = \int_0^{\infty}\mathrm{d}t\,t^{-1/2}\exp[-(2n+1-Y)t] \tag{26}$$

followed by the interchange of the order of integration and summation, result in the contribution from the infinite sum,

$$-\mathrm{i}\left(\frac{2}{\pi\varepsilon}\right)^{1/2}\int_0^{\infty}\mathrm{d}t\,t^{-1/2}\exp[(Y-1)t]\left[\sum_{n=N}^{\infty}\frac{1}{n!}\;\left(\frac{\mathrm{i}}{2}\right)^n\Psi_n(p,q)\;\exp(-2nt)\right]\;.$$

The interchange of the operations is justified in Appendix A through the uniform convergence of power series (31) and the Riesz/Young theorem (32). Writing the infinite series in the above term in the form

$$\begin{aligned} \sum_{n=N}^{\infty}\frac{1}{n!}\;\left(\frac{\mathrm{i}}{2}\right)^n\Psi_n(p,q)\;\exp(-2nt) \;&=\; \sum_{n=0}^{\infty}\frac{1}{n!}\;\left(\frac{\mathrm{i}}{2}\right)^n\Psi_n(p,q)\;\exp(-2nt)\\ &-\; \sum_{n=0}^{N-1}\frac{1}{n!}\;\left(\frac{\mathrm{i}}{2}\right)^n\Psi_n(p,q)\;\exp(-2nt) \end{aligned} \tag{27}$$

and application of the Mehler formula ‡ then yield the replacement of Eq.(25),

$$\begin{aligned} h^s_{\boldsymbol{B}^{-1}}(p,q) = &-\exp\left(\tfrac{3}{4}\pi\mathrm{i}\right)\left(\frac{2}{\varepsilon}\right)^{1/2}\sum_{n=0}^{N-1}\frac{1}{n!}\,\frac{1}{[\mathrm{i}\,(2n+1-Y)]^{1/2}}\;\left(\frac{\mathrm{i}}{2}\right)^n\Psi_n(p,q)\\ &-\mathrm{i}\left(\frac{1}{\pi\varepsilon}\right)^{1/2}\int_0^{\infty}\mathrm{d}t\,t^{-1/2}\exp(Yt)\;[F(t)-G(t|N)]\;, \end{aligned} \tag{28}$$

‡ The Mehler formula is given by $2^{1/2}\exp(-t)\;\sum_{n=0}^{\infty}(n!)^{-1}\;(\mathrm{i}/2)^n\Psi_n(p,q)\;[\exp(-2t)]^n = F(t)$ in this paper's notation, see Rainville (33, p.198); i.e., F is a *generator* of $\{2^{1/2}(n!)^{-1}\;(\mathrm{i}/2)^n\Psi_n\}$.

where

$$F(t) = \exp\left[-\tfrac{1}{2}\chi\tanh(2t) + \mathrm{i}Z\left(\mathrm{sech}(2t)-1\right)\right]\left(\mathrm{sech}(2t)\right)^{1/2} , \tag{29}$$

$$G(t|N) = 2^{1/2}\exp(-t)\sum_{n=0}^{N-1}\frac{1}{n!}\left(\frac{\mathrm{i}}{2}\right)^{n}\Psi_n(p,q)\,\exp(-2nt) , \tag{30}$$

and

$$\chi = \varepsilon^{-1}(\omega^2 q^2 + p^2) , \tag{31}$$

$$Z = \varepsilon^{-1}\omega\, qp . \tag{32}$$

The construction of $h^s_{\boldsymbol{B}}(p,q)$ via the standard composition equation follows again from Eq.(24). Substituting the representation for $h^s_{\boldsymbol{B}^{-1}}(p,q)$ given in Eq.(28) into Eq.(24) allows for the interchange of the differentiation operations with the summation and integration operations. This follows from the fact that (i) the series appearing in the expression are finite and (ii) the integrand is an integrable function with exponential decay for large t and admits uniform bounds for the function and its subsequent derivatives (31). Indeed, the point of the construction procedure was to replace the infinite series in Eq.(25) with an appropriately differentiable (equivalent) integral representation. The result of the calculation can be written in the form

$$\begin{aligned} h^s_{\boldsymbol{B}}(p,q) = {} & (2\varepsilon)^{1/2}\sum_{n=0}^{N-1}\frac{1}{n!}\left[-(2n+1-Y)\right]^{1/2}\left(\frac{\mathrm{i}}{2}\right)^{n}\Psi_n(p,q) \\ & -\mathrm{i}\left(\frac{\varepsilon}{\pi}\right)^{1/2}\int_0^{\infty}\mathrm{d}t\, t^{-1/2}\exp(Yt)\,\left[\mathsf{F}(t)-\mathsf{G}(t|N)\right] , \end{aligned} \tag{33}$$

which is the counterpart of Eq.(28), where

$$\begin{aligned} \mathsf{F}(t) = {} & \exp\left[-\tfrac{1}{2}\chi\tanh(2t) + \mathrm{i}Z\left(\mathrm{sech}(2t)-1\right)\right]\left(\mathrm{sech}(2t)\right)^{1/2} \\ & \times\left[Y - \chi\left(\mathrm{sech}(2t)\right)^2 - 2\mathrm{i}Z\,\mathrm{sech}(2t)\tanh(2t) - \tanh(2t)\right] , \end{aligned} \tag{34}$$

$$\mathsf{G}(t|N) = 2^{1/2}\exp(-t)\sum_{n=0}^{N-1}\frac{1}{n!}\left[-(2n+1-Y)\right]\left(\frac{\mathrm{i}}{2}\right)^{n}\Psi_n(p,q)\,\exp(-2nt) , \tag{35}$$

and the principal value of the square-root function appearing in Eq.(33) is taken.

The result in Eq.(33), in essence, supplements the approximate, *truncated* series representation for $h^s_{\boldsymbol{B}}(p,q)$ derived by Van Stralen (4), with an integral which results in the exact expression. As such, the expression in Eq.(33) is well-defined in the limit $N\to\infty$, the nonconvergent behavior of the (first) series being exactly cancelled by the appropriate contribution from the integral term in the neighborhood of $t=0$. The details of this cancellation will result in computationally convenient operator symbol representations, thus, focusing on the neighborhood of $t=0$, partitioning the integral on $[0,\infty)$ in Eq.(33) into the contiguous sets $[0,\alpha]$ and $[\alpha,\infty)$ with $\alpha>0$, and noting that

$$\begin{aligned} & \int_0^{\alpha}\mathrm{d}t\, t^{-1/2}\exp(Yt)\,\mathsf{G}(t|N) = \\ & 2^{3/2}\alpha^{1/2}\left[\sum_{n=0}^{N-1}\frac{1}{n!}\left[-(2n+1-Y)\right]\left(\frac{\mathrm{i}}{2}\right)^{n}\Psi_n(p,q)\right]\,{}_1F_1(1/2;3/2;-\alpha\,(2n+1-Y)) , \end{aligned} \tag{36}$$

allow for $h^s_{\boldsymbol{B}}(p,q)$ to be written in the form

$$\begin{aligned} h^s_{\boldsymbol{B}}(p,q) = {} & (2\varepsilon)^{1/2}\sum_{n=0}^{L-1}\frac{1}{n!}\left[-(2n+1-Y)\right]^{1/2}\left(\frac{\mathrm{i}}{2}\right)^{n}\Psi_n(p,q) \\ & \times\left[1+2\mathrm{i}\left(\frac{\alpha}{\pi}\right)^{1/2}\left[-(2n+1-Y)\right]^{1/2}{}_1F_1(1/2;3/2;-\alpha\,(2n+1-Y))\right] \\ & +\mathrm{i}\,(2\varepsilon)^{1/2}\sum_{n=L}^{N-1}\frac{1}{n!}\left(2n+1-Y\right)^{1/2}\left(\frac{\mathrm{i}}{2}\right)^{n}\Psi_n(p,q) \\ & \times\left[1-2\left(\frac{\alpha}{\pi}\right)^{1/2}\left(2n+1-Y\right)^{1/2}{}_1F_1(1/2;3/2;-\alpha\,(2n+1-Y))\right] \end{aligned} \tag{37}$$

$$-\mathrm{i}\left(\frac{\varepsilon}{\pi}\right)^{1/2}\int_0^{\alpha}\mathrm{d}t\,t^{-1/2}\exp(Yt)\,\mathsf{F}(t)-\mathrm{i}\left(\frac{\varepsilon}{\pi}\right)^{1/2}\int_{\alpha}^{\infty}\mathrm{d}t\,t^{-1/2}\exp(Yt)\,\left[\mathsf{F}(t)-\mathsf{G}(t|N)\right]\,,$$

where

$${}_1F_1(1/2;3/2;-\alpha\,(2n+1-Y))=\tfrac{1}{2}\alpha^{-1/2}\int_0^{\alpha}\mathrm{d}t\,t^{-1/2}\exp[-(2n+1-Y)t] \tag{38}$$

is the incomplete gamma function expressed as a confluent hypergeometric function as given in Magnus *et al.* (29, p.337).

With the following estimates, it will be established that the limit $N\to\infty$ in Eq.(37), *termwise*, exists. The *first* and *third* terms in Eq.(37) are independent of N and hence well-defined in the limit $N\to\infty$. The series in the *second* term of Eq.(37) can be bounded by

$$\begin{aligned}&\left|\sum_{n=L}^{N-1}\frac{1}{n!}\,(2n+1-Y)^{1/2}\,\left(\frac{\mathrm{i}}{2}\right)^n\Psi_n(p,q)\right.\\&\qquad\left.\times\left[1-2\left(\frac{\alpha}{\pi}\right)^{1/2}(2n+1-Y)^{1/2}{}_1F_1(1/2;3/2;-\alpha\,(2n+1-Y))\right]\right|\\&\le\sum_{n=L}^{N-1}\frac{1}{n!}\,(2n+1-Y)^{1/2}\,\left(\frac{1}{2}\right)^n|\Psi_n(p,q)|\\&\qquad\times\left|1-2\left(\frac{\alpha}{\pi}\right)^{1/2}(2n+1-Y)^{1/2}{}_1F_1(1/2;3/2;-\alpha\,(2n+1-Y))\right|\,.\end{aligned} \tag{39}$$

The oscillator function product admits the bound stated in Abramowitz and Stegun (34, p.787),

$$|\Psi_n(p,q)|<2^n n!\,\mathcal{K}^2\,, \tag{40}$$

with $\mathcal{K}\simeq 1.086435$ for $p,q\in\mathbb{R}$. Equations (26) and (38) establish the equality

$$\begin{aligned}&\frac{\pi^{1/2}}{(2n+1-Y)^{1/2}}\,\left[1-\frac{(2n+1-Y)^{1/2}}{\pi^{1/2}}\,2\alpha^{1/2}\,{}_1F_1(1/2;3/2;-\alpha\,(2n+1-Y))\right]\\&\qquad=\int_{\alpha}^{\infty}\mathrm{d}t\,t^{-1/2}\exp[-(2n+1-Y)t]\,,\end{aligned} \tag{41}$$

which, upon applying standard bounding techniques [§], yield the estimate

$$\begin{aligned}&\left|1-2\left(\frac{\alpha}{\pi}\right)^{1/2}(2n+1-Y)^{1/2}{}_1F_1(1/2;3/2;-\alpha\,(2n+1-Y))\right|\\&\qquad\le\left(\frac{1}{\alpha\pi}\right)^{1/2}\frac{1}{(2n+1-Y)^{1/2}}\,\exp[-\alpha\,(2n+1-Y)]\,.\end{aligned} \tag{42}$$

Combining Eqs.(40) and (42) with Eq.(39) then gives

$$\begin{aligned}&\left|\sum_{n=L}^{N-1}\frac{1}{n!}\,(2n+1-Y)^{1/2}\,\left(\frac{\mathrm{i}}{2}\right)^n\Psi_n(p,q)\right.\\&\qquad\left.\times\left[1-2\left(\frac{\alpha}{\pi}\right)^{1/2}(2n+1-Y)^{1/2}{}_1F_1(1/2;3/2;-\alpha\,(2n+1-Y))\right]\right|\\&<\mathcal{K}^2\left(\frac{1}{\alpha\pi}\right)^{1/2}\exp[-\alpha\,(1-Y)]\sum_{n=L}^{N-1}\exp(-2n\alpha)\,.\end{aligned} \tag{43}$$

The absolute values of the terms in the series are bounded by the terms in a convergent geometric series for $p,q\in\mathbb{R}$, thus establishing absolute and uniform convergence in the limit $N\to\infty$ and the bound

$$\left|\sum_{n=L}^{\infty}\frac{1}{n!}\,(2n+1-Y)^{1/2}\,\left(\frac{\mathrm{i}}{2}\right)^n\Psi_n(p,q)\right.$$

[§] The estimate, $\int_{\alpha}^{\infty}\mathrm{d}t\,t^{-1/2}\exp[-(2n+1-Y)t]\le\alpha^{-1/2}\int_{\alpha}^{\infty}\mathrm{d}t\,\exp[-(2n+1-Y)t]$
$=\alpha^{-1/2}(2n+1-Y)^{-1}\,\exp[-\alpha\,(2n+1-Y)]$.

$$\times \left[1 - 2\left(\frac{\alpha}{\pi}\right)^{1/2} (2n+1-Y)^{1/2}\, {}_1F_1(1/2;3/2;-\alpha\,(2n+1-Y))\right]\Bigg|$$
$$< \mathcal{K}^2 \left(\frac{1}{\alpha\pi}\right)^{1/2} \exp[-\alpha\,(2L+1-Y)]\,\frac{1}{1-\exp(-2\alpha)}\,. \tag{44}$$

The integral in the *fourth* and final term in Eq.(37), noting that $t \in [\alpha, \infty)$, can be written in the form (cf. Eqs.(34)-(35) and the implicit use of the Mehler formula)

$$\int_\alpha^\infty \mathrm{d}t\, t^{-1/2} \exp(Yt)\ [\mathsf{F}(t) - \mathsf{G}(t|N)] = \int_\alpha^\infty \mathrm{d}t\, t^{-1/2} \exp(Yt)$$
$$\times \left[2^{1/2}\exp(-t)\ \sum_{n=N}^\infty \frac{1}{n!}\,[-(2n+1-Y)]\left(\frac{\mathrm{i}}{2}\right)^n \Psi_n(p,q)\ \exp(-2nt)\right] \tag{45}$$

and – bringing the integration inside the summation – bounded by

$$\left|\int_\alpha^\infty \mathrm{d}t\, t^{-1/2} \exp(Yt)\ [\mathsf{F}(t) - \mathsf{G}(t|N)]\right|$$
$$< \mathcal{K}^2 \left(\frac{2}{\alpha}\right)^{1/2} \exp[-\alpha\,(2N+1-Y)]\,\frac{1}{1-\exp(-2\alpha)}\,, \tag{46}$$

applying the previous results in Eqs.(40) and (41)-(42). Taking the limit $N \to \infty$ in Eq.(46) then establishes that the fourth term gives a zero contribution.

Combining the previous results, and actually taking the limit $N \to \infty$ in Eq.(37), the expression for $h^s_{\boldsymbol{B}}(p,q)$ can now be written as an absolutely and uniformly convergent infinite series and a well-defined integral:

$$h^s_{\boldsymbol{B}}(p,q) = (2\varepsilon)^{1/2} \sum_{n=0}^\infty \frac{1}{n!}\ \left(\frac{\mathrm{i}}{2}\right)^n \Psi_n(p,q)$$
$$\times \left\{[-(2n+1-Y)]^{1/2} + 2\mathrm{i}\left(\frac{\alpha}{\pi}\right)^{1/2} [-(2n+1-Y)]\, {}_1F_1(1/2;3/2;-\alpha\,(2n+1-Y))\right\}$$
$$-\mathrm{i}\left(\frac{\varepsilon}{\pi}\right)^{1/2} \int_0^\alpha \mathrm{d}t\, t^{-1/2} \exp(Yt)\ \mathsf{F}(t)\,. \tag{47}$$

Backsubstituting Eq.(36) for $N = L$ in Eq.(47), the result in Eq.(47) can be expressed in the alternate form

$$h^s_{\boldsymbol{B}}(p,q) = (2\varepsilon)^{1/2} \sum_{n=0}^{L-1} \frac{1}{n!}\,[-(2n+1-Y)]^{1/2}\ \left(\frac{\mathrm{i}}{2}\right)^n \Psi_n(p,q)$$
$$+\mathrm{i}\,(2\varepsilon)^{1/2} \sum_{n=L}^\infty \frac{1}{n!}\,(2n+1-Y)^{1/2}\ \left(\frac{\mathrm{i}}{2}\right)^n \Psi_n(p,q) \tag{48}$$
$$\times \left[1 - 2\left(\frac{\alpha}{\pi}\right)^{1/2} (2n+1-Y)^{1/2}\, {}_1F_1(1/2;3/2;-\alpha\,(2n+1-Y))\right]$$
$$-\mathrm{i}\left(\frac{\varepsilon}{\pi}\right)^{1/2} \int_0^\alpha \mathrm{d}t\, t^{-1/2} \exp(Yt)\ [\mathsf{F}(t) - \mathsf{G}(t|L)]\ ,$$

which, in conjunction with the (arbitrary) choice of $\alpha > 0$, can be used to balance and control the magnitude of the terms in a numerical calculation of the operator symbol. As $\alpha \downarrow 0$ but $\alpha \neq 0$, the first two terms in Eq.(48) represent an increasingly better approximate modal decomposition of the operator symbol for an appropriately defined, finite region of the phase space (4).

Applying the analysis used to transform Eq.(33) into Eq.(48) to Eq.(28) converts the conditionally convergent infinite series representation for $h^s_{\boldsymbol{B}^{-1}}$ given in Eq.(21) into an absolutely and uniformly convergent infinite series and a well-defined integral.

C. The Weyl symbol

Exact expressions, in the desired modal form, for both the inverse square-root and square-root Helmholtz operator symbols in the Weyl calculus can be deduced from the preceding standard calculus results in a direct fashion requiring relatively little calculation. From the expression for $h^s_{\boldsymbol{B}^{-1}}(p,q)$ given in Eq.(28), it is evident that the transformation mapping $h^s_{\boldsymbol{B}^{-1}}(p,q) \to \Omega_{\boldsymbol{B}^{-1}}(p,q)$

expressed in Eq.(13) acts only on the functions $\Psi_n(p,q)$ and $F(t)$. Further, by construction, $F(t)$ in Eq.(29) is the $N \to \infty$ limit of $G(t|N)$ in Eq.(30), making $F(t)$ a generator of the set $\{\Psi_n(p,q)\}$. Consequently, the analogous function $\widetilde{F}(t)$ in the Weyl calculus will generate the appropriate transformation of the set $\{\Psi_n(p,q)\}$. Thus, it is only necessary to identify $\widetilde{F}(t)$ to ultimately write all of the exact expressions in the Weyl representation.

It is apparent by the construction in Eq.(28) that, for the case $Y < 1$ (where there are no propagating modes),

$$-\mathrm{i}\left(\frac{1}{\pi\varepsilon}\right)^{1/2} \int_0^\infty \mathrm{d}t\, t^{-1/2} \exp(Yt)\, F(t)$$

is $h^s_{\boldsymbol{B}^{-1}}(p,q)$. Since $\widetilde{F}(t)$ must play the analogous role for $\Omega_{\boldsymbol{B}^{-1}}(p,q)$ for $Y < 1$, carrying out transformation Eq.(13) with Eq.(29), it follows that

$$\widetilde{F}(t) = \exp\left[-\chi \tanh(t)\right] \operatorname{sech}(t) \tag{49}$$

(note that the (p,q) dependence is contained solely in the variable χ). Application of the generating function (Rainville (33, p.213))

$$\frac{\exp\left[-\dfrac{xv}{1-v}\right]}{1-v} = \sum_{n=0}^{\infty} L_n^{(0)}(x)\, v^n \ , \quad |v| < 1 \ , \tag{50}$$

immediately identifies the transformed orthogonal polynomial set through the expansion

$$\exp\left[-\chi \tanh(t)\right] \operatorname{sech}(t) = 2\exp(-t) \sum_{n=0}^{\infty} \Phi_n(\chi)\, \exp(-2nt) \tag{51}$$

as

$$\Phi_n(\chi) = \exp(-\chi)\,(-)^n L_n^{(0)}(2\chi) \ , \tag{52}$$

or

$$\Phi_n(\chi) = \exp(-\chi)\,\frac{1}{n!}\,(2\chi)^n\, {}_2F_0(-n,-n;-;-(1/2\chi)) \ , \tag{53}$$

where $L_n^{(0)}(\cdot)$ is the simple Laguerre polynomial (33), ${}_2F_0(-n,-n;-;-(1/2\cdot))$ is a generalized hypergeometric function as given in Rainville (33, chap.5), and the equivalence expressed in Eq.(52) and Eq.(53) follows directly from the definitions of the respective functions (33).

It is now conjectured with Eq.(49) and Eqs.(51)-(53) that the effect of the transformation from the standard to the Weyl calculus for the inverse square-root Helmholtz operator symbol is summarized by the correspondences

$$F(t) \longrightarrow \widetilde{F}(t) \tag{54}$$

and

$$\Psi_n(p,q) \longrightarrow 2^{1/2} n!(-2\mathrm{i})^n \Phi_n(\chi) \ . \tag{55}$$

Application of Eqs.(54) and (55) to the expressions (21) and (28) in the standard calculus then provides the results

$$\Omega_{\boldsymbol{B}^{-1}}(p,q) = -\exp\left(\tfrac{3}{4}\pi\mathrm{i}\right)\, \frac{2}{\varepsilon^{1/2}} \sum_{n=0}^{\infty} \frac{1}{[\mathrm{i}\,(2n+1-Y)]^{1/2}}\, \Phi_n(\chi) \tag{56}$$

and

$$\begin{aligned}\Omega_{\boldsymbol{B}^{-1}}(p,q) = &-\exp\left(\tfrac{3}{4}\pi\mathrm{i}\right)\, \frac{2}{\varepsilon^{1/2}} \sum_{n=0}^{N-1} \frac{1}{[\mathrm{i}\,(2n+1-Y)]^{1/2}}\, \Phi_n(\chi) \\ &-\mathrm{i}\left(\frac{1}{\pi\varepsilon}\right)^{1/2} \int_0^\infty \mathrm{d}t\, t^{-1/2} \exp(Yt)\, \left[\widetilde{F}(t) - \widetilde{G}(t|N)\right] \ ,\end{aligned} \tag{57}$$

where, with Eqs.(30) and (55),

$$\widetilde{G}(t|N) = 2\exp(-t) \sum_{n=0}^{N-1} \Phi_n(\chi)\, \exp(-2nt) \ . \tag{58}$$

For the case of the square-root Helmholtz operator symbol, Eq.(55) is supplemented with the correspondence

$$\mathsf{F}(t) \longrightarrow \widetilde{\mathsf{F}}(t) \,, \tag{59}$$

where $\mathsf{F}(t)$ is given by Eq.(34) and

$$\widetilde{\mathsf{F}}(t) = \exp\left[-\chi\tanh(t)\right]\mathrm{sech}(t)\left[Y - \chi\left(\mathrm{sech}(t)\right)^2 - \tanh(t)\right] \,, \tag{60}$$

following from Eqs.(13) and (34). Application of Eqs.(55) and (59) to the expression (33) in the standard calculus then gives the result

$$\begin{aligned}\Omega_{\boldsymbol{B}}(p,q) &= 2\varepsilon^{1/2}\sum_{n=0}^{N-1}[-(2n+1-Y)]^{1/2}\,\Phi_n(\chi) \\ &\quad -\mathrm{i}\left(\frac{\varepsilon}{\pi}\right)^{1/2}\int_0^\infty \mathrm{d}t\, t^{-1/2}\exp(Yt)\,\left[\widetilde{\mathsf{F}}(t) - \widetilde{\mathsf{G}}(t|N)\right] \,,\end{aligned} \tag{61}$$

where

$$\widetilde{\mathsf{G}}(t|N) = 2\exp(-t)\sum_{n=0}^{N-1}[-(2n+1-Y)]\Phi_n(\chi)\,\exp(-2nt) \tag{62}$$

(cf. Eq.(35)). The deduced constructions given in Eqs.(56)-(58) and (61)-(62) can be confirmed through the direct verification that $\Psi_n(p,q)$ and $2^{1/2}n!(-2\mathrm{i})^n\Phi_n(\chi)$ form a standard-Weyl 'transform pair' with respect to Eqs.(12)-(13).

The analysis leading to the expressions given in Eqs.(47) and (48) for $h^s_{\boldsymbol{B}}(p,q)$ as the sum of an absolutely and uniformly convergent infinite series and a well-defined integral then follows in essentially the same fashion for the Weyl symbol $\Omega_{\boldsymbol{B}}(p,q)$; the final results, following directly from the application of the correspondences given in Eqs.(55) and (59) to the standard calculus expressions, are given by

$$\begin{aligned}\Omega_{\boldsymbol{B}}(p,q) &= 2\varepsilon^{1/2}\sum_{n=0}^{\infty}\Phi_n(\chi) \\ &\quad\times\left\{[-(2n+1-Y)]^{1/2} + 2\mathrm{i}\left(\frac{\alpha}{\pi}\right)^{1/2}[-(2n+1-Y)]\,{}_1F_1(1/2;3/2;-\alpha\,(2n+1-Y))\right\} \\ &\qquad -\mathrm{i}\left(\frac{\varepsilon}{\pi}\right)^{1/2}\int_0^\alpha \mathrm{d}t\, t^{-1/2}\exp(Yt)\,\widetilde{\mathsf{F}}(t)\end{aligned} \tag{63}$$

and

$$\begin{aligned}\Omega_{\boldsymbol{B}}(p,q) &= 2\varepsilon^{1/2}\sum_{n=0}^{L-1}[-(2n+1-Y)]^{1/2}\,\Phi_n(\chi) \\ &\quad +\mathrm{i}\,2\varepsilon^{1/2}\sum_{n=L}^{\infty}(2n+1-Y)^{1/2}\,\Phi_n(\chi) \\ &\qquad\times\left[1 - 2\left(\frac{\alpha}{\pi}\right)^{1/2}(2n+1-Y)^{1/2}\,{}_1F_1(1/2;3/2;-\alpha\,(2n+1-Y))\right] \\ &\quad -\mathrm{i}\left(\frac{\varepsilon}{\pi}\right)^{1/2}\int_0^\alpha \mathrm{d}t\, t^{-1/2}\exp(Yt)\,\left[\widetilde{\mathsf{F}}(t) - \widetilde{\mathsf{G}}(t|L)\right] \,.\end{aligned} \tag{64}$$

The principal results of Section 2 are the Helmholtz operator symbol representations given in Eqs.(21), (47), (48), (56), (63) and (64).

3. Contour-integral operator symbol representations

It follows from the construction in Eq.(57) that the inverse square-root Helmholtz operator symbol can be written in the form

$$\Omega^{\mathrm{foc}}_{\boldsymbol{B}^{-1}}(p,q) = -\mathrm{i}\left(\frac{1}{\pi\varepsilon}\right)^{1/2}\int_0^\infty \mathrm{d}t\, t^{-1/2}\exp\left[Yt - \chi\tanh(t)\right]\mathrm{sech}(t) \,, \quad Y < 1 \,, \tag{65}$$

where there are no propagating modes. For the corresponding defocusing quadratic profile (compare Eq.(14)) defined by

$$K^2(z) = K_0^2 + \omega^2 z^2 \ ,$$

with $K_0, \omega \in \mathbb{R}_+$, the operator symbol integral representation (23)

$$\Omega^{\mathrm{def}}_{\boldsymbol{B}^{-1}}(p,q) = -\exp\left(\tfrac{3}{4}\pi\mathrm{i}\right)\left(\frac{1}{\pi\varepsilon}\right)^{1/2}\int_0^\infty \mathrm{d}t\, t^{-1/2}\exp\left[\mathrm{i}\left(Yt + X\tanh(t)\right)\right]\mathrm{sech}(t)\ , \tag{66}$$

where

$$X = \varepsilon^{-1}(\omega^2 q^2 - p^2) \tag{67}$$

(compare Eq.(31)), in conjunction with Eq.(65), lead to the relation

$$\Omega^{\mathrm{foc}}_{\boldsymbol{B}^{-1}}(p,q) = \lim_{\omega\to\mathrm{i}\omega}\Omega^{\mathrm{def}}_{\boldsymbol{B}^{-1}}(p,q)\ , \quad Y<1\ , \tag{68}$$

adopting an obvious superscript notation in this section for clarity. The analytic continuation result in Eq.(68) can be extended to the square-root Helmholtz operator symbol following the construction in Eq.(61) and noting the corresponding integral representation for the defocusing quadratic profile given in Fishman (23).

The principal goal in this section is to extend the integral representation in Eq.(65) and the subsequent analytic continuation result in Eq.(68) connecting the focusing and defocusing quadratic profiles (and the analogous results at the level of the square-root Helmholtz operator symbol) from $Y<1$ to $Y\in[0,\infty)$, thereby explicitly accounting for the presence of the propagating modes. The basic idea is to modify an ω-rotation/contour-integration construction, which underlies the Eq.(68) analytic continuation result for $Y<1$, by explicitly incorporating the periodicity of the associated, parabolic (Schrödinger) equation fundamental solution (propagator) into the Helmholtz operator symbol construction procedure inherent in Eq.(66).

A. The complex ω-rotation and contour integration: analytic continuation for $Y<1$

First, the ω-rotation/contour-integration construction for the $Y<1$ case will be outlined, followed by the explicit incorporation of the underlying periodicity to produce the modified construction leading to the desired integral representations for the Helmholtz operator symbols for $Y\in[0,\infty)$. The extended analytic continuation results, following directly from the integral representations, will then be established.

For the ω-rotation/contour-integration construction procedure, the starting point is the exact, closed-form expression for the Weyl symbol for the inverse square-root Helmholtz operator in Eq.(66), with the aid of Eqs.(18)-(19), written as (note the change of integration variable, $t\to t/\omega$)

$$\Omega^{\mathrm{def}}_{\boldsymbol{B}^{-1}}(p,q) = -\exp\left(\tfrac{3}{4}\pi\mathrm{i}\right)\left(\frac{\bar{k}}{\pi}\right)^{1/2}\int_0^\infty \mathrm{d}t\, t^{-1/2}\exp\left[\mathrm{i}\left(\bar{k}K_0^2 t + X\tanh(\omega t)\right)\right]\mathrm{sech}(\omega t). \tag{69}$$

In Eq.(69), let $\omega\to\omega^*=\omega\exp(\mathrm{i}\varphi)$, $0\le\varphi<\pi/2$, with the corresponding transformation $X\to X^*=\varepsilon^{-1}\exp(-\mathrm{i}\varphi)\left[\exp(2\mathrm{i}\varphi)\,\omega^2 q^2 - p^2\right]$, so that in the limit $\varphi\uparrow\pi/2$, $X^*\to\mathrm{i}\chi$. Consider the contour integral

$$\Omega \equiv -\exp\left(\tfrac{3}{4}\pi\mathrm{i}\right)\left(\frac{\bar{k}}{\pi}\right)^{1/2}\oint_{\mathcal{C}}\mathrm{d}\tau\,\tau^{-1/2}\exp\left[\mathrm{i}\left(\bar{k}K_0^2\tau + X^*\tanh(\omega^*\tau)\right)\right]\mathrm{sech}(\omega^*\tau)\ , \tag{70}$$

where $\mathcal{C}=\Gamma_1+\Gamma_2+\Gamma_3+\Gamma_4$ as illustrated in Fig. 1. For the integrand in Eq.(70), in the complex τ-plane, the branch point (associated with $\tau^{-1/2}$) is at the origin with the branch line chosen to lie along the negative real-axis, and the isolated singularities (associated with the zeros of cosh) are located at the points

$$\tau = \frac{1}{\omega}\exp\left[\mathrm{i}\left(\frac{\pi}{2}-\varphi\right)\right](2n+1)\,\frac{\pi}{2}\ , \quad n=\cdots,-2,-1,0,1,2,\cdots\ . \tag{71}$$

The ω-rotation and subsequent contour integration have been specifically constructed so that the contributions from Γ_1 and Γ_3 will ultimately result in the operator symbol for the focusing case and the analytic continuation of the operator symbol for the defocusing case, respectively. Application of the Cauchy integral theorem (35) followed by standard arguments (35) to establish that the contributions from Γ_2 and Γ_4 vanish, respectively, in the $\mathrm{R}\to\infty$ and $\rho\to 0$ limits for $0\le\varphi<\pi/2$ (Fig. 1) and $Y<1$ result in the equality

$$-\exp\left(\tfrac{3}{4}\pi\mathrm{i}\right)\left(\frac{\bar{k}}{\pi}\right)^{1/2}\int_0^\infty \mathrm{d}t\, t^{-1/2}\exp\left[\mathrm{i}\left(\bar{k}K_0^2 t + X^*\tanh(\omega^* t)\right)\right]\mathrm{sech}(\omega^* t) = \tag{72}$$

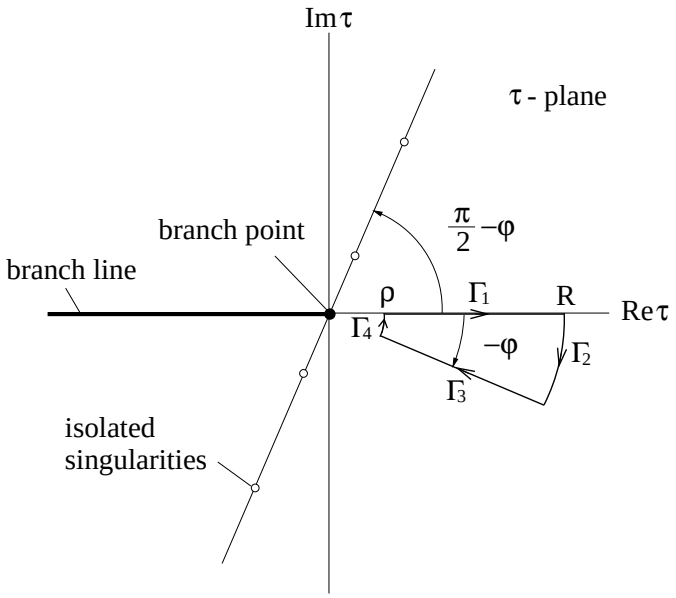

Figure 1. The contour of integration $\mathcal{C} = \Gamma_1 + \Gamma_2 + \Gamma_3 + \Gamma_4$ and the integrand singularity structure in the complex τ-plane for the Helmholtz operator symbol construction in Eq.(70).

$$-\exp\left(\tfrac{3}{4}\pi\mathrm{i}\right)\left(\frac{1}{\pi\varepsilon}\right)^{1/2}\exp\left(-\tfrac{1}{2}\mathrm{i}\varphi\right)\int_0^\infty \mathrm{d}t\, t^{-1/2}\exp\left[\mathrm{i}\left(\exp(-\mathrm{i}\varphi)\,Yt + X^*\tanh(t)\right)\right]\mathrm{sech}(t)\,,$$
$$0 \le \varphi < \tfrac{1}{2}\pi\,,\ Y < 1\,.$$

While the lhs of Eq.(72) is not well defined in the limit $\varphi \uparrow \pi/2$, the rhs of Eq.(72) is continuous at $\varphi = \pi/2$, suggesting that

$$\Omega^{\mathrm{foc}}_{\boldsymbol{B}^{-1}}(p,q) = -\mathrm{i}\left(\frac{1}{\pi\varepsilon}\right)^{1/2}\int_0^\infty \mathrm{d}t\, t^{-1/2}\exp\left[Yt - \chi\tanh(t)\right]\mathrm{sech}(t)\,,\quad Y<1\,,$$

which can be verified by establishing the equivalence of this equality and the corresponding spectral (modal) summation representation in Eq.(56) by proceeding from the identity in Eq.(51). The ω-rotation/contour-integration construction procedure results in the desired operator symbol integral representation, while explicitly illustrating the analytic continuation relationship between the focusing and defocusing quadratic profile cases, at least for $Y < 1$, i.e., in the absence of propagating modes.

B. Periodicity

The Weyl symbol construction procedure for the inverse square-root Helmholtz operator presented in (4, 23) is based on Eq.(6) in conjunction with (De Hoop and Gautesen (9, (7.1)))

$$\mathcal{B}^{-1}(z,z') = -2\mathrm{i}\bar{k}\,\mathrm{G}(0,z;0,z')\,, \tag{73}$$

which is just a restatement of Eq.(3), where G is the Helmholtz Green's function, satisfying

$$[\partial_x^2 + \partial_z^2 + \bar{k}^2K^2(z)]\,\mathrm{G}(x,z;x',z') = -\delta(x-x')\delta(z-z')\,, \tag{74}$$

supplemented with an outgoing-wave radiation condition (1, 23). The *parabolic* equation fundamental solution, $g(t,z;0,z')$ say, is related to $\mathrm{G}(x,z;x',z')$ through (23)

$$\mathrm{G}(x,z;0,z') = 2^{-3/2}\left(\frac{\mathrm{i}}{\bar{k}\pi}\right)^{1/2}\int_0^\infty \mathrm{d}t\, t^{-1/2}\exp\left[\tfrac{1}{2}\mathrm{i}\bar{k}\left(t + x^2t^{-1}\right)\right]\,g(t,z;0,z')\,, \tag{75}$$

and satisfies

$$\left[(\mathrm{i}/\bar{k})\,\partial_t + (1/2\bar{k}^2)\,\partial_z^2 + \tfrac{1}{2}(K^2(z)-1)\right]g(t,z;0,z') = 0 \tag{76}$$

supplemented by

$$g(0,z;0,z') = \delta(z-z')\,. \tag{77}$$

For the focusing quadratic profile, the parabolic equation fundamental solution takes the form implied in Fishman (23, (A1)) and given in Schulman (36, p.38),

$$g(t,z;0,z') = \left(\frac{\omega\bar{k}}{2\pi\mathrm{i}\,\sin(\omega t)}\right)^{1/2} \times \exp\left\{\tfrac{1}{2}\mathrm{i}\bar{k}\left[(K_0^2-1)\,t + \frac{\omega}{\sin(\omega t)}\left([z^2+(z')^2]\cos(\omega t) - 2zz'\right)\right]\right\} , \tag{78}$$

in accordance with the corresponding quantum mechanical harmonic oscillator formulation (27, 36). This function is, to within an exponential phase factor, periodic in t with period $(2\pi/\omega)$. Substituting Eq.(78) into Eq.(75), the subsequent result into Eq.(73), and applying the transform (6) lead to the lhs of Eq.(72) 'evaluated' at $\varphi = \pi/2$:

$$\Omega^{\mathrm{foc}}_{\boldsymbol{B}^{-1}}(p,q) \sim -\exp\left(\tfrac{3}{4}\pi\mathrm{i}\right)\left(\frac{\bar{k}}{\pi}\right)^{1/2}\int_0^\infty \mathrm{d}t\, t^{-1/2}\exp(-at)\,f(\omega t) , \tag{79}$$

where

$$a = -\mathrm{i}\bar{k}K_0^2 = -\mathrm{i}\omega Y \qquad \text{and} \qquad f(\omega t) = \exp\left[-\mathrm{i}\chi\,\mathrm{tan}(\omega t)\right]\sec(\omega t) .$$

The key to the extension of Eqs.(65) and (68) is the reduction of this semi-infinite integral to an integral over a single period through the application of the following theorem.

Theorem. Let $f(\omega t)$ be a $(2\pi/\omega)$-periodic function for $t \in (-\infty,\infty)$ and $\omega \in (0,\infty)$, and, further, let the following integral,

$$\int_0^\infty \mathrm{d}t\, t^{-1/2}\exp(-at)\,f(\omega t) , \quad \mathrm{Re}\{a\} > 0 \tag{80}$$

exist. Then the semi-infinite integral in Eq.(80) can be reduced to an integral over one period in the form

$$\int_0^\infty \mathrm{d}t\, t^{-1/2}\exp(-at)\,f(\omega t) = \left(\frac{\omega}{2\pi}\right)^{1/2}\int_0^{2\pi/\omega} \mathrm{d}t\,\zeta(1/2,(\omega t/2\pi),\exp(-2\pi a/\omega))\,\exp(-at)\,f(\omega t) , \tag{81}$$

where $\zeta(\sigma,\Delta,\xi)$ is the Lerch transcendental function defined by (29, 37)

$$\zeta(\sigma,\Delta,\xi) = \sum_{n=0}^{\infty}(n+\Delta)^{-\sigma}\xi^n , \quad \Delta \neq 0,-1,-2,\cdots , \quad |\xi| < 1 . \tag{82}$$

The Lerch transcendental function can be analytically continued into the cut complex ξ-plane via the integral representation (Erdélyi *et al.* (37, p.27))

$$\zeta(\sigma,\Delta,\xi) = \frac{1}{\Gamma(\sigma)}\int_0^\infty \mathrm{d}t\, t^{\sigma-1}\frac{\exp(-\Delta t)}{1-\xi\exp(-t)} , \quad \mathrm{Re}\{\Delta\} > 0 , \ \mathrm{Re}\{\sigma\} > 0 , \quad \xi \text{ not on the real axis between 1 and } \infty, \tag{83}$$

and where $\Gamma(\cdot)$ is the gamma function (29, 37). It is continued in Δ via the relationship given in Erdélyi *et al.* (37, p.27),

$$\zeta(\sigma,\Delta,\xi) = \xi^m\zeta(\sigma,m+\Delta,\xi) + \sum_{n=0}^{m-1}(n+\Delta)^{-\sigma}\xi^n , \quad m = 0,1,2,\cdots . \tag{84}$$

(A more detailed treatment of the Lerch transcendental function can be found in the references (29, 37).)

Proof. Starting with the integral on the rhs in Eq.(81) and applying Eq.(84) yield

$$\left(\frac{\omega}{2\pi}\right)^{1/2}\int_0^{2\pi/\omega} \mathrm{d}t\,\zeta(1/2,(\omega t/2\pi),\exp(-2\pi a/\omega))\,\exp(-at)\,f(\omega t) = \left(\frac{\omega}{2\pi}\right)^{1/2}\int_{m\,2\pi/\omega}^{(m+1)\,2\pi/\omega} \mathrm{d}t\,\zeta(1/2,(\omega t/2\pi),\exp(-2\pi a/\omega))\,\exp(-at)\,f(\omega t) + \int_0^{m\,2\pi/\omega} \mathrm{d}t\, t^{-1/2}\exp(-at)\,f(\omega t) , \quad m \geq 1 , \tag{85}$$

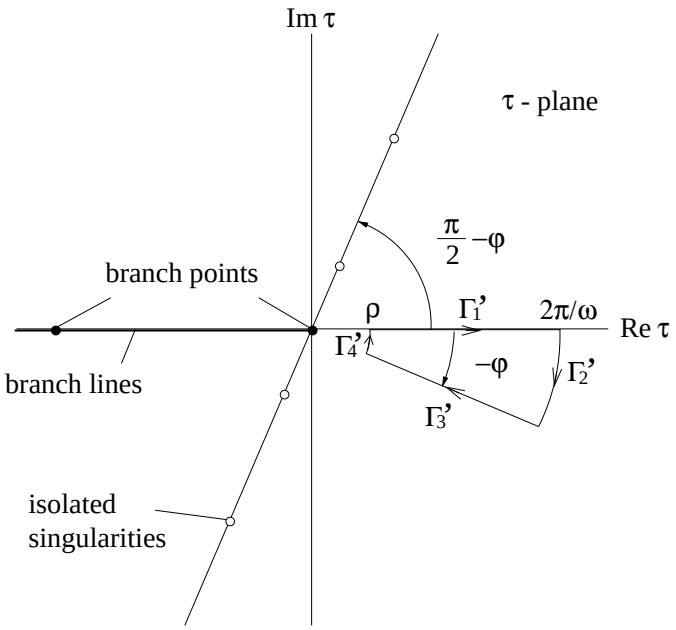

Figure 2. The contour of integration $\mathcal{C}' = \Gamma'_1 + \Gamma'_2 + \Gamma'_3 + \Gamma'_4$ and the integrand singularity structure in the complex τ-plane for the Helmholtz operator symbol construction in Eq.(88).

exploiting the periodicity of f. The second integral on the rhs of Eq.(85) can be written as

$$\int_0^{m\,2\pi/\omega} \mathrm{d}t\, t^{-1/2} \exp(-at)\, f(\omega t) = \int_0^{\infty} \mathrm{d}t\, t^{-1/2} \exp(-at)\, f(\omega t) - \int_{m\,2\pi/\omega}^{\infty} \mathrm{d}t\, t^{-1/2} \exp(-at)\, f(\omega t)\ . \tag{86}$$

On the other hand, consider the first integral on the rhs of Eq.(85). Substituting Eq.(82) into this integral, interchanging the order of integration and summation, and exploiting the periodicity of f result in

$$\left(\frac{\omega}{2\pi}\right)^{1/2} \int_{m\,2\pi/\omega}^{(m+1)\,2\pi/\omega} \mathrm{d}t\, \zeta(1/2, (\omega t/2\pi), \exp(-2\pi a/\omega))\, \exp(-at)\, f(\omega t) = \sum_{n=0}^{\infty} \int_{(m+n)\,2\pi/\omega}^{(m+n+1)\,2\pi/\omega} \mathrm{d}t\, t^{-1/2} \exp(-at)\, f(\omega t) = \int_{m\,2\pi/\omega}^{\infty} \mathrm{d}t\, t^{-1/2} \exp(-at)\, f(\omega t)\ . \tag{87}$$

Combining Eqs.(87), (86) and (85) results in the lhs of Eq.(81).

C. Symbol contour-integral representations for the focusing case

While the semi-infinite integral in the operator symbol construction for the focusing quadratic profile is not well defined at present, the above theorem and the previous ω-rotation/contour-integration construction for the case $Y < 1$ motivate the following construction procedure for $\Omega^{\mathrm{foc}}_{\boldsymbol{B}^{-1}}(p, q)$. Consider the contour integral (compare Eq.(70))

$$\Omega' \equiv -\exp\left(\tfrac{3}{4}\pi \mathrm{i}\right) \left(\frac{\bar{k}}{\pi}\right)^{1/2} \left(\frac{\omega}{2\pi}\right)^{1/2} \times \times \oint_{\mathcal{C}'} \mathrm{d}\tau\, \zeta(1/2, (\omega\tau/2\pi), \exp(2\pi \mathrm{i}\, Y)) \exp\left[\mathrm{i}\left(\bar{k} K_0^2 \tau + X^* \tanh(\omega^*\tau)\right)\right] \operatorname{sech}(\omega^*\tau) \tag{88}$$

for $Y \neq 0, 1, 2, \cdots$, where the contour $\mathcal{C}' = \Gamma'_1 + \Gamma'_2 + \Gamma'_3 + \Gamma'_4$ is defined in Fig. 2. For the integrand in Eq.(88), in the complex τ-plane, the branch points associated with $\zeta(1/2, (\omega\tau/2\pi), \exp(2\pi \mathrm{i}\, Y))$ are located at the points

$$\tau = -\frac{2\pi}{\omega} n\ , \quad n = 0, 1, 2, \cdots\ , \tag{89}$$

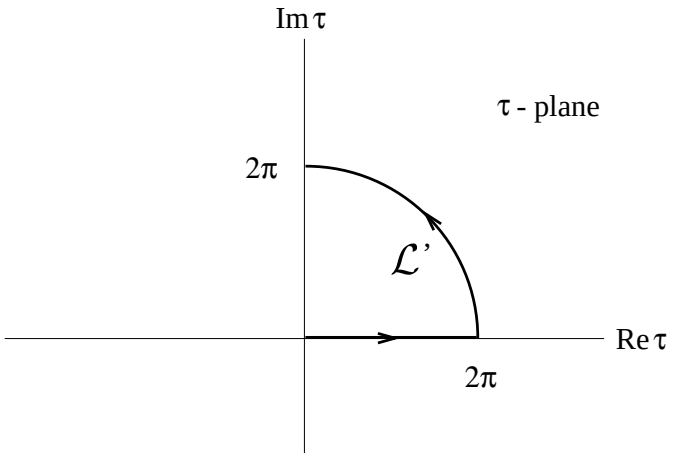

Figure 3. The contour of integration $\mathcal{L}'$ in the complex τ-plane for the Helmholtz operator symbol representation in Eq.(91).

with the associated branch lines chosen to lie along the negative real τ-axis, and the isolated singularities are located as in the previous construction for the case $Y < 1$. The series representation in Eq.(82) for $\zeta(1/2, (\omega\tau/2\pi), \exp(2\pi\mathrm{i}\,Y))$ is uniformly and absolutely convergent for $|\xi| < 1$, conditionally convergent for $|\xi| = 1$ and $\xi \neq 1$, and divergent for $\xi = 1$, where $\xi = \exp(2\pi\mathrm{i}\,Y)$. Thus, for the focusing quadratic profile, the Lerch transcendental function in Eq.(88) is defined by the series in Eq.(82), residing on the circle of convergence, away from $\xi = 1$, i.e., $Y \neq 0, 1, 2, \cdots$.

Application of the Cauchy integral theorem (35) to Eq.(88) followed by an evaluation of the contribution along Γ_4' in the $\rho \to 0$ limit result in

$$
\begin{aligned}
&-\exp\left(\tfrac{3}{4}\pi\mathrm{i}\right)\,\left(\frac{\omega\bar{k}}{2}\right)^{1/2}\,\frac{1}{\pi}\\
&\quad\times\int_0^{2\pi/\omega}\mathrm{d}t\,\zeta(1/2,(\omega t/2\pi),\exp(2\pi\mathrm{i}\,Y))\exp\left[\mathrm{i}\,(\bar{k}K_0^2 t+X^*\tanh(\omega^* t))\right]\,\mathrm{sech}(\omega^* t)\\
&=-\exp\left(\tfrac{3}{4}\pi\mathrm{i}\right)\,\frac{1}{(2\varepsilon)^{1/2}\pi}\exp(-\mathrm{i}\varphi)\\
&\quad\times\int_0^{2\pi}\mathrm{d}t\,\zeta(1/2,(t/2\pi)\exp(-\mathrm{i}\varphi),\exp(2\pi\mathrm{i}\,Y))\exp\left[\mathrm{i}\,(\exp(-\mathrm{i}\varphi)\,Yt+X^*\tanh(t))\right]\mathrm{sech}(t)\\
&\qquad+\exp\left(\tfrac{1}{4}\pi\mathrm{i}\right)\,\left(\frac{2}{\varepsilon}\right)^{1/2}\int_0^{\varphi}\mathrm{d}\theta\,\exp(-\mathrm{i}\theta)\,\zeta(1/2,\exp(-\mathrm{i}\theta),\exp(2\pi\mathrm{i}\,Y))\\
&\qquad\quad\times\exp\left[\mathrm{i}\,\left(2\pi\,Y\exp(-\mathrm{i}\theta)+X^*\tanh(2\pi\exp[\mathrm{i}(\varphi-\theta)])\right)\right]\mathrm{sech}(2\pi\exp[\mathrm{i}(\varphi-\theta)])\,,
\end{aligned}
\tag{90}
$$

$0 \leq \varphi < \pi/2$, $Y \neq 0, 1, 2, \cdots$. While the lhs in Eq.(90) is not well defined, at present, in the limit $\varphi \uparrow \pi/2$, the rhs in Eq.(90) is continuous at $\varphi = \pi/2$, suggesting that $\Omega^{\mathrm{foc}}_{\boldsymbol{B}^{-1}}(p,q)$ is given by the rhs of Eq.(90) evaluated at $\varphi = \pi/2$, i.e.,

$$
\begin{aligned}
\Omega^{\mathrm{foc}}_{\boldsymbol{B}^{-1}}(p,q) &= -\exp\left(\tfrac{1}{4}\pi\mathrm{i}\right)\,\frac{1}{(2\varepsilon)^{1/2}\pi}\\
&\quad\times\int_{\mathcal{L}'}\mathrm{d}\tau\,\zeta(1/2,(-\mathrm{i}/2\pi)\tau,\exp(2\pi\mathrm{i}\,Y))\exp\left[Y\tau-\chi\tanh(\tau)\right]\mathrm{sech}(\tau)\,,\quad Y\neq 0,1,2,\cdots\,,
\end{aligned}
\tag{91}
$$

where the contour $\mathcal{L}'$ in the complex τ-plane consists of the $\mathrm{Re}\{\tau\}$-axis from $\tau = 0$ to $\tau = 2\pi$ and the circular arc, $|\tau| = 2\pi$, from $\tau = 2\pi$ to $\tau = \mathrm{i}\,2\pi$, as illustrated in Fig. 3. Application of the Cauchy integral theorem (35) to Eq.(91) then yields the final integral representation

$$
\begin{aligned}
\Omega^{\mathrm{foc}}_{\boldsymbol{B}^{-1}}(p,q) &= -\exp\left(\tfrac{1}{4}\pi\mathrm{i}\right)\,\frac{1}{(2\varepsilon)^{1/2}\pi}\\
&\quad\times\int_{\mathcal{L}}\mathrm{d}\tau\,\zeta(1/2,(-\mathrm{i}/2\pi)\tau,\exp(2\pi\mathrm{i}\,Y))\exp\left[Y\tau-\chi\tanh(\tau)\right]\mathrm{sech}(\tau)\,,\quad Y\neq 0,1,2,\cdots\,,
\end{aligned}
\tag{92}
$$

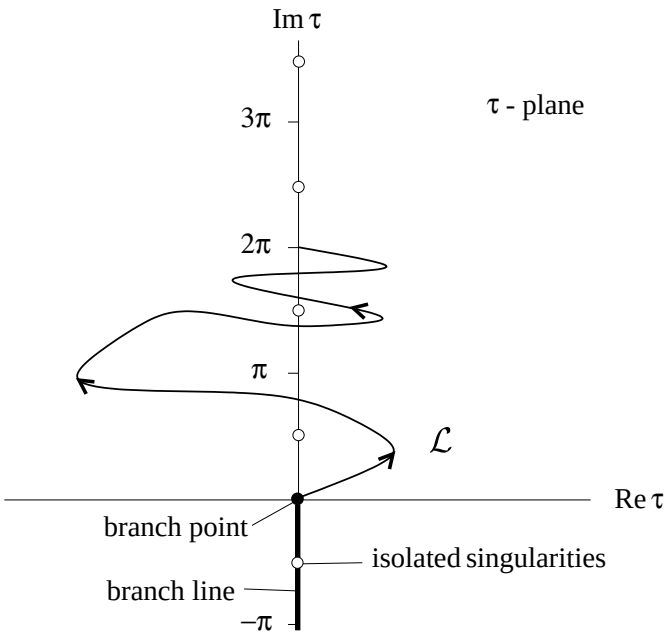

Figure 4. The contour of integration $\mathcal{L}$ and the integrand singularity structure in the complex τ-plane for the Helmholtz operator symbol representation in Eq.(92).

where the contour $\mathcal{L}$ in Eq.(92) starts at $\tau = 0$ and ends at $\tau = \mathrm{i}\,2\pi$, keeping the integrand singularities, which include branch points at (cf. Eq.(89))

$$\tau = -\mathrm{i}\,2\pi n\ , \quad n = 0, 1, 2, \cdots\ , \tag{93}$$

with the associated branch lines chosen to lie on the negative imaginary τ-axis, and isolated singularities at (cf. Eq.(71))

$$\tau = \mathrm{i}\,(2n+1)\,\frac{\pi}{2}\ , \quad n = \cdots, -2, -1, 0, 1, 2, \cdots\ , \tag{94}$$

'outside' the contour with respect to the half-plane $\mathrm{Re}\{\tau\} > 0$, as illustrated in Fig. 4. In Eq.(92), the occurrence of $\widetilde{F}$ defined in Eq.(49) is recognized. Now, the specific choice, $\mathcal{I}_\tau$, for the contour $\mathcal{L}$, shown in Fig. 5, provides the appropriate definition for the lhs integral in Eq.(90) in the limit $\varphi \uparrow \pi/2$, viz.,

$$\begin{aligned}
&-\exp\left(\tfrac{3}{4}\pi\mathrm{i}\right)\ \left(\frac{\omega\bar{k}}{2}\right)^{1/2}\ \frac{1}{\pi} \\
&\quad\times\int_0^{2\pi/\omega} \mathrm{d}t\ \zeta(1/2, (\omega t/2\pi), \exp(2\pi\mathrm{i}\,Y))\exp\left[\mathrm{i}\,(\bar{k}K_0^2 t + X^*\tanh(\omega^* t))\right]\ \mathrm{sech}(\omega^* t) \\
&\to -\exp\left(\tfrac{3}{4}\pi\mathrm{i}\right)\ \frac{1}{(2\varepsilon)^{1/2}\pi} \\
&\quad\times\int_0^{2\pi} \mathrm{d}t\ \zeta(1/2, (t/2\pi), \exp(2\pi\mathrm{i}\,Y))\exp\left[\mathrm{i}\,(Yt - \chi\tan(t))\right]\sec(t)\ ,
\end{aligned}$$

where the path of integration along $[0, 2\pi]$ is understood to pass 'below' the integrand singularities at $t = \pi/2$ and $3\pi/2$ (cf. Eq.(79)).

Verification of Eq.(92) – The operator symbol representation given in Eq.(92) can be verified in the following manner. Choosing the contour $\mathcal{L}$ to lie entirely in the half-plane $\mathrm{Re}\{\tau\} > 0$ and avoid the integrand singularities, and applying Eq.(84) for $m = 1$ to Eq.(92) result in

$$-\exp\left(\tfrac{1}{4}\pi\mathrm{i}\right)\ \frac{1}{(2\varepsilon)^{1/2}\pi}\ \int_{\mathcal{L}} \mathrm{d}\tau\,\zeta(1/2, (-\mathrm{i}/2\pi)\tau, \exp(2\pi\mathrm{i}\,Y))\exp\left[Y\tau - \chi\tanh(\tau)\right]\mathrm{sech}(\tau)$$

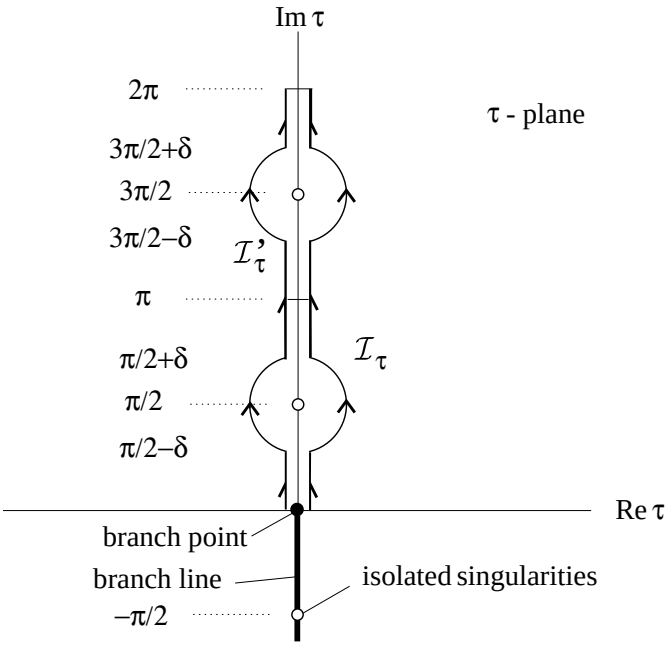

Figure 5. The contours of integration $\mathcal{I}_\tau$ and $\mathcal{I}'_\tau$ in the complex τ-plane used for the proper definition of the left-hand side integral in Eq.(90) and the high-frequency asymptotic constructions in Eqs.(129) and (147); $0 < \delta < \pi/2$ in general and $0 < \delta \ll 1$ for the specific asymptotic evaluations.

$$= -\mathrm{i}\left(\frac{1}{\pi\varepsilon}\right)^{1/2} \int_{\mathcal{L}} \mathrm{d}\tau\, \tau^{-1/2} \exp\left[Y\tau - \chi\tanh(\tau)\right] \operatorname{sech}(\tau) - \exp\left(\tfrac{1}{4}\pi\mathrm{i}\right) \frac{\exp(2\pi\mathrm{i}\,Y)}{(2\varepsilon)^{1/2}\pi}$$
$$\times \int_{\mathcal{L}} \mathrm{d}\tau\, \zeta(1/2, 1-(\mathrm{i}/2\pi)\tau, \exp(2\pi\mathrm{i}\,Y)) \exp\left[Y\tau - \chi\tanh(\tau)\right] \operatorname{sech}(\tau)\ , Y \neq 0, 1, 2, \cdots\ . \tag{95}$$

Examining the *first* term on the rhs in Eq.(95) and applying the generating function result in Eqs.(51) and (52), interchanging the order of integration and summation, which is justified by the uniform convergence of power series within their radius of convergence and the application of the Riesz/Young theorem (31, 32), and carrying out the remaining τ-integration result in

$$-\mathrm{i}\left(\frac{1}{\pi\varepsilon}\right)^{1/2} \int_{\mathcal{L}} \mathrm{d}\tau\, \tau^{-1/2} \exp\left[Y\tau - \chi\tanh(\tau)\right] \operatorname{sech}(\tau)$$
$$= -\exp\left(\tfrac{3}{4}\pi\mathrm{i}\right) \frac{2^{5/2}}{\varepsilon^{1/2}} \sum_{n=0}^{\infty} \Phi_n(\chi)\, {}_1F_1(1/2; 3/2; -\mathrm{i}\,2\pi\,(2n+1-Y))\ , \tag{96}$$

utilizing the complex form of the integral representation of the incomplete gamma function expressed as a confluent hypergeometric function (29) given in Eq.(38). Applying standard confluent hypergeometric function identities (29, 37) then yields the expression

$$-\exp\left(\tfrac{3}{4}\pi\mathrm{i}\right) \frac{2}{\varepsilon^{1/2}} \sum_{n=0}^{\infty} \frac{1}{[\mathrm{i}\,(2n+1-Y)]^{1/2}}\, \Phi_n(\chi) \tag{97}$$
$$+\exp\left(\tfrac{3}{4}\pi\mathrm{i}\right)\, 2\, \frac{\exp(2\pi\mathrm{i}\,Y)}{(\pi\varepsilon)^{1/2}} \sum_{n=0}^{\infty} \frac{1}{[\mathrm{i}\,(2n+1-Y)]^{1/2}}\, \Phi_n(\chi)\, U(1/2; 1/2; \mathrm{i}\,2\pi\,(2n+1-Y))$$

for the first term on the rhs in Eq.(95), where $U(\cdot;\cdot;\cdot)$ is the second solution of the confluent hypergeometric differential equation as given in Magnus *et al.* (29, chap.vi) and Erdélyi *et al.* (37, chap.vi). The large n asymptotic expansions (29, 37) for both $L_n^{(0)}(2\chi)$ and $U(1/2; 1/2; \mathrm{i}\,2\pi\,(2n+1-Y))$ establish the convergence of the two series in Eq.(97). Following from the spectral (modal) summation representation of the inverse square-root Helmholtz operator symbol given in Eq.(56), the first term in Eq.(97) is seen to be exactly $\Omega^{\mathrm{foc}}_{\boldsymbol{B}^{-1}}(p, q)$.

Examining the *second* term on the rhs in Eq.(95) and applying the generating function result in Eqs.(51) and (52), the integral representation in Eq.(83), interchanging the order of integration and summation, and carrying out an elementary exponential

integration over the contour $\mathcal{L}$ in the complex τ-plane result in the expression

$$-\exp\left(\tfrac{3}{4}\pi\mathrm{i}\right)\; 2^{3/2}\frac{\exp(2\pi\mathrm{i}\,Y)}{(\pi\varepsilon)^{1/2}}\;\sum_{n=0}^{\infty}\Phi_n(\chi)\;\int_0^{\infty}\mathrm{d}t\,t^{-1/2}\,[t+\mathrm{i}\,2\pi\,(2n+1-Y)]^{-1}\,\exp(-t)\;. \tag{98}$$

Utilizing the integral representation (Magnus *et al.* (29, p.277))

$$\begin{aligned}&\int_0^{\infty}\mathrm{d}t\,t^{-1/2}\,[t+\mathrm{i}\,2\pi\,(2n+1-Y)]^{-1}\,\exp(-t)\\&\quad=\frac{1}{[2\mathrm{i}\,(2n+1-Y)]^{1/2}}\;U(1/2;1/2;\mathrm{i}\,2\pi\,(2n+1-Y))\end{aligned} \tag{99}$$

in Eq.(98) then results in the expression

$$\begin{aligned}&-\exp\left(\tfrac{3}{4}\pi\mathrm{i}\right)\,2\,\frac{\exp(2\pi\mathrm{i}\,Y)}{(\pi\varepsilon)^{1/2}}\\&\quad\times\sum_{n=0}^{\infty}\frac{1}{[\mathrm{i}\,(2n+1-Y)]^{1/2}}\;\Phi_n(\chi)\,U(1/2;1/2;\mathrm{i}\,2\pi\,(2n+1-Y))\end{aligned} \tag{100}$$

for the second term on the rhs in Eq.(95), which exactly cancels the second term of expression (97). Hence, adding the terms in expressions (97) and (100), in view of Eq.(56), then establishes the contour-integral representation for $\Omega^{\mathrm{foc}}_{\boldsymbol{B}^{-1}}(p,q)$ given by Eq.(92).

The expression for $\Omega^{\mathrm{foc}}_{\boldsymbol{B}}(p,q)$ follows from the equation composing $\Omega^{\mathrm{foc}}_{\boldsymbol{B}^{-1}}$ with $\Omega^{\mathrm{foc}}_{\boldsymbol{B}^2}=K_0^2-\omega^2q^2-p^2$ (cf. Eq.(11)) in accordance with the Weyl calculus (23) (compare Eq.(24)), i.e.,

$$\begin{aligned}&\Omega^{\mathrm{foc}}_{\boldsymbol{B}}(p,q)=\\&\quad\left[(K_0^2-\omega^2q^2-p^2)+(1/2\bar{k})^2\partial_q^2+(\omega/2\bar{k})^2\partial_p^2+(\mathrm{i}p/\bar{k})\,\partial_q-(\mathrm{i}q\omega^2/\bar{k})\,\partial_p\right]\Omega^{\mathrm{foc}}_{\boldsymbol{B}^{-1}}(p,q)\;.\end{aligned} \tag{101}$$

Substitution of Eq.(92) into Eq.(101) allows for the subsequent interchange of the differentiation and integration operations following from the uniform convergence properties of the appropriate integrals involved (31). The resulting calculation takes the final form

$$\begin{aligned}\Omega^{\mathrm{foc}}_{\boldsymbol{B}}(p,q)=&-\exp\left(\tfrac{1}{4}\pi\mathrm{i}\right)\;\left(\frac{\varepsilon}{2}\right)^{1/2}\frac{1}{\pi}\;\int_{\mathcal{L}}\mathrm{d}\tau\,\zeta(1/2,(-\mathrm{i}/2\pi)\tau,\exp(2\pi\mathrm{i}\,Y))\\&\times\exp\left[Y\tau-\chi\tanh(\tau)\right]\mathrm{sech}(\tau)\left[Y-\chi\,(\mathrm{sech}(\tau))^2-\tanh(\tau)\right],\;Y\neq0,1,2,\cdots,\end{aligned} \tag{102}$$

in which the occurrence of $\widetilde{\mathsf{F}}(t)$ defined in Eq.(60) is recognized.

Standard symbols – The corresponding results for the standard operator symbols follow directly from the relationship in Eq.(12) and take the form

$$\begin{aligned}h^{s;\mathrm{foc}}_{\boldsymbol{B}^{-1}}(p,q)=&-\exp\left(\tfrac{1}{4}\pi\mathrm{i}\right)\;\frac{1}{(2\varepsilon)^{1/2}\pi}\int_{\mathcal{L}}\mathrm{d}\tau\,\zeta(1/2,(-\mathrm{i}/2\pi)\tau,\exp(2\pi\mathrm{i}\,Y))\\&\times\exp\left[Y\tau-\tfrac{1}{2}\chi\tanh(2\tau)+\mathrm{i}Z\,(\mathrm{sech}(2\tau)-1)\right](\mathrm{sech}(2\tau))^{1/2},\;Y\neq0,1,2,\cdots,\end{aligned} \tag{103}$$

(equivalent to replacing in Eq.(92) $\widetilde{F}$ by F, cf. Eq.(29)), and

$$\begin{aligned}h^{s;\mathrm{foc}}_{\boldsymbol{B}}(p,q)=&-\exp\left(\tfrac{1}{4}\pi\mathrm{i}\right)\;\left(\frac{\varepsilon}{2}\right)^{1/2}\frac{1}{\pi}\;\int_{\mathcal{L}}\mathrm{d}\tau\,\zeta(1/2,(-\mathrm{i}/2\pi)\tau,\exp(2\pi\mathrm{i}\,Y))\\&\times\exp\left[Y\tau-\tfrac{1}{2}\chi\tanh(2\tau)+\mathrm{i}Z\,(\mathrm{sech}(2\tau)-1)\right](\mathrm{sech}(2\tau))^{1/2}\\&\times\left[Y-\chi\,(\mathrm{sech}(2\tau))^2-2\mathrm{i}Z\,\mathrm{sech}(2\tau)\tanh(2\tau)-\tanh(2\tau)\right],\;Y\neq0,1,2,\cdots,\end{aligned} \tag{104}$$

(equivalent to replacing in Eq.(102) $\widetilde{\mathsf{F}}$ by F, cf. Eq.(34)). In Eqs.(103) and (104), the contour $\mathcal{L}$ is now confined to the half-plane $\mathrm{Re}\{\tau\}\geq0$, avoiding the integrand singularities, and the function $(\mathrm{sech}(2\tau))^{1/2}$ is analytic in the neighborhood of the contour and is given by the power series which results from the reduction of the generator F when $p=q=0$.

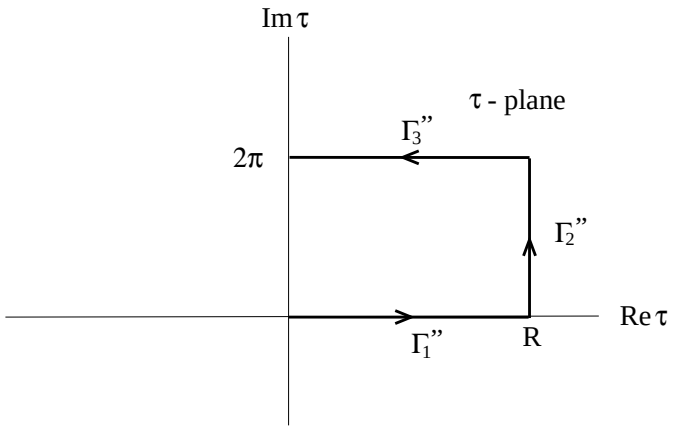

Figure 6. The contour of integration $\mathcal{L} = \mathcal{C}'' = \Gamma_1'' + \Gamma_2'' + \Gamma_3''$ in the complex τ-plane chosen for the evaluation of the Helmholtz operator symbol representation in Eq.(105).

D. Symbol contour-integral representations for the defocusing case

The corresponding Helmholtz operator symbols for the defocusing quadratic profile can be expressed by contour-integral representations analogous to those given in Eq.(92) and
Eqs.(102)-(104) for the focusing case. The Weyl symbol for the inverse square-root Helmholtz operator is given by

$$\Omega^{\mathrm{def}}_{\boldsymbol{B}^{-1}}(p,q) = -\mathrm{i}\,\frac{1}{(2\varepsilon)^{1/2}\pi} \times \int_{\mathcal{L}} \mathrm{d}\tau\, \zeta(1/2,(-\mathrm{i}/2\pi)\tau,\exp(-2\pi\,Y))\exp\left[\mathrm{i}\,(Y\tau + X\tanh(\tau))\right]\mathrm{sech}(\tau)\,, \quad Y \neq 0\,. \tag{105}$$

Verification of Eq.(105) – Following from the Cauchy integral theorem (35), the contour $\mathcal{L}$ in the complex τ-plane can be specifically chosen as $\mathcal{C}'' = \Gamma_1'' + \Gamma_2'' + \Gamma_3''$, as illustrated in Fig. 6, to be evaluated in the limit $\mathrm{R} \to \infty$. Applying Eq.(84) for $m = 1$ to the contribution to Eq.(105) along Γ_1'' gives

$$\begin{aligned} &-\mathrm{i}\,\frac{1}{(2\varepsilon)^{1/2}\pi}\int_0^\infty \mathrm{d}t\,\zeta(1/2,(-\mathrm{i}/2\pi)t,\exp(-2\pi\,Y))\exp\left[\mathrm{i}\,(Yt + X\tanh(t))\right]\mathrm{sech}(t) \\ &\quad = -\exp\left(\tfrac{3}{4}\pi\mathrm{i}\right)\left(\frac{1}{\pi\varepsilon}\right)^{1/2}\int_0^\infty \mathrm{d}t\,t^{-1/2}\exp\left[\mathrm{i}\,(Yt + X\tanh(t))\right]\mathrm{sech}(t) - \mathrm{i}\,\frac{\exp(-2\pi\,Y)}{(2\varepsilon)^{1/2}\pi} \\ &\qquad \times \int_0^\infty \mathrm{d}t\,\zeta(1/2,1-(\mathrm{i}/2\pi)t,\exp(-2\pi\,Y))\exp\left[\mathrm{i}\,(Yt + X\tanh(t))\right]\mathrm{sech}(t)\,, \quad Y \neq 0\,, \end{aligned} \tag{106}$$

when the limit $\mathrm{R} \to \infty$ is taken. Following from the exact operator symbol representations for the defocusing case established by Fishman (23) and given in Eq.(66), the first term on the rhs in Eq.(106) is seen to be exactly $\Omega^{\mathrm{def}}_{\boldsymbol{B}^{-1}}(p,q)$. It is readily established that the contribution to Eq.(105) along Γ_2'' vanishes in the limit $\mathrm{R} \to \infty$. Utilizing the periodicity of the hyperbolic functions,

$$\tanh(z + \mathrm{i}\,2\pi) = \tanh(z) \qquad \text{and} \qquad \mathrm{sech}(z + \mathrm{i}\,2\pi) = \mathrm{sech}(z)\,, \tag{107}$$

in the evaluation of the contribution to Eq.(105) along Γ_3'' then results in the term

$$\mathrm{i}\,\frac{\exp(-2\pi\,Y)}{(2\varepsilon)^{1/2}\pi}\int_0^\infty \mathrm{d}t\,\zeta(1/2,1-(\mathrm{i}/2\pi)t,\exp(-2\pi\,Y))\exp\left[\mathrm{i}\,(Yt + X\tanh(t))\right]\mathrm{sech}(t)\,, \quad Y \neq 0\,, \tag{108}$$

in the limit $\mathrm{R} \to \infty$. Adding the terms in Eqs.(106) and (108), in view of the integral representation in Eq.(66), then establishes the inverse square-root Helmholtz operator symbol representation given in Eq.(105). (Note that specifying the contour $\mathcal{L} = \mathcal{C}''$ in Eq.(92) for the focusing case recovers the contour-integral representation in Eq.(65) for $Y < 1$.)

The construction of $\Omega^{\mathrm{def}}_{\boldsymbol{B}}(p,q)$ via the Weyl composition equation (23), in a manner analogous to Eqs.(101)-(102), then provides the representation

$$\Omega^{\mathrm{def}}_{\boldsymbol{B}}(p,q) = -\left(\frac{\varepsilon}{2}\right)^{1/2}\frac{1}{\pi}\int_{\mathcal{L}} \mathrm{d}\tau\,\zeta(1/2,(-\mathrm{i}/2\pi)\tau,\exp(-2\pi\,Y))$$

$$\times \exp\left[\mathrm{i}\left(Y\tau + X\tanh(\tau)\right)\right]\mathrm{sech}(\tau)\left[\mathrm{i}Y + \mathrm{i}X\left(\mathrm{sech}(\tau)\right)^2 - \tanh(\tau)\right]\,,\ Y \neq 0\,. \tag{109}$$

Standard symbols – The corresponding integral representations for the standard operator symbols again follow from Eq.(12) in the form

$$h^{s;\mathrm{def}}_{\boldsymbol{B}^{-1}}(p,q) = -\mathrm{i}\,\frac{1}{(2\varepsilon)^{1/2}\pi}\int_{\mathcal{L}}\mathrm{d}\tau\,\zeta(1/2,(-\mathrm{i}/2\pi)\tau,\exp(-2\pi Y))$$
$$\times\exp\left[\mathrm{i}\left(Y\tau + \tfrac{1}{2}X\tanh(2\tau) + Z\left(\mathrm{sech}(2\tau)-1\right)\right)\right]\left(\mathrm{sech}(2\tau)\right)^{1/2}\ ,\quad Y\neq 0\,, \tag{110}$$

and

$$h^{s;\mathrm{def}}_{\boldsymbol{B}}(p,q) = -\left(\frac{\varepsilon}{2}\right)^{1/2}\frac{1}{\pi}\int_{\mathcal{L}}\mathrm{d}\tau\,\zeta(1/2,(-\mathrm{i}/2\pi)\tau,\exp(-2\pi Y))$$
$$\times\exp\left[\mathrm{i}\left(Y\tau + \tfrac{1}{2}X\tanh(2\tau) + Z\left(\mathrm{sech}(2\tau)-1\right)\right)\right]\left(\mathrm{sech}(2\tau)\right)^{1/2}$$
$$\times\left[\mathrm{i}Y + \mathrm{i}X\left(\mathrm{sech}(2\tau)\right)^2 - 2\mathrm{i}Z\,\mathrm{sech}(2\tau)\tanh(2\tau) - \tanh(2\tau)\right]\ ,\quad Y\neq 0\,. \tag{111}$$

E. Analytic continuation for $Y \in [0,\infty)$

The contour-integral representations for the Helmholtz operator symbols given in Eq.(105) and Eqs.(109)-(111) for the defocusing quadratic profile and Eq.(92) and Eqs.(102)-(104) for the focusing case, in conjunction with the appropriate analytic structure in the complex variable ω associated with the contour integrals, immediately establish the extended analytic continuation results

$$\Omega^{\mathrm{foc}}_{\boldsymbol{B}^{-1}}(p,q) \;=\; \lim_{\omega\to\mathrm{i}\omega}\Omega^{\mathrm{def}}_{\boldsymbol{B}^{-1}}(p,q)\,,\quad Y\in[0,\infty)\,,\ Y\neq 1,3,5,\cdots\,, \tag{112}$$

$$\Omega^{\mathrm{foc}}_{\boldsymbol{B}}(p,q) \;=\; \lim_{\omega\to\mathrm{i}\omega}\Omega^{\mathrm{def}}_{\boldsymbol{B}}(p,q)\,,\quad Y\in[0,\infty)\,, \tag{113}$$

while

$$h^{s;\mathrm{foc}}_{\boldsymbol{B}^{-1}}(p,q) \;=\; \lim_{\omega\to\mathrm{i}\omega}h^{s;\mathrm{def}}_{\boldsymbol{B}^{-1}}(p,q)\,,\quad Y\in[0,\infty)\,,\ Y\neq 1,3,5,\cdots\,, \tag{114}$$

$$h^{s;\mathrm{foc}}_{\boldsymbol{B}}(p,q) \;=\; \lim_{\omega\to\mathrm{i}\omega}h^{s;\mathrm{def}}_{\boldsymbol{B}}(p,q)\,,\quad Y\in[0,\infty)\,. \tag{115}$$

The equalities in Eqs.(112)-(115) extend the applicability of the previous analytic continuation results summarized in Eq.(68) from $Y<1$ to $Y\in[0,\infty)$, with the extension to the previously omitted, integer Y values following from the spectral (modal) summation representations and several additional contour-integral representations briefly discussed in Appendix B.

The principal results of Section 3 are the Helmholtz operator symbol representations in Eq.(92) and Eqs.(102)-(104) for the focusing case, Eq.(105) and Eqs.(109)-(111) for the defocusing case, and the analytic continuation formulas in Eqs.(112)-(115) connecting them.

4. Time-Fourier versus time-Laplace domain

In the analysis of two-way wave scattering, the generalized Bremmer series that couples the one-way waves plays a fundamental role. The convergence properties of this series are understood in the time-Laplace domain (De Hoop (11)) and require Sobolev order estimates of the square-root 'Helmholtz' operator uniform in the Laplace parameter. However, most algorithms that compute terms in the generalized Bremmer series are carried out in the time-Fourier domain. The quadratic profile provides a canonical medium in which the transformation of the square-root 'Helmholtz' operator from the time-Fourier to the time-Laplace domain, and vice versa, can be carried out explicitly and understood.

In the space-Laplace domain, the formally exact wave equation for (one-way) propagation in a transversely inhomogeneous half-space supplemented with appropriate right-traveling-wave radiation and initial-value conditions is given by (11)

$$(1/\bar{k})\,\partial_x w^+ + \boldsymbol{B}_s\,w^+ = 0\,, \tag{116}$$

(compare Eq.(1)), where

$$\boldsymbol{B}_s = \boldsymbol{B}_s(z,\partial_z) = [K^2(z) - (1/\bar{k})^2\partial_z^2]^{1/2} \tag{117}$$

is now the strictly elliptic square-root 'Helmholtz' operator (compare Eq.(2)). Note that, here,

$$w^+(x,z;s)=\int_0^\infty \mathrm{d}t\ \exp(-st)w^+(x,z;t)\ .$$

The phase space analysis remains largely the same, and can be summarized by the lattice multivariate (path) integral, with Hamiltonian equal to the square-root 'Helmholtz' operator symbol (11),

$$\mathcal{G}_s^+(x,z;x',z')=H(x-x')\lim_{M\to\infty}\int_{\mathbb{R}^{2M-1}}\prod_{i=1}^{M}(\bar{k}/2\pi)\mathrm{d}p^{(i)}\prod_{j=1}^{M-1}\mathrm{d}z^{(j)}$$
$$\times\exp\left[-\bar{k}\sum_{k=1}^{M}\left\{-\mathrm{i}\,p^{(k)}(z^{(k)}-z^{(k-1)})+h^s_{\boldsymbol{B}_s}(p^{(k)},z^{(k)})M^{-1}\Delta x\right\}\right] \tag{118}$$

(cf. Eq.(10)).

The mappings between the square-root 'Helmholtz' operator symbols constructed in the time-Fourier domain in Sections 2 and 3 and the corresponding symbols associated with the time-Laplace domain operator in Eq.(117) follow from the specific form of the quadratic profile representation and the analytic continuation results in Eqs.(113) and (115). Treating only the Weyl representation here, first, for the defocusing case, it follows from Eqs.(2) and (113) that

$$\Omega^{\mathrm{def}}_{\boldsymbol{B}_s}(p,q)=-\mathrm{i}\lim_{\omega\to\mathrm{i}\omega,K_0\to\mathrm{i}K_0}\Omega^{\mathrm{def}}_{\boldsymbol{B}}(p,q)=-\mathrm{i}\lim_{K_0\to\mathrm{i}K_0}\Omega^{\mathrm{foc}}_{\boldsymbol{B}}(p,q)\ . \tag{119}$$

Substituting representation (109) into Eq.(119) yields

$$\Omega^{\mathrm{def}}_{\boldsymbol{B}_s}(p,q)=\exp\left(-\tfrac{1}{4}\pi\mathrm{i}\right)\left(\frac{\varepsilon}{2}\right)^{1/2}\frac{1}{\pi}\int_{\mathcal{L}}\mathrm{d}\tau\,\zeta(1/2,(-\mathrm{i}/2\pi)\tau,\exp(-2\pi\mathrm{i}\,Y))$$
$$\times\exp\left[-(Y\tau+\chi\tanh(\tau))\right]\mathrm{sech}(\tau)\left[Y+\chi\,(\mathrm{sech}(\tau))^2+\tanh(\tau)\right],\ Y\neq 0,1,2,\cdots, \tag{120}$$

while the subsequent choice of contour $\mathcal{L}=\mathcal{C}''$ in Fig. 6 yields the equivalent form (see Fishman (23, (32)-(34)))

$$\Omega^{\mathrm{def}}_{\boldsymbol{B}_s}(p,q)=\left(\frac{\varepsilon}{\pi}\right)^{1/2}\int_0^\infty \mathrm{d}t\,t^{-1/2}\exp\left[-(Yt+\chi\tanh(t))\right]\mathrm{sech}(t)$$
$$\times\left[Y+\chi\,(\mathrm{sech}(t))^2+\tanh(t)\right]\ . \tag{121}$$

(compare Eq.(125)). For the focusing quadratic profile, it likewise follows that

$$\Omega^{\mathrm{foc}}_{\boldsymbol{B}_s}(p,q)=\lim_{\omega\to\mathrm{i}\omega}\Omega^{\mathrm{def}}_{\boldsymbol{B}_s}(p,q)=-\mathrm{i}\lim_{\omega\to\mathrm{i}\omega,K_0\to\mathrm{i}K_0}\Omega^{\mathrm{foc}}_{\boldsymbol{B}}(p,q)=-\mathrm{i}\lim_{\omega\to-\omega,K_0\to\mathrm{i}K_0}\Omega^{\mathrm{def}}_{\boldsymbol{B}}(p,q). \tag{122}$$

Substituting the representations (120) and (121) into Eq.(122), then results in the equivalent expressions

$$\Omega^{\mathrm{foc}}_{\boldsymbol{B}_s}(p,q)=\left(\frac{\varepsilon}{2}\right)^{1/2}\frac{1}{\pi}\int_{\mathcal{L}}\mathrm{d}\tau\,\zeta(1/2,(-\mathrm{i}/2\pi)\tau,\exp(-2\pi\,Y))$$
$$\times\exp\left[\mathrm{i}\,(Y\tau-X\tanh(\tau))\right]\mathrm{sech}(\tau)\left[-\mathrm{i}Y+\mathrm{i}X\,(\mathrm{sech}(\tau))^2+\tanh(\tau)\right],\ Y\neq 0\ , \tag{123}$$

and

$$\Omega^{\mathrm{foc}}_{\boldsymbol{B}_s}(p,q)=\exp\left(\tfrac{1}{4}\pi\mathrm{i}\right)\left(\frac{\varepsilon}{\pi}\right)^{1/2}\int_0^\infty \mathrm{d}t\,t^{-1/2}\exp\left[\mathrm{i}\,(Yt-X\tanh(t))\right]\mathrm{sech}(t)$$
$$\times\left[-\mathrm{i}Y+\mathrm{i}X\,(\mathrm{sech}(t))^2+\tanh(t)\right]\ . \tag{124}$$

The operator symbol representations in Eqs.(120) and (123) will prove useful in the construction and analysis of the square-root 'Helholtz' operator in the right-half of the complex Laplace plane, which will be presented elsewhere.

5. Asymptotic operator symbol expansions

The contour-integral representations for the Helmholtz operator symbols developed in Section 3 enable the high- and low-frequency, asymptotic operator symbol expansions to be derived in a straightforward fashion. Only the expressions for $\Omega^{\mathrm{foc}}_{\boldsymbol{B}}(p,q)$ will be presented; the other cases can be derived in a similar manner. (The superscript notation introduced in Section 3 will now be suppressed since all subsequent results will apply to the focusing case.)

A. Low-frequency asymptotic operator symbol expansion

In the low-frequency limit, $\varepsilon \to \infty$ and $Y \to 0$, enabling Y to be restricted to $Y < 1$, corresponding to $L = 0$, where there are no propagating modes. In the absence of propagating modes, the expression for the square-root Helmholtz operator symbol in the Weyl calculus reduces to (cf. Eq.(61) with Eq.(60)),

$$\Omega_{\boldsymbol{B}}(p,q) = -\mathrm{i}\left(\frac{\varepsilon}{\pi}\right)^{1/2} \int_0^\infty \mathrm{d}t\, t^{-1/2} \exp\left[Yt - \chi \tanh(t)\right] \mathrm{sech}(t)$$
$$\times \left[Y - \chi\left(\mathrm{sech}(t)\right)^2 - \tanh(t)\right] \ , \quad Y < 1 \ . \tag{125}$$

Expanding the exponential in the integrand and ordering the resulting terms in powers of ε yield a sum of integrals, each of which can be expressed in terms of the generalized zeta function ζ^*. On the one hand, ζ^* is defined as a special case of the Lerch transcendental function introduced in Eq.(82), viz.,

$$\zeta^*(\sigma,\Delta) = \sum_{n=0}^{\infty} (-)^n (n+\Delta)^{-\sigma} \ , \quad \Delta \neq 0, -1, -2, \cdots \ , \tag{126}$$

and its appropriate analytic continuations (29, 37). On the other hand, ζ^* is represented through the integral

$$\int_0^\infty \mathrm{d}t\, t^{s-1} \mathrm{sech}(t) \tanh(t) = 2^{2-s}\Gamma(s)\zeta^*(s-1,1/2) \ , \quad \mathrm{Re}\{s\} > 0 \ , \tag{127}$$

following from the result in Magnus *et al.* (29, p.34). Employing this integral representation, and integrating by parts the various terms in the above mentioned expansion then yield ¶

$$\Omega_{\boldsymbol{B}}(p,q) \overset{\varepsilon \to \infty}{\sim} \mathrm{i}\, 2^{1/2} \Big\{ 2\zeta^*(-1/2,1/2)\, \varepsilon^{1/2}$$
$$- \left[2^{-1}\zeta^*(1/2,1/2) K_0^2 + 2^2 \zeta^*(-3/2,1/2)(\omega^2 q^2 + p^2)\right] \varepsilon^{-1/2}$$
$$- \left[2^{-4}\zeta^*(3/2,1/2) K_0^4 - \zeta^*(-1/2,1/2) K_0^2 (\omega^2 q^2 + p^2)\right.$$
$$\left. - (2^{-1}\zeta^*(-1/2,1/2) + 2\zeta^*(-5/2,1/2))(\omega^2 q^2 + p^2)^2\right] \varepsilon^{-3/2} + \cdots \Big\} \ . \tag{128}$$

The low-frequency asymptotic expansion given in Fishman (23, (29)) for the defocusing quadratic profile in conjunction with the analytic continuation property given in Eq.(113) lead to the same result. As expected, $\Omega_{\boldsymbol{B}}(p,q)$ is purely imaginary for $Y < 1$, in the absence of propagating modes.

B. High-frequency asymptotic operator symbol expansion

The high-frequency, $\varepsilon \to 0$, asymptotic evaluation of $\Omega_{\boldsymbol{B}}(p,q)$ starts with a delicate choice $\mathcal{I}_\tau$ of the contour $\mathcal{L}$ in the integral representation (102). Essentially, the contour $\mathcal{I}_\tau$ follows the imaginary τ-axis, circling around the isolated singularities – leading to an oscillatory integral representation for the Weyl operator symbol.

Changing the variables of integration, $\tau = \mathrm{i}t$ along the 'linear segments' of the contour, and $\tau = \mathrm{i}[\pi/2 + \delta\exp(\mathrm{i}\vartheta)]$ and $\tau = \mathrm{i}[3\pi/2 + \delta\exp(\mathrm{i}\vartheta)]$ with $\vartheta \in [-\pi, 0]$ along the 'semicircular segments', then results in the explicit representation

$$\Omega_{\boldsymbol{B}}(p,q) = \mathrm{i}\left[\int_0^{\pi/2-\delta} \mathrm{d}t\, \mathcal{R}(t) + \int_{\pi/2+\delta}^{3\pi/2-\delta} \mathrm{d}t\, \mathcal{R}(t) + \int_{3\pi/2+\delta}^{2\pi} \mathrm{d}t\, \mathcal{R}(t)\right]$$
$$+ \exp\left(\tfrac{1}{4}\pi\mathrm{i}\right) \exp\left(\tfrac{1}{2}\pi\mathrm{i}\, Y\right) \left(\frac{\varepsilon}{2}\right)^{1/2} \frac{1}{\pi}\, \delta \int_0^\pi \mathrm{d}\vartheta\, \exp(-\mathrm{i}\vartheta)$$
$$\times \left[\exp(\pi\mathrm{i}\, Y)\, \zeta(1/2, 3/4 + (\delta/2\pi)\exp(-\mathrm{i}\vartheta), \exp(2\pi\mathrm{i}\, Y))\right.$$
$$\left. - \zeta(1/2, 1/4 + (\delta/2\pi)\exp(-\mathrm{i}\vartheta), \exp(2\pi\mathrm{i}\, Y))\right]$$
$$\times \exp\left[\mathrm{i}\, \left(Y\delta\exp(-\mathrm{i}\vartheta) + \chi\cot(\delta\exp(-\mathrm{i}\vartheta))\right)\right] \csc(\delta\exp(-\mathrm{i}\vartheta))$$

¶ The various terms contain integrals of the type, $\int_0^\infty \mathrm{d}t\, t^s \mathrm{sech}(t) = 2^{-s}(s+1)^{-1}\Gamma(s+2)\zeta^*(s+1,1/2)$,
$\int_0^\infty \mathrm{d}t\, t^{s+1} \mathrm{sech}^3(t) = 2^{-s-2}\Gamma(s+2)\zeta^*(s+2,1/2) - 2^{-s}\Gamma(s+2)\zeta^*(s,1/2)$, and
$\int_0^\infty \mathrm{d}t\, t^s \mathrm{sech}^3(t)\tanh(t) = 2^{-s}(1/3)\,\Gamma(s+1)\zeta^*(s,1/2) - 2^{2-s}(1/3)\,\Gamma(s+1)\zeta^*(s-2,1/2)$.

$$\times \left[Y - \chi\left(\csc(\delta\exp(-\mathrm{i}\vartheta))\right)^2 + \mathrm{i}\cot(\delta\exp(-\mathrm{i}\vartheta))\right] \ , \quad Y \neq 0, 1, 2, \cdots \ , \tag{129}$$

where

$$\mathcal{R}(t) \equiv -\exp\left(\tfrac{1}{4}\pi\mathrm{i}\right)\left(\frac{\varepsilon}{2}\right)^{1/2}\frac{1}{\pi}\,\zeta(1/2, (t/2\pi), \exp(2\pi\mathrm{i}\,Y)) \\ \times \exp\left[\mathrm{i}\left(Yt - \chi\tan(t)\right)\right]\sec(t)\left[Y - \chi\left(\sec(t)\right)^2 - \mathrm{i}\tan(t)\right] \ , \tag{130}$$

and $0 < \delta < \pi/2$. An asymptotic evaluation of $\Omega_{\boldsymbol{B}}(p, q)$ in the $\varepsilon \to 0$ limit can then, for the most part, be reduced to a *stationary phase* evaluation (38, 39) of the first three integrals in Eqs.(129)-(130) in conjunction with a Laplace method evaluation (38, 39) of the semicircular (ϑ-)integral contributions in Eq.(129).

The principal part of $\Omega_{\boldsymbol{B}}(p, q)$ is found to be

$$\left[\varepsilon\left(Y - \chi\right)\right]^{1/2} = \left[K_0^2 - \omega^2 q^2 - p^2\right]^{1/2} \ ;$$

hence, the analysis naturally divides into two cases: (**1**) $Y > \chi > 0$ (locally-propagating regime) and (**2**) $\chi > Y > 0$ (locally-evanescent regime).

Case 1: $Y > \chi > 0$. Applying the stationary phase and the Laplace methods to the operator symbol integral representations given in Eqs.(129) and (130), the dominant contributions are found to result from exterior and interior end points, interior critical points, and the singular points of the integrand. Since the Cauchy integral theorem (35) implies that the representation is independent of the particular choice of δ for $0 < \delta < \pi/2$, this can be exploited in the detailed calculation. The principal idea is to choose δ so that (i) the dominant contributions can be divided into three disjoint groups which can be calculated independently and added in the end to produce the final result, and (ii) the contribution from the singular points of the integrand can be evaluated in an expeditious manner.

The first group comprises the contributions from the exterior end points at $t = 0$ and 2π. The second group comprises the contributions from the interior critical points. The series and integral representations of the Lerch transcendental function, given, respectively, in Eq.(82) and Eq.(83), readily establish that, in the context of the high-frequency asymptotic analysis, in the function $\mathcal{R}$,

- $\zeta(1/2, (t/2\pi), \exp(2\pi\mathrm{i}\,Y))$ is solely an amplitude function, while
- $\forall t \in [0, 2\pi]$:

$$\zeta(1/2, (t/2\pi), \exp(2\pi\mathrm{i}\,Y)) \neq 0 \ , \tag{131}$$

and $\zeta(1/2, (t/2\pi), \exp(2\pi\mathrm{i}\,Y))$ is finite except at $t = 0$.

Thus, the oscillatory part of $\mathcal{R}$ is the exponential,

$$\exp\left[\mathrm{i}\left(Yt - \chi\tan(t)\right)\right] \ ,$$

which implicitly contains the 'large' parameter ε^{-1}. The ('interior') critical points, $\tau_0 = \mathrm{i}t_0$ say, associated with its phase, follow from the equality $Y - \chi\left(\sec(t)\right)^2 = 0$, and are given by t_0, $\pi - t_0$, $\pi + t_0$, and $2\pi - t_0$, where

$$t_0 = \arctan\left(\left[(Y/\chi) - 1\right]^{1/2}\right) \tag{132}$$

$$= \tfrac{1}{2}\mathrm{i}\log\left(\frac{\mathrm{i} + \left[(Y/\chi) - 1\right]^{1/2}}{\mathrm{i} - \left[(Y/\chi) - 1\right]^{1/2}}\right) \ , \tag{133}$$

with the principal branches understood. (Observe, that as $(Y/\chi) \to \infty$, then $t_0 \uparrow \pi/2$ and the critical points tend to the isolated singularities, while as $(Y/\chi) \to 1$, $t_0 \downarrow 0$ and the critical points tend to the exterior end points, 0 and 2π, and to π.)

The third group comprises the contributions from the four interior end points at $t = \pi/2 \pm \delta$ and $t = 3\pi/2 \pm \delta$ in conjunction with the two semicircular (ϑ-)integrals deriving from the δ-neighborhoods of the isolated singular points at $t = \pi/2$ and $t = 3\pi/2$.

With the exception of the two previously mentioned limits of coalescing critical points, the contributions to the high-frequency asymptotic operator symbol evaluation from the three groups are disjoint if there are no critical points on the intervals on the imaginary τ-axis, $[\pi/2 - \delta, \pi/2 + \delta]$ and $[3\pi/2 - \delta, 3\pi/2 + \delta]$. Thus, for fixed εY and $\varepsilon\chi$, to ensure that $t_0 < \pi/2 - \delta$, requires the condition,

$$Y/\chi < \left(\csc(\delta)\right)^2 \ . \tag{134}$$

On the other hand, the radius δ of the semicircles must be sufficiently large to avoid a residual contribution from the isolated singularities when $t_0 \uparrow \pi/2$.

The further refinement of the contour $\mathcal{I}_\tau$ in relation to the calculation of the contributions from the δ-neighborhoods of the two isolated singularities requires some attention. The exponential occurring in the integrand of the semicircular contributions to Eq.(129) can be written in the form

$$\exp\left[\mathrm{i}\ \left(Y\delta\exp(-\mathrm{i}\vartheta)+\chi\cot(\delta\exp(-\mathrm{i}\vartheta))\right)\right]=\exp[h_R(\vartheta)+\mathrm{i}\,h_I(\vartheta)]\ ,$$

where

$$h_R(\vartheta)=Y\delta\sin(\vartheta)+\tfrac{1}{2}\mathrm{i}\,\chi\ [\cot(\delta\exp(-\mathrm{i}\vartheta))-\cot(\delta\exp(\mathrm{i}\vartheta))] \tag{135}$$

and

$$h_I(\vartheta)\ =Y\delta\cos(\vartheta)+\tfrac{1}{2}\ \chi\ [\cot(\delta\exp(-\mathrm{i}\vartheta))+\cot(\delta\exp(\mathrm{i}\vartheta))] \tag{136}$$

with $\vartheta\in[0,\pi]$. The estimation of the contributions from the two semicircular (ϑ-)integrals in Eq.(129) is governed by $h_R(\vartheta)$ in Eq.(135). The function h_R (cf. Eq.(135)) can be written in the form

$$h_R(\vartheta)\ =Y\delta\sin(\vartheta)+\chi\,\frac{\sinh(2\delta\sin(\vartheta))}{\cos(2\delta\cos(\vartheta))-\cosh(2\delta\sin(\vartheta))}\ .$$

It follows that $h_R(\vartheta)$ is a symmetric function of ϑ with respect to $\pi/2$ for $\vartheta\in[0,\pi]$. Also, note that $h_R(0)=h_R(\pi)=0$. For sufficiently small δ, it is straightforward to establish that $h_R(\vartheta)$ is monotonically decreasing for $\vartheta\in[0,\pi/2)$ and monotonically increasing for $\vartheta\in(\pi/2,\pi]$ with a global minimum at $\pi/2$, transitioning for increasing δ to a 'double-well-like' structure with a local or global maximum at $\pi/2$ and two, symmetrically located global minima. Condition (134), while ensuring that $h_R'(0)=-h_R'(\pi)<0$, is not sufficient to imply that $h_R(\vartheta)<0\ \forall\vartheta\in(0,\pi)$. Requiring that $h_R(\pi/2)<0$ using Eq.(135), resulting in the additional condition,

$$Y/\chi<\delta^{-1}\coth(\delta)\ , \tag{137}$$

ensures the latter condition. Ensuring that $h_R(\vartheta)<0\ \forall\vartheta\in(0,\pi)$ implies that the exponential function in the semicircular contributions to Eq.(129) is dominated by the exponential decay in the high-frequency limit. Condition (137), however, is not sufficient to ensure that $h_R(\vartheta)$ has a single, global minimum at $\pi/2$. Requiring that $h_R''(\pi/2)>0$ ensures the latter condition, resulting in the additional and final condition on δ,

$$Y/\chi<(\mathrm{csch}(\delta))^2(2\delta\coth(\delta)-1)\ . \tag{138}$$

Ensuring that $h_R(\vartheta)$ has a single, global minimum at $\pi/2$ not only ensures that the integrands corresponding to the contributions from the two isolated singular points are exponentially small for $\vartheta\in(0,\pi)$, but that, in addition, the dominant contributions in the Laplace method (38, 39) calculation come entirely from the neighborhoods of the maxima at the end points $\vartheta=0$ and π.

In summary, the contour $\mathcal{I}_\tau$ is specifically constructed such that for fixed εY and $\varepsilon\chi$, a sufficiently small δ is chosen so as to satisfy the infimum of inequalities (134), (137) and (138), which simply yields (the subsequent inequalities hold for sufficiently small δ)

$$Y/\chi<(\mathrm{csch}(\delta))^2(2\delta\coth(\delta)-1)<\delta^{-1}\coth(\delta)<(\csc(\delta))^2\ . \tag{139}$$

The choice of δ in Eq.(139) ensures that (i) the dominant contributions to the operator symbol integral representation given in Eqs.(129) and (130), with the general method of stationary phase (38, 39), can be divided into the following three disjoint groups:

(a) the exterior end points at $t=0$ and 2π,
(b) the four interior critical points at t_0, $\pi-t_0$, $\pi+t_0$, and $2\pi-t_0$, and
(c) the four interior end points at $t=\pi/2\pm\delta$ and $3\pi/2\pm\delta$ in conjunction with the two semicircular (ϑ-)integrals deriving from the δ-neighborhoods of the singular points at $t=\pi/2$ and $3\pi/2$,

and (ii) the contribution from the two isolated singular points can be reduced to a Laplace method end point calculation.

(a). Application of Eq.(84) and exploitation of the periodicity of the trigonometric functions,

$$\tan(t+2\pi)=\tan(t)\qquad\text{and}\qquad\sec(t+2\pi)=\sec(t)\ , \tag{140}$$

reduce the exterior end point contributions from $t=0$ and 2π in Eqs.(129) and (130) to a single end point contribution from $t=0$ (of the semi-infinite integral representation, employing Eq.(81)),

$$\Omega_{\boldsymbol{B}}^{\mathrm{alg}}(p,q)\sim-\exp\left(\tfrac{3}{4}\pi\mathrm{i}\right)\ \left(\frac{\varepsilon}{\pi}\right)^{1/2}\ \int_0\mathrm{d}t\,t^{-1/2}\exp\left[\mathrm{i}\,(Yt-\chi\tan(t))\right]\sec(t)$$

$$\times \left[Y - \chi \left(\sec(t) \right)^2 - \mathrm{i} \tan(t) \right] \tag{141}$$

(compare Eq.(79)). The standard evaluation of the end point contribution in Erdélyi (38, pp.52-56) [‖] applied to Eq.(141) then yields the algebraic branch of the asymptotic operator symbol expansion,

$$\Omega_{\boldsymbol{B}}^{\mathrm{alg}}(p,q) \overset{\varepsilon \to 0}{\sim} \left[\varepsilon \left(Y - \chi \right) \right]^{1/2} + \tfrac{1}{8} \varepsilon^2 \left(\varepsilon Y \right) \left[\varepsilon \left(Y - \chi \right) \right]^{-5/2} + \mathrm{l.o.t.} \quad . \tag{142}$$

The first two (non-vanishing) terms in the algebraic branch of the asymptotic operator symbol expansion are $\mathcal{O}(1)$ and $\mathcal{O}(\varepsilon^2)$, respectively, in contrast to the standard operator symbol expansion which contains an $\mathcal{O}(\varepsilon)$ term (20). This difference is a reflection of the symmetry inherent in the Weyl construction (16, 17).

Equation (142) can also directly be derived from the analytic continuation of the corresponding asymptotic result for the defocusing quadratic profile presented in Fishman (23, (27)) through the relationship given in Eq.(113). The algebraic branch coincides with the outcome of the *polyhomogeneous* calculus of operator symbols (1, 15, 16).

(b). The stationary phase evaluation of the contributions from the four interior critical points, accounting for Eq.(131), is accomplished in the standard manner as in Erdélyi (38, pp.52-56) [‖] . The contributions from t_0 and $\pi + t_0$ are combined as well as the ones from $\pi - t_0$ and $2\pi - t_0$. While carrying out these combinations, the following identity,

$$-2^{3/2} \zeta(3/2, 2\Delta, -\xi) = \xi \, \zeta(3/2, \Delta + 1/2, \xi^2) - \zeta(3/2, \Delta, \xi^2) \, , \tag{143}$$

is invoked; it follows readily from Eq.(82) or Eq.(83). The result yields the oscillatory branch of the asymptotic operator symbol expansion,

$$\begin{aligned} \Omega_{\boldsymbol{B}}^{\mathrm{osc}}(p,q) &\overset{\varepsilon \to 0}{\sim} \tfrac{1}{2} \varepsilon \, \pi^{-3/2} (\varepsilon \chi)^{-1/2} [(Y/\chi) - 1]^{-1/4} \\ &\times \Big\{ \mathrm{i} \, \exp(\pi \mathrm{i} Y) \zeta(3/2, 1 - (t_0/\pi), -\exp(\pi \mathrm{i} Y)) \, \exp[-\mathrm{i} \left(Y t_0 - \chi \left[(Y/\chi) - 1 \right]^{1/2} \right)] \\ &\quad - \zeta(3/2, (t_0/\pi), -\exp(\pi \mathrm{i} Y)) \exp[\mathrm{i} \left(Y t_0 - \chi \left[(Y/\chi) - 1 \right]^{1/2} \right)] \Big\} + \mathrm{l.o.t.} \quad . \end{aligned} \tag{144}$$

The leading term in the oscillatory branch of the asymptotic operator symbol expansion is $\mathcal{O}(\varepsilon)$, with the contributions of $\mathcal{O}(\varepsilon^{1/2})$, which are proportional to the singular amplitudes $\zeta(1/2, (t_0/2\pi), \exp(2\pi \mathrm{i} Y))$, $\zeta(1/2, 1 - (t_0/2\pi), \exp(2\pi \mathrm{i} Y))$, and $\zeta(1/2, (1/2) \pm (t_0/2\pi), \exp(2\pi \mathrm{i} Y))$, having vanished.

(c). The interior end point contributions are calculated in the standard manner as in Erdélyi (38, pp.52-56) as before. The specific choice of δ in Eq.(139) reduces the ϑ-integral contributions to a standard Laplace method end point calculation as in Erdélyi (38, pp.36-39); as expected, these contributions exactly cancel the corresponding interior end point contributions. The result is a total group **(c)** contribution of 0 to within exponentially small terms. Thus,

$$\Omega_{\boldsymbol{B}}^{\mathrm{sng}}(p,q) \overset{\varepsilon \to 0}{\sim} \mathcal{O}(\text{exponentially small terms}) \, . \tag{145}$$

(a) + (b) + (c). The asymptotic contributions from groups **(a)–(c)** represented in Eqs.(142), (144), and (145) can be added together to produce the desired final result,

$$\begin{aligned} \Omega_{\boldsymbol{B}}(p,q) &\overset{\varepsilon \to 0}{\sim} \left[\varepsilon \left(Y - \chi \right) \right]^{1/2} + \tfrac{1}{8} \varepsilon^2 \left(\varepsilon Y \right) \left[\varepsilon \left(Y - \chi \right) \right]^{-5/2} \\ &\quad + \tfrac{1}{2} \varepsilon \, \pi^{-3/2} (\varepsilon \chi)^{-1/2} [(Y/\chi) - 1]^{-1/4} \\ &\quad \times \Big\{ \mathrm{i} \, \exp(\pi \mathrm{i} Y) \zeta(3/2, 1 - (t_0/\pi), -\exp(\pi \mathrm{i} Y)) \, \exp[-\mathrm{i} \left(Y t_0 - \chi \left[(Y/\chi) - 1 \right]^{1/2} \right)] \end{aligned}$$

[‖] For an oscillatory integral, $I = \int_\alpha^\beta \mathrm{d}t \, \exp[\mathrm{i} \varepsilon^{-1} h(t)] \, g(t)$, where $h'(t) = (t - \alpha)^{\rho - 1} (\beta - t)^{\sigma - 1} h_1(t)$ with $h(t)$ monotonically increasing on $t \in [\alpha, \beta]$, and $g(t) = (t - \alpha)^{\lambda - 1} (\beta - t)^{\mu - 1} g_1(t)$, with special points located at $t = \alpha$ and β, the desired expansion is $I_K \sim B_K(\varepsilon^{-1}) - A_K(\varepsilon^{-1})$. Here, $A_K(\varepsilon^{-1}) = -\sum_{k=0}^{K-1} (\rho \, k!)^{-1} \Gamma((k + \lambda)/\rho) \, \exp\left[\frac{1}{2} \pi \mathrm{i} (k + \lambda)/\rho \right] \varepsilon^{(k+\lambda)/\rho} \exp[\mathrm{i} \varepsilon^{-1} h(\alpha)] \, \lim_{u \downarrow 0} \mathcal{F}_A^{(k)}(u)$, while $B_K(\varepsilon^{-1}) = -\sum_{k=0}^{K-1} (\sigma \, k!)^{-1} \Gamma((k + \mu)/\sigma) \, \exp\left[-\frac{1}{2} \pi \mathrm{i} (k + \mu)/\sigma \right] \varepsilon^{(k+\mu)/\sigma} \exp[\mathrm{i} \varepsilon^{-1} h(\beta)] \, \lim_{v \downarrow 0} \mathcal{F}_B^{(k)}(v)$, where $[u(t)]^\rho = h(t) - h(\alpha)$, $\mathcal{F}_A(u) = [u(t)]^{1-\lambda} g(t) \, [u'(t)]^{-1}$, while $[v(t)]^\sigma = h(\beta) - h(t)$, $\mathcal{F}_B(v) = [v(t)]^{1-\mu} g(t) \, [v'(t)]^{-1}$. For the specific calculations, $h(t) = \varepsilon \left(Y t - \chi \tan(t) \right)$, while $g(t)$ is divided into two terms, one proportional to $\sec(t) \left[Y - \chi \left(\sec(t) \right)^2 \right]$ and one proportional to $-\mathrm{i} \sec(t) \tan(t)$, to account for the different values of λ and μ in each case.

$$-\zeta(3/2,(t_0/\pi),-\exp(\pi\mathrm{i}\,Y))\exp[\mathrm{i}\,(Y t_0-\chi\,[(Y/\chi)-1]^{1/2})]\Big\}+\text{l.o.t.}\quad . \tag{146}$$

The convergence of the Lerch transcendental functions in Eq.(146), following from Eq.(82), removes the restrictions on Y, originating from the contour-integral representation in Eq.(102). Most importantly, while the asymptotic expression in Eq.(146) was ultimately derived for a particularly convenient choice of δ, it follows from the Cauchy integral theorem (35), that this expression holds for all, fixed, $\delta\in(0,\pi/2)$, providing the desired *non*uniform asymptotic expansion.

$\chi=0$ (**normal propagation at** $q=0$). While the limit $Y/\chi\to\infty$ (implying, in the construction, the limit $\delta\to 0$) cannot be taken in Eq.(146) due to the coalescing pairs of interior critical points (t_0 and $\pi-t_0$ at $\pi/2$ and $\pi+t_0$ and $2\pi-t_0$ at $3\pi/2$), necessitating a uniform asymptotic expansion analysis (39), the high-frequency asymptotic expansion of $\Omega_{\boldsymbol{B}}(0,0)$ can be determined in the following fashion. Choosing $\mathcal{L}=\mathcal{I}'_\tau$, as illustrated in Fig. 5, in Eq.(102) yields the operator symbol representation

$$\Omega_{\boldsymbol{B}}(p,q)=\int_{\mathcal{I}'_\tau}\mathrm{d}\tau\,\mathcal{R}(-\mathrm{i}\tau)+2\pi\mathrm{i}\,\left[\mathrm{Res}_{\tau=\mathrm{i}\,\pi/2}\mathcal{R}(-\mathrm{i}\,\cdot)+\mathrm{Res}_{\tau=\mathrm{i}\,3\pi/2}\mathcal{R}(-\mathrm{i}\,\cdot)\right]\ ,\qquad Y\neq 0,1,2,\cdots\ , \tag{147}$$

following from the Cauchy integral theorem (35). In this case, for fixed εY and $\varepsilon\chi$, a sufficiently small $\delta>0$ can be chosen such that

$$(\mathrm{csch}(\delta))^2(2\delta\coth(\delta)-1)<\delta^{-1}\coth(\delta)<(\csc(\delta))^2<Y/\chi\ . \tag{148}$$

With δ satisfying this inequality, it follows that (i) the interior critical points now reside on the intervals $(\pi/2-\delta,\pi/2+\delta)$ and $(3\pi/2-\delta,3\pi/2+\delta)$ and (ii) the corresponding ϑ-integral integrands following from Eqs.(147) and (130) are exponentially small on $\vartheta\in(0,\pi)$, with the dominant contributions resulting from the neighborhoods of the maxima at the end points $\vartheta=0$ and π. The first point establishes the absence of any contributions from group **(b)**, while the second point, in conjunction with the interior end point contribution calculation, again establish that the group **(c)** contribution is exponentially small. Thus, in this case,

$$\Omega_{\boldsymbol{B}}(p,q)\overset{\varepsilon\to 0}{\sim}\Omega^{\mathrm{alg}}_{\boldsymbol{B}}(p,q)+\lim_{\varepsilon\to 0}2\pi\mathrm{i}\,\left[\mathrm{Res}_{\tau=\mathrm{i}\,\pi/2}\mathcal{R}(-\mathrm{i}\,\cdot)+\mathrm{Res}_{\tau=\mathrm{i}\,3\pi/2}\mathcal{R}(-\mathrm{i}\,\cdot)\right]\ ,\qquad Y\neq 0,1,2,\cdots\ . \tag{149}$$

For the case $p=q=0$ ($\chi=0$), the residues in Eq.(149) can be evaluated in a straightforward fashion (35). Both, poles of first order, associated with the factor $Y\sec(t)$, and poles of second order, associated with the factor $-\mathrm{i}\sec(t)\tan(t)$, occur. Adding the contributions yields,

$$\begin{aligned}\Omega_{\boldsymbol{B}}(0,0)\overset{\varepsilon\to 0}{\sim}&\,(\varepsilon Y)^{1/2}+\exp\left(\tfrac{3}{4}\pi\mathrm{i}\right)\,\frac{\varepsilon^{1/2}}{\pi}\,\zeta(3/2,1/2,-\exp(\pi\mathrm{i}\,Y))\exp(\pi\mathrm{i}\,Y/2)\\&+\tfrac{1}{8}\varepsilon^2\,(\varepsilon\,Y)^{-3/2}+\text{l.o.t.}\ ,\end{aligned} \tag{150}$$

using, again, Eq.(143); here, the residues of the poles of first order have cancelled. Again, the restrictions on Y are removed by the convergence of the Lerch transcendental function in Eq.(150).

The connection between the contour-integral representation in Eq.(102) and the subsequent asymptotic expansions, and the spectral (modal) summation becomes more apparent upon expressing the operator symbol asymptotic expansions in Eqs.(146) and (150) in alternative forms, viz., through the application of the Lerch functional equation as given in Magnus *et al.* (29, p.34),

$$\begin{aligned}\zeta(\sigma,\Delta,\xi)=&\,\mathrm{i}\,\xi^{-\Delta}(2\pi)^{\sigma-1}\Gamma(1-\sigma)\\&\times\Big\{\exp[-\pi\mathrm{i}\,(\sigma/2)]\,\zeta(1-\sigma,(2\pi\mathrm{i})^{-1}\log(\xi),\exp(-2\pi\mathrm{i}\,\Delta))\\&-\exp[\pi\mathrm{i}\,((\sigma/2)+2\Delta)]\,\zeta(1-\sigma,1-(2\pi\mathrm{i})^{-1}\log(\xi),\exp(2\pi\mathrm{i}\,\Delta))\Big\}\ ,\end{aligned} \tag{151}$$

where the principal branch of the $\log(\cdot)$ function is understood. Introducing η according to $Y=2L-1+\eta$, $\eta\in[0,2]$ (cf. the estimate below Eq.(19)), and applying Eq.(151) to Eq.(150) yield

$$\begin{aligned}\Omega_{\boldsymbol{B}}(0,0)\overset{\varepsilon\to 0}{\sim}&\,(\varepsilon Y)^{1/2}-2^{3/2}\varepsilon^{1/2}(-)^L\mu\,[\zeta^*(-1/2,\mathtt{d}/2)-\mathrm{i}\,\zeta^*(-1/2,1-(\mathtt{d}/2))]\\&+\tfrac{1}{8}\varepsilon^2\,(\varepsilon\,Y)^{-3/2}+\text{l.o.t.}\ ,\end{aligned} \tag{152}$$

where the generalized zeta function is defined by the appropriate analytic continuations of Eq.(126) (29, 37), with

$$\mathsf{d} = \mathsf{d}(\eta) \quad = \quad \begin{cases} \eta & \text{if } \eta \in [0,1] \,, \\ \eta - 2 & \text{if } \eta \in (1,2] \,, \end{cases} \tag{153}$$

$$\mu = \mu(\eta) \quad = \quad \begin{cases} 1 & \text{if } \eta \in [0,1] \,, \\ -1 & \text{if } \eta \in (1,2] \,. \end{cases} \tag{154}$$

Rather than being asymptotic, both of the expressions for $\mathrm{Im}\{\Omega_{\boldsymbol{B}}(0,0)\}$ in Eqs.(150) and (152), resulting from the evaluation of the residues in Eq.(149), are exact. This follows on starting with $\mathrm{Im}\{\Omega_{\boldsymbol{B}}(0,0)\}$ in Eq.(152) and using Eq.(84) with $m = 1$ to show that

$$\begin{aligned} &- [\zeta^*(-1/2, (\eta/2) - 1) - \mathrm{i}\,\zeta^*(-1/2, 2 - (\eta/2))] \\ &\qquad = \zeta^*(-1/2, \eta/2) - \mathrm{i}\,\zeta^*(-1/2, 1 - (\eta/2)) \,, \quad \text{for } \eta \in (1,2], \end{aligned} \tag{155}$$

establishing that Eq.(152) is valid for $\eta \in [0,2]$ with $\mathsf{d} = \eta$ and $\mu = 1$. Then, use of the identity

$$(\xi\,\partial_\xi + \Delta)\,\zeta(\sigma, \Delta, \xi) = \zeta(\sigma - 1, \Delta, \xi) \,, \tag{156}$$

which follows directly from Eq.(82), application of Eq.(83), and comparison with
$\mathrm{Im}\{\Omega^{\mathrm{foc}}_{\boldsymbol{B}}(0,0)\}$ in Eq.(61) for $N = L$ complete the proof. The Lerch functional equation (151) makes explicit the number of propagating modes L in the operator symbol, contour-integral representation in Eq.(102).

Case 2: $\chi > Y > 0$. For the high-frequency asymptotic evaluation of the operator symbol integral representation in Eqs.(129) and (130) in this case, there are (i) exterior end point contributions from $t = 0$ and 2π, (ii) no interior critical points on the imaginary τ-axis, following from Eq.(132), and (iii) contributions of exponentially small order from group **(c)**, following from Eq.(139) and the discussion preceding Eq.(145). Returning to Eq.(102) and the original contour $\mathcal{L}$, a critical point is encountered on the real τ-axis: it follows from the equality $Y - \chi\,(\mathrm{sech}(\tau))^2 = 0$, and is given by

$$\tau_0 \quad = \quad \mathrm{arctanh}\left([1 - (Y/\chi)]^{1/2}\right) \tag{157}$$

$$\quad = \quad \tfrac{1}{2}\log\left(\frac{1 + [1 - (Y/\chi)]^{1/2}}{1 - [1 - (Y/\chi)]^{1/2}}\right) \,, \tag{158}$$

with the principal branches taken. The contribution from this critical point is a term of exponentially small order, supplementing the algebraic branch deriving from group **(a)**. The most direct way to derive the resulting expansion is to exploit the analytic continuation result in Eq.(113) in conjunction with the corresponding asymptotic result for the defocusing quadratic profile, derived by a stationary phase evaluation, in Fishman (23, (27),(28)). The final expression is

$$\begin{aligned} \Omega_{\boldsymbol{B}}(p,q) &\overset{\varepsilon \to 0}{\sim} [\varepsilon\,(Y - \chi)]^{1/2} + \tfrac{1}{8}\varepsilon^2\,(\varepsilon Y)\,[\varepsilon\,(Y - \chi)]^{-5/2} \\ &\quad + \tfrac{1}{2}\varepsilon\,\tau_0^{-3/2}(\varepsilon\chi)^{-1/2}[1 - (Y/\chi)]^{-1/4}\exp[Y\tau_0 - \chi\,[1 - (Y/\chi)]^{1/2}] + \text{l.o.t.} \quad . \end{aligned} \tag{159}$$

The principal results of Section 5 are the low-frequency asymptotic expansion in Eq.(128) and the high-frequency asymptotic expansions in Eqs.(146), (150), (152), and (159). Taken together, Eqs.(146) and (159) provide the nonuniform, high-frequency asymptotic, operator symbol expansion for the full range of the phase space variables p and q. As previously discussed, the high-frequency results are not valid in the $Y/\chi \to \infty$ limit due to the coalescing pairs of interior critical points. The high-frequency results will also fail in the limit of $Y/\chi \to 1$ due to the coalescing of (i) the interior critical point at t_0 and the exterior end point at $t = 0$, (ii) the interior critical point at $2\pi - t_0$ and the exterior end point at $t = 2\pi$, and (iii) the two interior critical points at $\pi - t_0$ and $\pi + t_0$ at $t = \pi$. To address these two limiting cases, uniform methods must be applied (39). The nonuniform expansions, however, do establish and illustrate the fundamental oscillatory character of the square-root Helmholtz operator symbol in the high-frequency limit (1, 23). In the elliptic pseudodifferential operator calculus, only the nonuniform algebraic branch given in Eq.(142) is obtained in the asymptotic analysis (1, 14, 15, 16, 17).

6. One-way propagation

A. Propagating and nonpropagating operator symbol constituents

It is clear from the derivation of the spectral (modal) summation representations presented in Section 2 that the Helmholtz operator symbols naturally divide into their propagating and nonpropagating modal contributions. In the Weyl calculus, in both Eq.(61) with $N = L$ and Eq.(64), the first, finite sum of L terms represents the propagating modal contribution to the square-root Helmholtz operator symbol, while the remaining terms comprise the nonpropagating modal contribution, with a corresponding decomposition in both Eq.(33) with $N = L$ and Eq.(48) in the standard calculus. From the propagating and nonpropagating modal decomposition, adopting an obvious superscript notation, it then follows that $\Omega_{\boldsymbol{B}} = \Omega_{\boldsymbol{B}}{}^{\mathrm{P}} + \Omega_{\boldsymbol{B}}^{\mathrm{NP}}$ with

$$\Omega_{\boldsymbol{B}}{}^{\mathrm{P}}(p,q) = \mathrm{Re}\{\Omega_{\boldsymbol{B}}(p,q)\}\,, \tag{160}$$

$$\Omega_{\boldsymbol{B}}^{\mathrm{NP}}(p,q) = \mathrm{i}\,\mathrm{Im}\{\Omega_{\boldsymbol{B}}(p,q)\}\,. \tag{161}$$

Correspondingly, decomposing the previously mentioned propagating and nonpropagating modal contributions into their real and imaginary parts, and further noting the even/odd symmetry with respect to p (or q) establish that $h_{\boldsymbol{B}}^{s} = h_{\boldsymbol{B}}^{s;\ \mathrm{P}} + h_{\boldsymbol{B}}^{s;\mathrm{NP}}$ for the standard symbol, with

$$h_{\boldsymbol{B}}^{s;\ \mathrm{P}} = \exp(-\mathrm{i}\bar{k}\,pq)\ \left\{\mathrm{EP}\left[\mathrm{Re}\{\exp(\mathrm{i}\bar{k}\,pq)\,h_{\boldsymbol{B}}^{s}(p,q)\}\right] + \mathrm{i}\,\mathrm{OP}\left[\mathrm{Im}\{\exp(\mathrm{i}\bar{k}\,pq)\,h_{\boldsymbol{B}}^{s}(p,q)\}\right]\right\}, \tag{162}$$

and

$$h_{\boldsymbol{B}}^{s;\mathrm{NP}} = \exp(-\mathrm{i}\bar{k}\,pq)\ \left\{\mathrm{OP}\left[\mathrm{Re}\{\exp(\mathrm{i}\bar{k}\,pq)\,h_{\boldsymbol{B}}^{s}(p,q)\}\right] + \mathrm{i}\,\mathrm{EP}\left[\mathrm{Im}\{\exp(\mathrm{i}\bar{k}\,pq)\,h_{\boldsymbol{B}}^{s}(p,q)\}\right]\right\}, \tag{163}$$

where the even and odd parts of a function $f(x)$ are defined by

$$\mathrm{EP}[f(x)] = \tfrac{1}{2}\,[f(x) + f(-x)]\ , \tag{164}$$

and

$$\mathrm{OP}[f(x)] = \tfrac{1}{2}\,[f(x) - f(-x)]\ , \tag{165}$$

respectively, and are taken with respect to either p or q in Eqs.(162) and (163).

Equations (160)-(163) can be applied to any exact representation of the square-root Helmholtz operator symbol. In particular, equating the Weyl operator symbol constructions (61) and (102) in Sections 2 and 3, respectively, yields

$$\Omega_{\boldsymbol{B}}{}^{\mathrm{P}}(p,q) = 2\varepsilon^{1/2}\ \sum_{n=0}^{L-1}[-(2n+1-Y)]^{1/2}\ \Phi_n(\chi) \tag{166}$$

or

$$\Omega_{\boldsymbol{B}}{}^{\mathrm{P}}(p,q) = \mathrm{Re}\Bigg\{-\exp\left(\tfrac{1}{4}\pi\mathrm{i}\right)\ \left(\frac{\varepsilon}{2}\right)^{1/2}\frac{1}{\pi}\int_{\mathcal{L}}\mathrm{d}\tau\,\zeta(1/2,(-\mathrm{i}/2\pi)\tau,\exp(2\pi\mathrm{i}\,Y))$$
$$\times\exp\left[Y\tau-\chi\tanh(\tau)\right]\mathrm{sech}(\tau)\left[Y-\chi\left(\mathrm{sech}(\tau)\right)^2-\tanh(\tau)\right]\Bigg\},\ Y\neq 0,1,2,\cdots\ , \tag{167}$$

and

$$\Omega_{\boldsymbol{B}}^{\mathrm{NP}}(p,q) = -\mathrm{i}\left(\frac{\varepsilon}{\pi}\right)^{1/2}\ \int_0^{\infty}\mathrm{d}t\,t^{-1/2}\exp(Yt)\ \left[\widetilde{\mathsf{F}}(t)-\widetilde{\mathsf{G}}(t|L)\right] \tag{168}$$

or

$$\Omega_{\boldsymbol{B}}^{\mathrm{NP}}(p,q) = \mathrm{i}\,\mathrm{Im}\Bigg\{-\exp\left(\tfrac{1}{4}\pi\mathrm{i}\right)\ \left(\frac{\varepsilon}{2}\right)^{1/2}\frac{1}{\pi}\int_{\mathcal{L}}\mathrm{d}\tau\,\zeta(1/2,(-\mathrm{i}/2\pi)\tau,\exp(2\pi\mathrm{i}\,Y))$$
$$\times\exp\left[Y\tau-\chi\tanh(\tau)\right]\mathrm{sech}(\tau)\left[Y-\chi\left(\mathrm{sech}(\tau)\right)^2-\tanh(\tau)\right]\Bigg\},\ Y\neq 0,1,2,\cdots\ , \tag{169}$$

with analogous results following from the application of Eq.(64).

Following from Eqs.(166)-(169) and the constructions presented in Section 5, the high- and low-frequency, asymptotic expansions for the propagating and nonpropagating constituents of the square-root Helmholtz operator symbol can be obtained. In the

high-frequency, $\varepsilon \to 0$, limit, for example, utilizing Eqs.(146) and (159) result in

$$\Omega_{\boldsymbol{B}}{}^{\mathrm{P}}(p,q) \overset{\varepsilon\to 0}{\sim} \begin{cases} \mathrm{Re}\{\text{rhs of Eq.(146)}\} \quad , \quad Y > \chi > 0 \, , \\ \\ \mathrm{Re}\{\text{rhs of Eq.(159)}\} \quad , \quad \chi > Y > 0 \, , \end{cases} \tag{170}$$

with a corresponding set of expressions for the nonpropagating operator symbol constituent. The decomposition into the propagating and nonpropagating constituents in conjunction with the high-frequency asymptotic expansions relate the number of propagating modes L to specific structural features of the square-root Helmholtz operator symbol. The oscillatory asymptotic branch in Eqs.(144) and (146) is governed by the exponential phase functions,
$\pm\left(Y t_0 - \chi\,[(Y/\chi)-1]^{1/2}\right)$. Taking $Y/\chi \gg 1$ and $p^2 \gg \omega^2 q^2$ in Eqs.(132) and (144) then yield the dominant exponential phase function (to within a sign),

$$\left(Y t_0 - \chi\,[(Y/\chi)-1]^{1/2}\right) \overset{Y/\chi\gg 1}{\sim} \left(Y\,(\pi/2) - 2\,Y^{1/2}\chi^{1/2}\right) \overset{p^2\gg\omega^2 q^2}{\sim} \left(Y\,(\pi/2) - 2\,Y^{1/2}\varepsilon^{-1/2}p\right) .$$

Thus, in the lowest order,

$$Y \simeq \varepsilon\,(\pi/T_p)^2 \, , \tag{171}$$

where T_p is the period of oscillation of $\Omega_{\boldsymbol{B}}{}^{\mathrm{P}}$ as a function of p. An estimate of the number of propagating modes L follows immediately from the estimate following Eq.(19), with more sophisticated expressions following in a natural manner.

Moreover, the addition of one propagating mode through the increase in K_0^2 and/or decrease in ε, mathematically represented by taking $L \to L+1$ ($Y \to Y+2$), corresponds to a change in the sign of the scaled, nonpropagating, square-root Helmholtz operator symbol constituent ($\mathrm{i}\,\mathrm{Im}\{\Omega_{\boldsymbol{B}}(0,0)\}\,\varepsilon^{-1/2}$) in Eq.(152) in the high-frequency limit.

B. The one-way propagator

The infinitesimal, one-way propagator, in conjunction with the special structure of the Weyl and standard symbols for the square-root Helmholtz operator, reveal both the multiresolution and generalized screen nature of the propagation process. The fundamental solution of the one-way wave equation can be written in the form $\mathcal{G}^+(x,z;x',z') = H(x-x')\,g^+(x,z;x',z')$ with $g^+(x,z;x',z')$ denoting the *one-way propagator*. Following from Eq.(10) with $M=1$, the infinitesimal, one-way propagator follows as

$$g^+(x,z;x',z') = \int_{\mathbb{R}} (\bar{k}/2\pi)\mathrm{d}p\, \exp\left[\mathrm{i}\bar{k}\,\left\{p(z-z') + \Omega_{\boldsymbol{B}}\left(p,\tfrac{1}{2}(z+z')\right)(x-x')\right\}\right] \, . \tag{172}$$

In the limit $x \downarrow x'$, the propagator can be asymptotically expanded to the lowest order in the form

$$\begin{aligned} g^+(x,z;x',z') &\sim \delta(z-z') \\ &\quad + \mathrm{i}\bar{k}\,(x-x') \int_{\mathbb{R}} (\bar{k}/2\pi)\mathrm{d}p\, \exp\left[\mathrm{i}\bar{k}\,p(z-z')\right] \Omega_{\boldsymbol{B}}\left(p,\tfrac{1}{2}(z+z')\right) \, , \end{aligned} \tag{173}$$

where the integral term is recognized as the Schwartz kernel $\mathcal{B}(z,z')$ (cf. Eqs.(6) and (8)) and is understood in the distributional sense (4, 30).

Recognizing from Eq.(63) that the Weyl operator symbol $\Omega_{\boldsymbol{B}}(p,q)$ can be written as the sum of an absolutely and uniformly convergent infinite series and a well-defined integral, it follows that in the limit $|p| \to \infty$, the series contribution tends to 0 while the integral contribution reproduces the pseudodifferential operator limit $\Omega_{\boldsymbol{B}}(p,q) \sim \mathrm{i}\,|p|$. In the limit $\alpha \downarrow 0$, but $\alpha \neq 0$, discarding the integral contribution and approximating $\Omega_{\boldsymbol{B}}(p,q)$ by the infinite series alone result in a convergent integral in Eq.(173), corresponding to an essentially correct treatment of all of the modal contributions except the 'large n' values in the (generally) deep evanescent regime. Denoting this approximation by $g^+(x,z;x',z') \sim g_\alpha^+(x,z;x',z')$, the expansion in Eq.(173) takes the form

$$\begin{aligned} g_\alpha^+(x,z;x',z') &\sim \delta(z-z') + \mathrm{i}\bar{k}\,(x-x')\,2\sum_{n=0}^{\infty} \\ &\left\{[-\varepsilon\,(2n+1-Y)]^{1/2} + 2\mathrm{i}\left(\frac{\alpha}{\pi}\right)^{1/2}\varepsilon^{1/2}[-(2n+1-Y)]\,{}_1F_1(1/2;3/2;-\alpha\,(2n+1-Y))\right\} \\ &\qquad \times \int_{\mathbb{R}} (\bar{k}/2\pi)\mathrm{d}p\,(-)^n L_n^{(0)}(2\chi)\,\exp(-\chi)\exp[\mathrm{i}\bar{k}\,p(z-z')] \, , \end{aligned} \tag{174}$$

where $\chi := \varepsilon^{-1}\left(\frac{1}{4}\omega^2(z+z')^2 + p^2\right)$. The last line of this equation can be written in the form

$$\int_{\mathbb{R}} (\bar{k}/2\pi)\mathrm{d}p\,(-)^n L_n^{(0)}(2\chi)\,\exp(-\chi)\exp[\mathrm{i}\bar{k}\,p(z-z')]$$
$$= \int_{\mathbb{R}} (\bar{k}/2\pi)\mathrm{d}p\,\exp(-\varepsilon^{-1}p^2)\exp(2\mathrm{i}\bar{k}\,pz)$$
$$\times(-)^n L_n^{(0)}(2\chi)\,\exp\left[-\tfrac{1}{4}\varepsilon^{-1}\omega^2(z+z')^2\right]\exp[\mathrm{i}\bar{k}\,p(z+z')]\,. \tag{175}$$

In Eqs.(173)-(175), a forward constituent transform is identified as the windowed Fourier transform

$$\frac{1}{\sqrt{2}}\int_{\mathbb{R}} \mathrm{d}z'\,\exp\left[-\frac{\Omega}{2}\frac{(z+z')^2}{2}\right]\exp\left[-\mathrm{i}\bar{k}\,p\sqrt{2}\,\frac{(z+z')}{\sqrt{2}}\right] \quad ,$$

where $\Omega = \omega\bar{k}$ is a dilation parameter, with a corresponding constituent 'inverse' transform, $\sqrt{2}\int_{\mathbb{R}}(\bar{k}/2\pi)\mathrm{d}p$, revealing the multiresolution (40) nature of the propagation process.

The standard calculus analogue of the (modal) expansion in Eq.(174) is given by

$$g_\alpha^+(x,z;x',z') \sim \delta(z-z') + \mathrm{i}\bar{k}\,(x-x')\,2^{1/2}\sum_{n=0}^{\infty}\frac{1}{n!}\left(\frac{\mathrm{i}}{2}\right)^n \phi_n\left((\omega\bar{k})^{1/2}z\right)$$
$$\times\left\{[-\varepsilon\,(2n+1-Y)]^{1/2} + 2\mathrm{i}\left(\frac{\alpha}{\pi}\right)^{1/2}\varepsilon^{1/2}[-(2n+1-Y)]\,{}_1F_1(1/2;3/2;-\alpha\,(2n+1-Y))\right\}$$
$$\times\int_{\mathbb{R}}(\bar{k}/2\pi)\mathrm{d}p\,\phi_n\left((\bar{k}/\omega)^{1/2}p\right)\exp(-\mathrm{i}\bar{k}\,pz')\,. \tag{176}$$

Equation (176) reveals the structure of a 'generalized screen' expansion representation (41): a Fourier transform ($z' \to p$), followed by a multiplication (Hermite polynomials) in the p-domain, followed by a (Gaussian weighted) inverse transform ($p \to z$), followed by a multiplication in the z-domain.

The sequence of operations in the infinitesimal propagation process, outlined in the multiresolution and generalized screen analyses above, is inherent in the path-integral structure of the fundamental solution (1, 2, 11, 18, 19, 20, 21, 36) in Eq.(10). Moreover, the path-integral representation reduces to the spectral (modal) representation for the fundamental solution, which, for the (range-independent) focusing quadratic profile, takes the form

$$\mathcal{G}^+(x,z;x',z') = H(x-x')\sum_{n=0}^{\infty}\exp\left\{\mathrm{i}\bar{k}\,[-\varepsilon\,(2n+1-Y)]^{1/2}\,(x-x')\right\}$$
$$\times\exp\left\{-2\bar{k}\,\left(\frac{\alpha}{\pi}\right)^{1/2}\varepsilon^{1/2}[-(2n+1-Y)]\,{}_1F_1(1/2;3/2;-\alpha\,(2n+1-Y))\,(x-x')\right\}$$
$$\times\frac{\varepsilon^{1/2}\bar{k}}{\pi^{1/2}}\,\frac{1}{n!\,2^n}\,\Theta_n(z,z')\,. \tag{177}$$

(For $\alpha \downarrow 0$, but $\alpha \neq 0$, Eq.(177) corresponds to the approximation associated with g_α^+ outlined above, while for $\alpha = 0$, it represents the exact fundamental solution.) In Eq.(177), a transform pair can be identified through the identity

$$\sum_{n=0}^{\infty}\frac{\varepsilon^{1/2}\bar{k}}{\pi^{1/2}}\,\frac{1}{n!\,2^n}\,\Theta_n(z,z') = \sum_{n=0}^{\infty}\frac{(\omega\bar{k})^{1/2}}{\pi^{1/2}}\,\frac{1}{n!\,2^n}\,\phi_n\left((\omega\bar{k})^{1/2}z\right)\phi_n\left((\omega\bar{k})^{1/2}z'\right) = \delta(z-z')\,.$$

Thus, the ϕ_n, subjected to the appropriate normalization, form an orthonormal basis. With Eq.(177), in the action of the propagator, the integration over z' constitutes a 'forward' transform, whereas the summation over n constitutes the associated 'inverse' transform; the propagator is 'diagonal' in the transform domain. Unlike the global operator diagonalization in the spectral (modal) propagator representation, the infinitesimal propagator representations can be viewed as a 'diagonalization' in the phase space strip about a localized coordinate point (24).

7. Exact symbols for operator rational approximations to B

The square-root Helmholtz operator can be approximated by operator rational approximations in general, and additive, operator rational approximations in particular (1, 3, 4, 5, 6, 10, 23). These operator approximations implicitly correspond to uniform operator

symbol constructions over appropriate regions of phase space, and immediately result in approximate, partial differential, one-way wave equations (1, 3, 4, 5, 6, 10, 23). With a continued-fraction approach, the square-root Helmholtz operator $\boldsymbol{B}$ is approximated to Nth-order by

$$\boldsymbol{B} = [\boldsymbol{I} + \boldsymbol{L}]^{1/2} \simeq \boldsymbol{I} + \sum_{j=1}^{N} [\boldsymbol{I} + \mathrm{b}_{j,N}\boldsymbol{L}]^{-1} \mathrm{a}_{j,N}\boldsymbol{L} \ , \tag{178}$$

where

$$\boldsymbol{L} = \boldsymbol{B}^2 - \boldsymbol{I} = [(K^2(z) - 1)\,\boldsymbol{I} + (1/\bar{k})^2 \partial_z^2] \ , \tag{179}$$

the operator sum in Eq.(178) is supplemented with a right-traveling- (outgoing-)wave radiation condition, and the approximation coefficients $\{\mathrm{a}_{j,N}, \mathrm{b}_{j,N}\}$ are determined in the homogeneous medium limit by a variety of approximation-theoretic criteria (1, 3, 4, 5, 6, 10, 23, 42). For every case where an exact square-root Helmholtz operator symbol can be constructed, the operator symbols corresponding exactly to the operator sum in Eq.(178) can be written in closed form (1, 23). Let the Weyl symbol $\Omega_{[\beta\boldsymbol{I}+\gamma\boldsymbol{L}]^{-1}}(p,q)$ correspond with the operator $[\beta\boldsymbol{I} + \gamma\boldsymbol{L}]^{-1}$, then Eq.(178) can be simplified as

$$\boldsymbol{B} \simeq \boldsymbol{B}^{\mathrm{ARA}} = \boldsymbol{I} + \sum_{j=1}^{N} c_{j,N}[\boldsymbol{I} - [\boldsymbol{I} + \mathrm{b}_{j,N}\boldsymbol{L}]^{-1}] \ ,$$

so that the exact, additive, rational approximation operator symbol in the Weyl calculus is given by (1, 23)

$$\Omega_{\boldsymbol{B}}^{\mathrm{ARA}}(p,q) = 1 + \sum_{j=1}^{N} c_{j,N}[1 - \Omega_{[\boldsymbol{I}+b_{j,N}\boldsymbol{L}]^{-1}}(p,q)] \ , \tag{180}$$

where

$$\mathrm{c}_{j,N} = \frac{\mathrm{a}_{j,N}}{\mathrm{b}_{j,N}} \ . \tag{181}$$

The operator symbol $\Omega_{[\beta\boldsymbol{I}+\gamma\boldsymbol{L}]^{-1}}(p,q)$ is the fundamental function in the construction. It follows from (i) the relevant results in Fishman (23) for the defocusing quadratic profile in conjunction with the analytic continuation result in Eq.(112) and (ii) the previous construction of $\Omega_{\boldsymbol{B}^{-1}}(p,q)$ for the focusing quadratic profile in Eq.(56) that

$$\Omega_{[\beta\boldsymbol{I}+\gamma\boldsymbol{L}]^{-1}}(p,q) = \frac{2}{\varepsilon\gamma} \sum_{n=0}^{\infty} [-(2n + 1 - \widehat{Y})]^{-1} \ \Phi_n(\chi) \tag{182}$$

for the spectral (modal) summation representation, and from (iii) the observation that the appropriate Lerch transcendental function $\zeta(\sigma, \Delta, \xi)$ involved in the construction of $\Omega_{[\beta\boldsymbol{I}+\gamma\boldsymbol{L}]^{-1}}(p,q)$ appears in the analogue of Eq.(92) with $\sigma = 0$, that

$$\begin{aligned} \Omega_{[\beta\boldsymbol{I}+\gamma\boldsymbol{L}]^{-1}}(p,q) &= -\frac{1}{\varepsilon\gamma} \ \frac{1}{1 - \exp(2\pi\mathrm{i}\,\widehat{Y})} \\ &\times \int_{\mathcal{L}} \mathrm{d}\tau \ \exp\left[\widehat{Y}\tau - \chi\tanh(\tau)\right] \mathrm{sech}(\tau) \ , \quad \widehat{Y} \neq 0, 1, 2, \cdots \ , \end{aligned} \tag{183}$$

for the contour-integral representation. In Eqs.(182) and (183),

$$\widehat{Y} = Y + \varepsilon^{-1}[(\beta/\gamma) - 1] \ . \tag{184}$$

Appendix B contains an additional representation for $\Omega_{[\beta\boldsymbol{I}+\gamma\boldsymbol{L}]^{-1}}(p,q)$. Combining Eqs.(182) and (183) with Eq.(180) results in the exact, closed-form representations of the Weyl symbol for the additive, rational operator approximations of the square-root Helmholtz operator.

Finally, expressions analogous to Eqs.(182), (183), and (B3), in conjunction with Eqs.(180)-(181), can be written for the operator symbols in the standard calculus in a straightforward manner.

8. Numerical results

The square-root Helmholtz operator symbol for the focusing quadratic profile can be numerically computed, in both the Weyl and standard calculi, from the spectral (modal) summation and contour-integral formulas. For the spectral (modal) summation

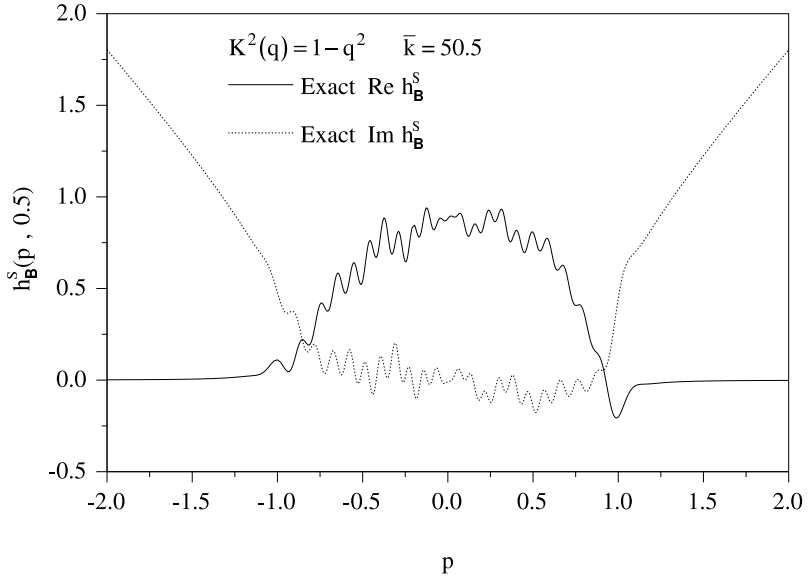

Figure 7. $h^s_{\boldsymbol{B}}(p, 0.5)$ vs. p for the focusing quadratic profile. The exact standard operator symbol is computed from Eq.(104).

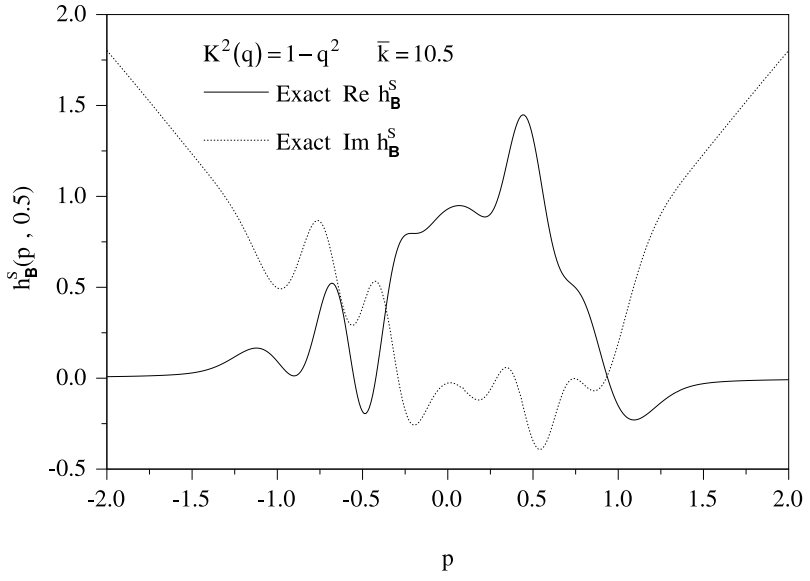

Figure 8. $h^s_{\boldsymbol{B}}(p, 0.5)$ vs. p for the focusing quadratic profile. The exact standard operator symbol is computed from Eq.(104).

representations, for the standard operator symbol, for example, Eq.(48) is computed. The finite and infinite sums are rewritten and evaluated in the manner outlined in detail by Van Stralen (4), while the remaining finite integral is computed by an adaptive recursive Newton-Cotes 8 panel rule (4, 43), with α chosen relative to the magnitude of the integrand in a manner which balances the location of the second, infinite series within its circle of convergence against the magnitude of the integrand and the range of integration in that final term. In this scheme, it immediately follows from the estimates in Eq.(42) and Eq.(44) that the limit $\alpha \to 0$ corresponds to the infinite sum approaching its radius of convergence, requiring an ever increasing number of terms for an accurate numerical computation, and a relatively simple numerical integration, while the limit $\alpha \to \infty$ corresponds to the sum approaching the center of its circle of convergence, requiring an ever decreasing number of terms for an accurate numerical computation, and a more involved numerical integration (44). The expression in Eq.(48) is independent of the particular choice of α, which was verified in the numerical computations. The corresponding computation in the Weyl calculus of Eq.(64) is treated in a similar fashion. For the

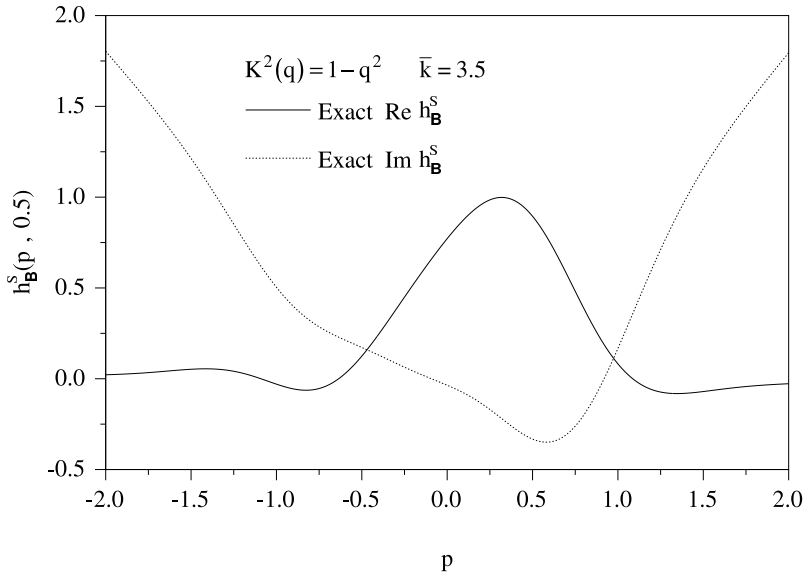

Figure 9. $h^s_{\boldsymbol{B}}(p, 0.5)$ vs. p for the focusing quadratic profile. The exact standard operator symbol is computed from Eq.(104).

contour-integral representations, the Weyl and standard operator symbols are computed from Eq.(102) and Eq.(104), respectively. In both cases, the contour $\mathcal{L}$ in the complex τ-plane is chosen as $\mathcal{C}''$ in Fig. 6 with R taken to be finite. Applying Eq.(84) and exploiting the periodicity of the hyperbolic functions in Eq.(107) in the same manner used in proceeding from Eq.(106) to Eq.(108) reduce the contour integral to a single integral along Γ_1'' and two integrals along Γ_2''. The Lerch transcendental function is computed from Eq.(83) by the Romberg numerical integration method (45) applied to the three resulting integrals. R is chosen to make $\mathrm{R}\,Y$ an $\mathcal{O}(1)$ quantity, thereby balancing the numerical effects of the singularities at $\tau = \mathrm{i}\,\pi/2$ and $\mathrm{i}\,3\pi/2$ for the limit $\mathrm{R} \to 0$ with the attempt to construct an $\mathcal{O}(1)$ quantity from the integration of extremely large magnitude integrands in the limit $\mathrm{R} \to \infty$. In both the Weyl and standard cases, the computations are, in principle, independent of the choice of R, which was verified numerically for a reasonable range of the parameter. In the subsequent numerical computations, the spectral (modal) summation and contour-integral methods resulted in identical curves. Further, for the case $Y < 1$, these two computational methods were found to be in complete agreement with the results obtained from numerically integrating Eq.(125) and its standard calculus analog, Eq.(33), with $N = 0$. The exact operator symbol curves presented in this section were computed from the contour-integral representations.

It follows from Eqs.(48) and (104) that the standard, square-root Helmholtz operator symbol $h^s_{\boldsymbol{B}}(p, q)$ is (i) invariant under the interchange $p \leftrightarrow \omega q$, (ii) a symmetric function of p (q) for q (p)$= 0$, (iii) an asymmetric function of p (q) for q (p)$\neq 0$, and (iv) a (an) symmetric (antisymmetric) function of p and q for the imaginary (real) part of the symbol for $Y < 1$ in the absence of propagating modes. The third and fourth points are illustrated in Figs. 7-10 by plotting $h^s_{\boldsymbol{B}}(p, 0.5)$ for the specific quadratic case $K^2(q) = 1 - q^2$ and $\bar{k} = 50.5$, 10.5, 3.5, and 0.5, respectively. Figure 10 for $\bar{k} = 0.5$ illustrates the fourth point. The sequence of figures also illustrates the transition from the high- to the low-frequency regime for a choice of q within the well, with the square-root function plus superimposed oscillatory behavior, characteristic of the locally-homogeneous, high-frequency limit (1, 4, 23), gradually transforming to the absorption-dominated curves, corresponding to the absence of propagating modes, in the low-frequency limit. Figure 11 displays $h^s_{\boldsymbol{B}}(p, 1.5)$ for the same profile and $\bar{k} = 10.5$, illustrating the dominant absorptive behavior for a choice of q outside the well. Figure 12 illustrates $h^s_{\boldsymbol{B}}(0, q)$ for the same profile and $\bar{k} = 10.5$, and will be applied in demonstrating the waveguiding properties of the focusing quadratic profile in the final Sec. **??**. All of the Figs. 7-12 are consistent with the appropriate analytic continuation of the corresponding results for the defocusing quadratic profile presented by Fishman (23).

It follows from Eqs.(64) and (102) that the Weyl, square-root Helmholtz operator symbol $\Omega_{\boldsymbol{B}}(p, q)$ is (i) solely a function of the variable χ, following from the symplectic structure in the Weyl composition equation (11) and the quadratic dependence of $K^2(q)$ (16, 23), (ii) invariant under the interchange $p \leftrightarrow \omega q$, (iii) a symmetric function of p and q, and (iv) purely imaginary for $Y < 1$ in the absence of propagating modes. Figures 13-17 illustrate $\Omega_{\boldsymbol{B}}(p, 0)$ for the specific quadratic case $K^2(q) = 1 - q^2$ and $\bar{k} = 50.5$, 10.5, 3.5, 0.95, and 0.1, respectively. As in the case for the standard operator symbol, the sequence of figures again illustrates the characteristic behavior and transition from the high- to the low-frequency regime for a choice of q within the

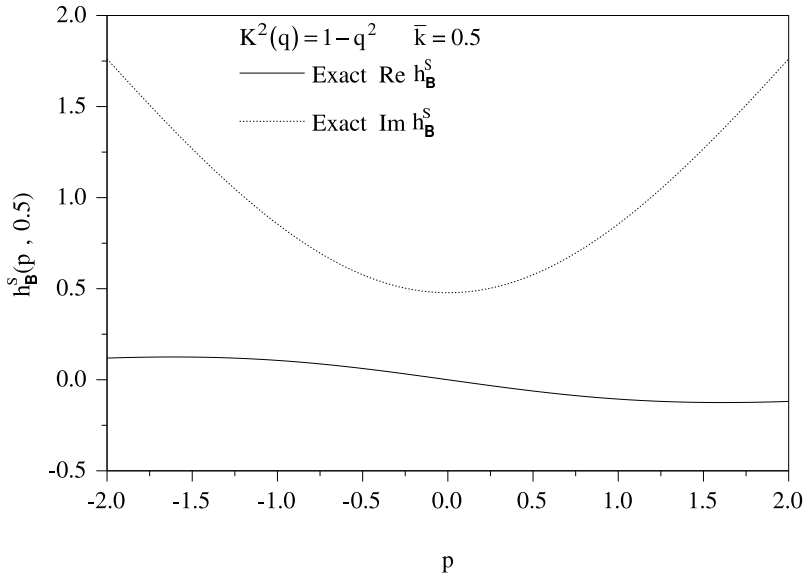

Figure 10. $h^s_{\boldsymbol{B}}(p, 0.5)$ vs. p for the focusing quadratic profile. The exact standard operator symbol is computed from Eq.(104).

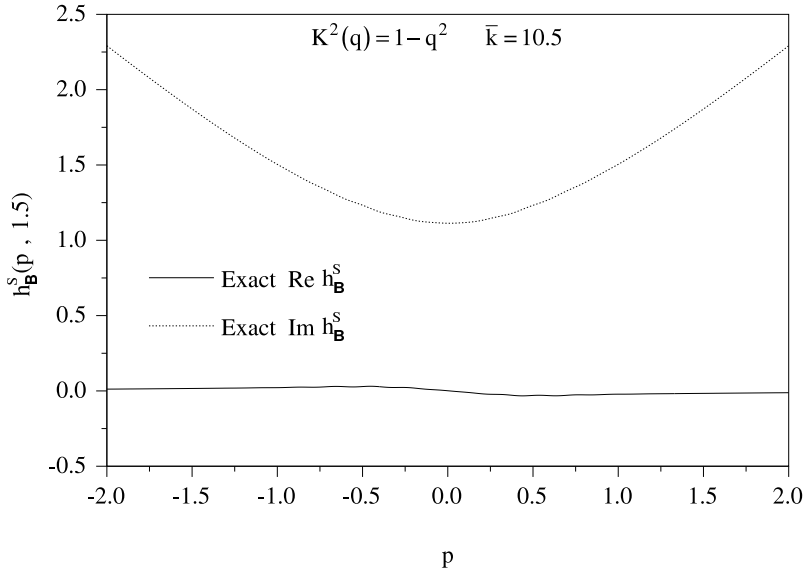

Figure 11. $h^s_{\boldsymbol{B}}(p, 1.5)$ vs. p for the focusing quadratic profile. The exact standard operator symbol is computed from Eq.(104).

well. Analogous behavior to that displayed for the standard operator symbol in Fig. 11, for a choice of q outside the well, follows immediately from Fig. 14 and the variable dependence on χ. Once again, all of the Figs. 13-17 are consistent with the appropriate analytic continuation of the corresponding results for the defocusing quadratic profile presented by Fishman (23). The differences in the symmetry properties between the standard and the Weyl, Helmholtz operator symbols, exhibited in the formulas and illustrated in the preceding figures, are a reflection of the different operator-ordering schemes underlying the two pseudodifferential operator calculi (17).

The effectiveness of both the low- and high-frequency asymptotic, Helmholtz operator symbol expansions derived in Sec. **??** is readily demonstrated. Figures 16 and 17 compare the exact result in Eq.(102) and the low-frequency asymptotic result in Eq.(128) for $\varepsilon = 1.0526$ and 10, respectively, suggesting the increasing accuracy as $\varepsilon \to \infty$ and the manner of breakdown of Eq.(128). The same results are obtained using Eq.(125) for the exact operator symbol calculation for $Y < 1$. In Figs. 13-15, the exact result in

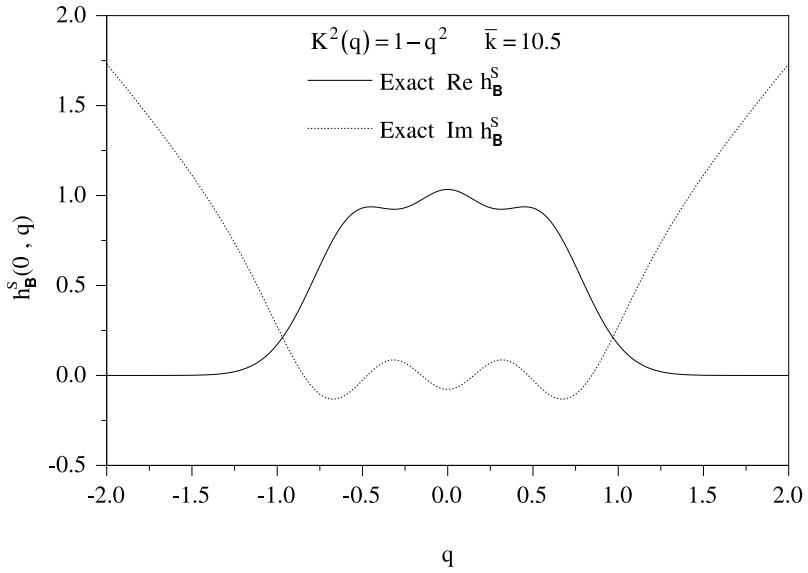

Figure 12. $h^s_{\boldsymbol{B}}(0,q)$ vs. q for the focusing quadratic profile. The exact standard operator symbol is computed from Eq.(104).

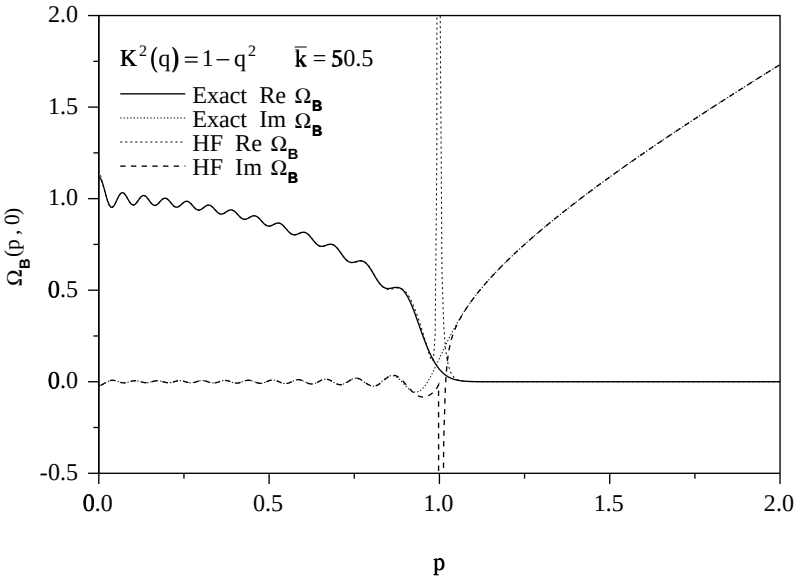

Figure 13. $\Omega_{\boldsymbol{B}}(p,0)$ vs. p for the focusing quadratic profile. The exact Weyl operator symbol (Eq.(102)) is compared with the Weyl, high-frequency (HF) approximate, operator symbol (Eqs.(146) and (159)).

Eq.(102) and the high-frequency asymptotic results in Eq.(146) and Eq.(159) are compared for $\varepsilon = 0.0198$, 0.0952, and 0.2857, respectively. The sequence of figures demonstrates the accuracy of the nonuniform, asymptotic expansions outside the $Y/\chi \to 1$ and $Y/\chi \to \infty$ regimes as $\varepsilon \to 0$. In particular, the nonuniformity associated with the $Y/\chi \to \infty$ regime is seen to be confined to a very narrow region about $p = 0$. The lowest-order estimate of the number of propagating modes L, following from Eq.(171), yields 25, 4, and 1, respectively, for the previously mentioned ε sequence. Comparison with the exact number of modes, 25, 5, and 2, respectively, again illustrates the increasing accuracy of the asymptotic analysis as $\varepsilon \to 0$. In Fig. 18, the exact result in Eq.(102) for $\Omega_{\boldsymbol{B}}(0,0)$ is compared with the corresponding, high-frequency asymptotic expression in Eq.(150) for the specific quadratic case $K^2(q) = 1 - q^2$ and $\bar{k} \in [0,2]$ ($\varepsilon \in (\infty, 0.5]$), illustrating the increasing accuracy of Eq.(150) as $\varepsilon \to 0$. Figure 18 further illustrates the exact, rather than the asymptotic, nature of the expression for $\mathrm{Im}\{\Omega_{\boldsymbol{B}}(0,0)\}$ in Eq.(150).

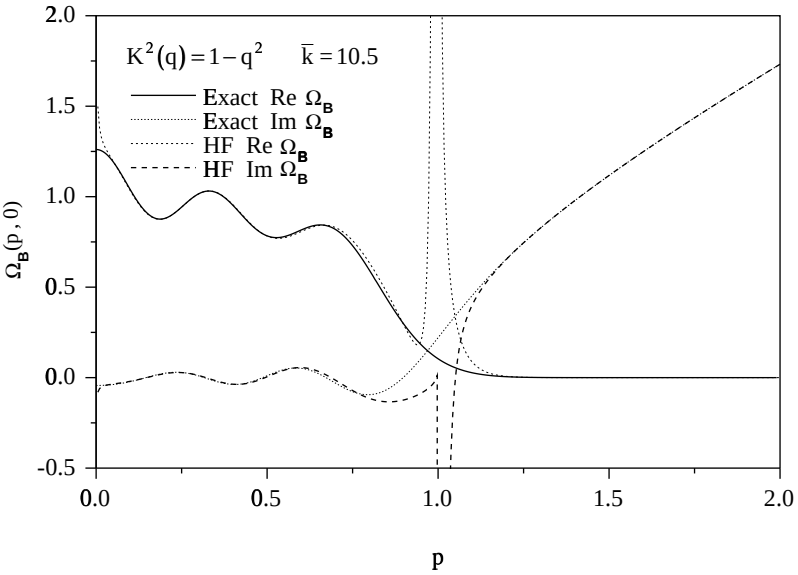

Figure 14. $\Omega_{\boldsymbol{B}}(p, 0)$ vs. p for the focusing quadratic profile. The exact Weyl operator symbol (Eq.(102)) is compared with the Weyl, high-frequency (HF) approximate, operator symbol (Eqs.(146) and (159)).

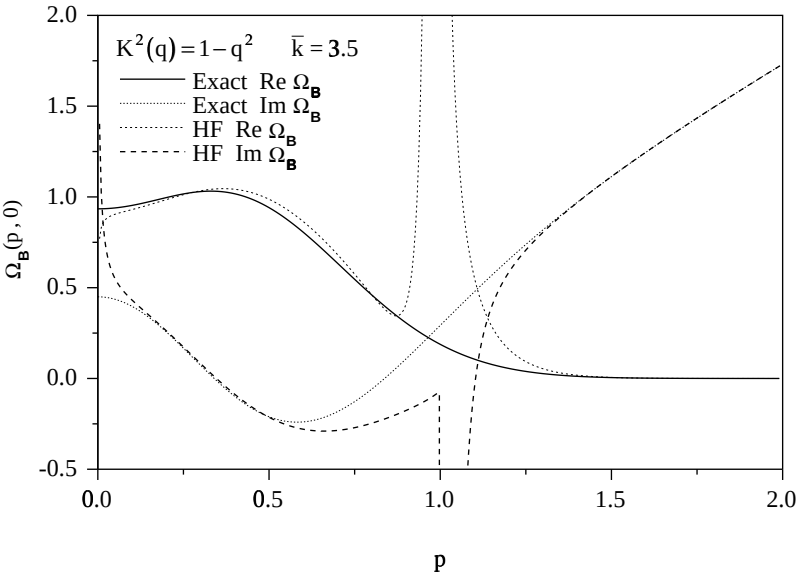

Figure 15. $\Omega_{\boldsymbol{B}}(p, 0)$ vs. p for the focusing quadratic profile. The exact Weyl operator symbol (Eq.(102)) is compared with the Weyl, high-frequency (HF) approximate, operator symbol (Eqs.(146) and (159)).

In the high-frequency, $\varepsilon \to 0$, limit, the Weyl composition equation (11) can be approximated by

$$\Omega_{\boldsymbol{B}^2}(p, q) = K^2(q) - p^2 \simeq [\Omega_{\boldsymbol{B}}(p, q)]^2 \ , \tag{185}$$

which can serve as the basis for an approximate, high-frequency reconstruction (23). This is illustrated in Fig. 19 where $\Omega^2_{\boldsymbol{B}}(0, q)$ (computed from Eq.(102)) is compared with $K^2(q) = 1 - q^2$ for $\bar{k} = 50.5$, 10.5, and 3.5 ($\varepsilon = 0.0198$, 0.0952, and 0.2857). The accuracy of the reconstruction increases as $\varepsilon \to 0$, with the deviation from zero imaginary part serving, in some sense, as a measure of the accuracy of the profile reconstruction for real profiles (23).

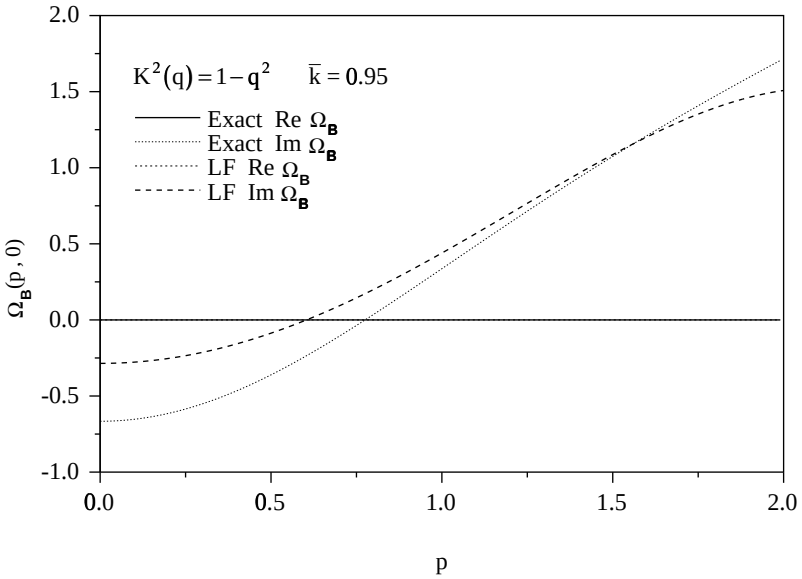

Figure 16. $\Omega_{\boldsymbol{B}}(p, 0)$ vs. p for the focusing quadratic profile. The exact Weyl operator symbol (Eq.(102)) is compared with the Weyl, low-frequency (LF) approximate, operator symbol (Eq.(128)).

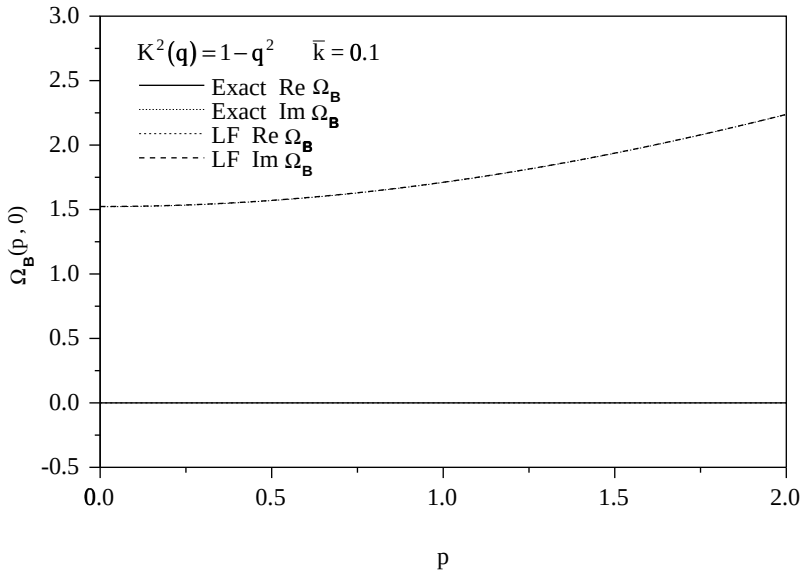

Figure 17. $\Omega_{\boldsymbol{B}}(p, 0)$ vs. p for the focusing quadratic profile. The exact Weyl operator symbol (Eq.(102)) is compared with the Weyl, low-frequency (LF) approximate, operator symbol (Eq.(128)).

9. Discussion

The Helmholtz operator symbols for the focusing quadratic profile have been exactly constructed by two complementary methods: (i) a spectral (modal) summation approach in Section 2 deriving from standard representations and constructions in spectral analysis and (ii) a contour-integral approach in Section 3 based on extracting the operator symbols from the appropriate Green's function, or corresponding parabolic (Schrödinger) propagator, data. As the name implies, the former method is natural for partitioning the operator symbol into its propagating and nonpropagating components, as well as for examining the individual modal contributions, while the latter method is natural for examining the total operator symbol, in particular, for deriving both the high- and

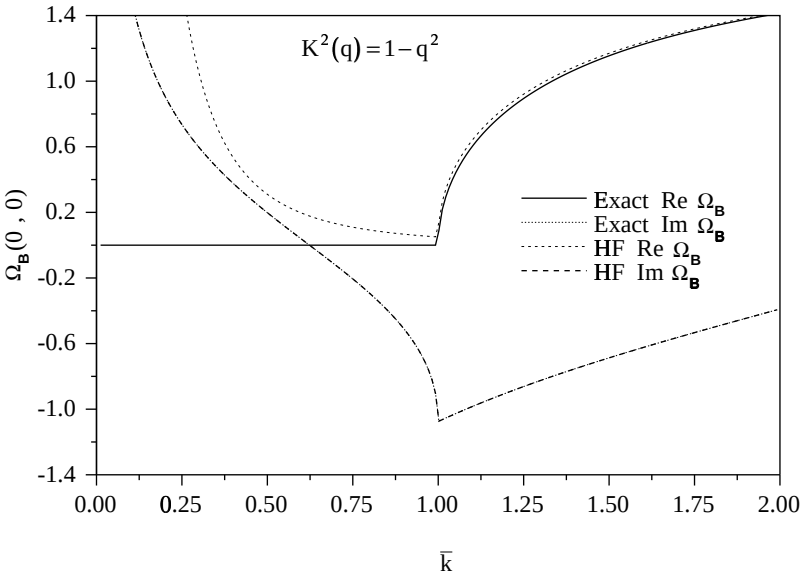

Figure 18. $\Omega_{\boldsymbol{B}}(0, 0)$ vs. $\bar{k}$ for the focusing quadratic profile. The exact Weyl operator symbol (Eq.(102)) is compared with the Weyl, high-frequency (HF) approximate, operator symbol (Eq.(150)).

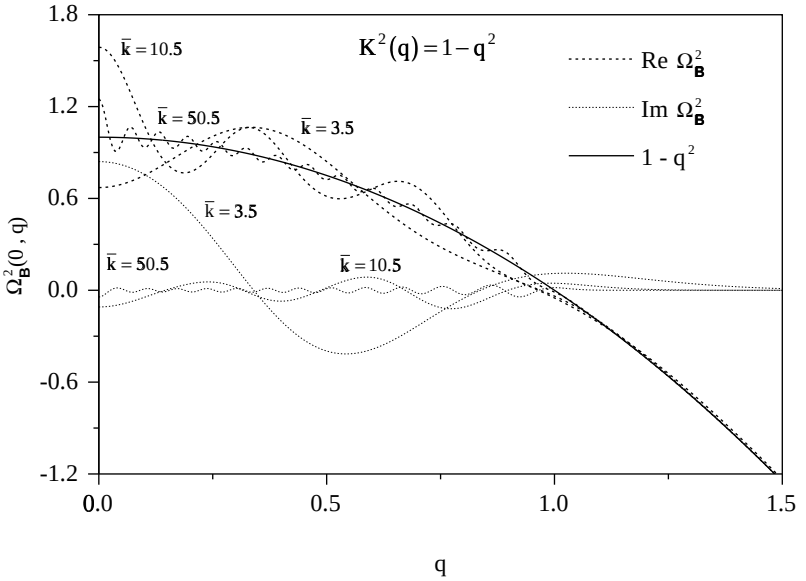

Figure 19. $\Omega_{\boldsymbol{B}}^2(0, q)$ vs. q for the focusing quadratic profile. The exact focusing quadratic profile, $K^2(q) = 1 - q^2$, is compared with the square of the exact Weyl operator symbol computed from Eq.(102).

low-frequency asymptotic expansions. The two approaches can be combined, as in Section 6, to derive both integral representations and asymptotic expansions for the individual propagating and nonpropagating modal sums, as indicated in Eqs.(166)-(170). In particular, for the propagating contribution to the square-root Helmholtz operator symbol, in the high-frequency limit, a sum of a finite, but ever-increasing, number of terms (cf. Eq.(166)) is asymptotically analyzed in a straightforward manner through the contour-integral equivalence as indicated in Eq.(170). Furthermore, even though the periodicity of the associated parabolic (Schrödinger) propagator is explicitly exploited in the contour-integral construction and the discrete nature of the spectrum is, likewise, exploited in the spectral (modal) summation construction for the focusing quadratic case, the two complementary operator symbol construction procedures and their combined usage are quite general, and applicable to other profiles. Indeed, for the Helmholtz operator

symbols in the defocusing quadratic case, which were constructed by the same procedures (4, 23), the associated spectrum has no discrete contributions and the associated parabolic (Schrödinger) propagator is not periodic.

The fractional, Helmholtz operator symbols constructed in Sections 2 and 3 represent the appropriate Helmholtz operator roots associated with the physical, right-traveling wave field. In the spectral (modal) summation construction, this condition is enforced through the appropriate infinitesimal shifting of the resolvent singularities in the integral representation (1, 4, 23), while, in the contour-integral construction, the correspondence to the physical roots follows immediately from the extraction of the operator symbols from the physical, outgoing wave Green's function or the corresponding parabolic (Schrödinger) propagator (23). As such, the Helmholtz operator symbols must satisfy the appropriate composition equations and be consistent with the physical, right-traveling- (outgoing-)wave radiation condition (1, 4, 23), as was demonstrated for the defocusing quadratic profile case by Fishman (23). This is briefly outlined for the focusing quadratic profile case in Appendix C. Satisfying the appropraite composition equations alone is not sufficient to ensure the construction of the physical, Helmholtz operator symbols; the correspondence with the radiation condition is essential. For example, if the $\omega \rightarrow -\mathrm{i}\omega$ limit is taken in the analytic continuation formulas (112)-(115), the resulting symbols will still satisfy the appropriate composition equations (at least in a formal, asymptotic sense (15, 17)), however, they will no longer be consistent with the physical radiation condition, and, thus, will not correspond to the physical operator roots. The construction of the physical, Helmholtz operator symbols has been briefly discussed by Fishman (23).

The exact, square-root Helmholtz operator symbol constructions given in Eqs.(102) and (104) in conjunction with the numerical results presented in Section 8 illustrate the waveguiding properties of the focusing quadratic profile. At the level of the marching range step, which follows immediately from Eq.(10), the infinitesimal, down-range wave field is given by (19, 20, 21, 23)

$$w^+(x+\Delta x,z) \simeq \int_{\mathbb{R}} (\bar{k}/2\pi)\mathrm{d}p\, \exp(\mathrm{i}\bar{k}\, pz)\, \exp[\mathrm{i}\bar{k}\, h^s_{\boldsymbol{B}}(p,z)\Delta x]\, \widetilde{w^+}(x,p)\ . \tag{186}$$

Taking the initial wave field at x to be represented by a very broad Gaussian function, which is essentially constant over the non-absorptive range of the profile ($K^2(z) > 0$), results in a very narrow Gaussian function, sharply peaked about $p = 0$, for the corresponding $\widetilde{w^+}(x,p)$, leading to the approximation

$$w^+(x+\Delta x,z) \simeq \exp[\mathrm{i}\bar{k}\, h^s_{\boldsymbol{B}}(0,z)\Delta x]\ . \tag{187}$$

For the cases corresponding to propagating modes, it follows from Fig. 12 (and the $p \leftrightarrow \omega q$ invariance of $h^s_{\boldsymbol{B}}(p,q)$ in the quadratic case) that the energy within the effective waveguide will be redistributed, with the wave field in the absorptive regions being suppressed. In particular, the oscillatory character of the operator symbol ensures the strict conservation of the integrated energy flux (1, 19), while the phase space regions with $\mathrm{Im}\{h^s_{\boldsymbol{B}}(p,q)\} < 0$ ultimately allow for the down-range focusing correctly corresponding to the modal energy distribution.

While the focusing quadratic profile is, in some respects, nonphysical, the corresponding Helmholtz operator symbols, nevertheless, establish canonical symbol features for more general profiles containing locally-quadratic wells. This should not be surprising. In the context of a modal analysis, the low-lying eigenfunctions and corresponding eigenvalues in such wells will exhibit a quadratic character. This is the same phenomenon expressed at the level of the operator symbol. This will be illustrated in detail elsewhere.

The Helmholtz operator symbol results presented in Sections 2-7 can be immediately extended to the generalized, focusing quadratic profile defined by

$$K^2(z) = K_0^2 + 2\lambda z - \omega^2 z^2\ ,$$

with $K_0, \omega \in \mathbb{R}_+$ and $\lambda \in \mathbb{R}$. Since the effect of the linear term is to shift the equilibrium position and the overall phase in the corresponding harmonic oscillator problem, it immediately follows from Fishman (23) and the analytic continuation results in Section 3 that all of the Helmholtz operator symbol representations derived for the focusing quadratic profile ($\lambda = 0$) hold for the generalized profile with the following identifications,

$$\chi \quad \longrightarrow \quad \varepsilon^{-1}\left[\omega^2(q-\lambda/\omega^2)^2 + p^2\right]\ , \tag{188}$$

$$Y \quad \longrightarrow \quad \varepsilon^{-1}\left[K_0^2 + \lambda^2/\omega^2\right]\ , \tag{189}$$

$$Z \quad \longrightarrow \quad \varepsilon^{-1}\left[\omega\,(q-\lambda/\omega^2)\,p\right]\ , \tag{190}$$

while

$$q \longrightarrow q - \lambda/\omega^2\ . \tag{191}$$

The linear term is seen to increase the effective Y parameter in Eq.(189), tending, in general, to increase the number of propagating modal components, consistent with the increased ability of the positive (non-absorptive) part of the generalized focusing quadratic

profile to support 'bound states'. Exact symbol constructions for the Helmholtz operators can also be extended to the higher-dimensional, separable and coupled, focusing quadratic cases following from the results in Fishman (23) and the appropriate incorporation of the periodicity in the associated parabolic (Schrödinger) propagator.

The general, spectral and contour-integral, Helmholtz operator symbol construction procedures presented here and in Fishman (23) can be applied, as previously suggested, to other cases of interest. The hyperbolic function profile, $K^2(z) = K_0^2 + D\tanh(\nu z) + E\mathrm{sech}^2(\nu z)$ (23, 46), is appropriate for physical modeling, encompasses a range of perturbation limits, illustrates the operator symbol transition from high to low frequency, and accommodates the effects associated with both symmetrical and asymmetrical wells in addition to large gradients, for example. Particularly interesting limiting cases include the delta profile, $K^2(z) = K_0^2 + 2\Lambda\delta(z)$ (47, 48), the discontinuity profile, $K^2(z) = K_1^2 + \Delta K^2 H(z)$, where $H(\cdot)$ is, again, the Heaviside function and $\Delta K^2 = K_2^2 - K_1^2$ (27, 49), and the reflectionless profiles with L prescribed bound states (49, 50). In addition, rectangular wells (4, 27) along with a combination of the delta and quadratic profiles (48) can be considered. These detailed constructions will be presented elsewhere, and are of particular interest owing to their ability to illuminate the differences in the high-frequency asymptotic, operator symbol structure between smooth and nonsmooth profiles. Moreover, the very recent, extensive listing of exact solutions for the Schrödinger (time-dependent) and corresponding Helmholtz (time-independent) quantum mechanical equations (51) in conjunction with the operator symbol construction procedures presented here and in Fishman (23) allow, in principle, for the consideration of additional cases.

The Helmholtz operator symbols (in the frequency domain) lie outside of the well-established theory and corresponding calculus of elliptic pseudodifferential operators (1, 15). As a result, that well-developed calculus cannot provide the uniform characterization of these operator symbols over phase space which is crucial for many applications (1). In the high-frequency asymptotic approximations, in addition to the algebraic terms associated with the elliptic calculus, the contributions of exponential order, corresponding to the infinitely smooth part of the kernel, must be properly included. This has been discussed in detail by Fishman *et al.* (1), where uniform, high- and low-frequency approximations were derived for the square-root Helmholtz operator symbol. (The corresponding analysis, at the level of the operator kernel, is presented in De Hoop and Gautesen (9).) Exact operator symbol constructions and their corresponding asymptotic expansions further illuminate this new asymptotic structure. Specifically, for the focusing quadratic profile, the exact operator symbol plots for the high-frequency regime given in Figs. 7-9 and 11-15 and the high-frequency asymptotic, operator symbol expansions given in Eq.(146) and Eq.(159) and illustrated in Figs. 13-15 together demonstrate the oscillatory character associated with the Helmholtz operator symbols (1, 23). The results presented here and in Fishman (23) further illustrate that, for the quadratic case, the location of the oscillatory branch of the Weyl operator symbol is confined to (i) the locally-propagating regime in the focusing case and, correspondingly, (ii) the locally-evanescent regime in the defocusing case. Furthermore, the discussion surrounding Eq.(171) establishes the detailed connection between these oscillations and the underlying profile. More generally, the analysis underlying the results presented in Fishman *et al.* (1) establishes that for bounded profiles, $K_{\min}^2 < K^2(z) < K_{\max}^2$, the oscillatory branch of the Weyl, Helmholtz operator symbol is of finite extent with respect to p, essentially lying within the interval $p \in [K_{\min}, K_{\max}]$ for $p \in [0, \infty)$. The oscillatory branch location correspondences between the locally-propagating regime and focusing porfiles and the locally-evanescent regime and defocusing profiles, illustrated above for the quadratic case, are found to hold in the more general cases.

The exact construction of the Helmholtz operator symbols for the focusing quadratic profile impacts several areas of direct and inverse wave propagation modeling in extended inhomogeneous environments. Substituting the exact results in Eqs.(102) and (104) into the one-way wave equations (8) and (7), respectively, and fixing the range point at $x = x_b$ provide an exact realization of the computational (nonreflecting) boundary condition for the transversely inhomogeneous Helmholtz equation for the focusing quadratic case (1). Combining Eq.(104) and Eq.(10) results in a formally exact, explicit, path-integral representation for the fundamental solution of the one-way Helmholtz equation (7) for the focusing quadratic profile (1, 2, 18, 19, 20, 21). Furthermore, Eq.(102) provides an explicit example of the function which effects the formally exact 'τ-integration' in the Feynman/Fradkin path-integral representation (52, 53). Moreover, the formal, phase space path-integral representation, in terms of the square-root Helmholtz operator symbol, can be compared to the mathematically rigorous constructions recently presented by LaChapelle (54), based on an extension of the Cartier/DeWitt-Morette functional integration scheme (55), and Dynin (56), motivated by a backward Euler approximation of the corresponding, first-order, pseudodifferential (phase space) evolution equation and product integral constructions. The Dynin analysis, in particular, may ultimately provide the means to establish a rigorous mathematical basis for the formal, phase space path-integral constructions. The exact symbol representations for the well-known, operator rational approximations of the square-root Helmholtz operator, which provide the basis for the practical computational realization of the 'parabolic equation' method (1, 3, 4, 5, 6, 10, 23), are constructed in Section 7 for the focusing quadratic profile. Previously, the corresponding operator symbols for the defocusing quadratic profile were numerically compared with the exact constructions for several, recent, rational approximation schemes (1, 10, 23). The Helmholtz operator symbols can be connected to Galerkin (basis

set expansion) methods (57, 58, 59) for the Helmholtz equation through Eq.(7), Eq.(47), and expansion in the oscillator basis set ϕ_n.

The path-integral representation for the fundamental solution (one-way propagator) inherently contains both the asymptotic ray and modal representations of the wave field, and, in this sense, is a particularly useful representation. Concerning the numerical evaluation of the one-way propagator, although, for the quadratic profile, the propagator path-integral representation can be exactly evaluated through a spectral summation (the square-root Helmholtz operator is then compact), for more general profiles, the infinitesimal propagator controls any wave field continuation algorithm. The infinitesimal propagator is expressed in terms of the square-root Helmholtz operator symbol. From the quadratic profile case, it is seen that (i) using the Weyl calculus (and associated Weyl transform), the infinitesimal propagator follows a multiresolution analysis, and (ii) using the standard calculus, a screen representation for the propagator is obtained. Thus, the microlocal analysis associated with the operator symbols is tied to a multiresolution analysis for wave propagation.

Returning to the fully-coupled, two-way, elliptic wave propagation problem, the generalized Bremmer series (9, 10, 11) provides a means to incorporate the one-way constructions directly into the two-way scattering process. The generalized Bremmer series couples the one-way wave constituents, and generates all multiply-scattered waves. The convergence properties of this series are understood in the time-Laplace domain, and require Sobolev order estimates of the square-root 'Helmholtz' operator uniform in the Laplace parameter. However, most algorithms that (approximately) compute terms in the generalized Bremmer series are accomplished in the time-Fourier domain (10). The closed-form expressions, derived for the square-root Helmholtz operator in the quadratic profile, should prove to be useful in obtaining these Sobolev order estimates in the time-Fourier domain. It is anticipated that such an estimate would hold for more general profiles. Furthermore, the generalized Bremmer series representation for waves can be interpreted as a method of 'tracing waves', the wave-theoretical analogue of the geometrical (asymptotic) method of 'tracing rays' (Weinberg and Burridge (60)). Such methods play a key role in the 'bootstrapping' approach to inverse scattering (see, for example, Claerbout (61)).

Equation (171) can be viewed from both a 'direct' and 'inverse' perspective. From the 'direct' perspective, viewed as a characterization of the operator symbol, given ε, the dimensionless parameter characterizing the medium variability on the wavelength scale, and measuring T, the number of propagating modes L follows immediately from Eq.(171). The accuracy of this lowest-order estimate was illustrated in Section 8 in connection with Figs. 13-15.

From the 'inverse' perspective, viewed as a reconstruction from data with known $\bar{k}$, combining Eq.(150) with Eq.(171) and treating T and $\Omega_{\boldsymbol{B}}(0,0)$ as the data result in estimates for both the focusing quadratic profile parameters and the number of propagating modes L. While the relationship between the profile and the asymptotic, Helmholtz operator symbol structure has been illustrated here for the specific case of the focusing quadratic profile, it can be extended to general profiles through both the uniform, high- and low-frequency asymptotic expansions presented in Fishman *et al.* (1). Of course, $K^2(q)$ can, in principle, be reconstructed from the composition equation Eq.(11), which was illustrated in Section 8 and by Fishman (23) for the focusing and defocusing quadratic cases, respectively, in the high-frequency limit. These ideas have a natural extension to the scattering and DtN operator symbols in the inverse analysis of the general, range-dependent Helmholtz equation (1, 2, 12, 13).

In summary, the inverse square-root and square-root Helmholtz operators (and, subsequently, the scattering and Dirichlet-to-Neumann operators) play a fundamental role in many direct and inverse scattering/propagation problems. These operators do not belong to the class of strictly elliptic pseudodifferential operators and their calculus. Even though the operator symbol constructions and subsequent characterizations presented in this paper are restricted to the specific, quadratic profile, many of the results are believed to be (at least, qualitatively) canonical, and should apply to a wide class of, even singular, medium profiles. In this regard, this paper provides a hint on the extension of this polyhomogeneous calculus for symbols of elliptic pseudodifferential operators to a calculus for non-strictly elliptic operators, such as the ones listed above. This should impact the continuing development of uniform asymptotic symbol expansions (1, 9) for these propagation and scattering operators.

Acknowledgments

The research reported in this paper has been financially supported by the Naval Research Laboratory, the sponsors of the Consortium Project at the Center for Wave Phenomena, a Special Research Fund of the Executive Board of the Delft University of Technology, Delft, the Netherlands, and research grants from the Stichting Fund for Science, Technology and Research (a companion organization to the Schlumberger Foundation in the USA). The authors gratefully acknowledge all of these sources of support. Richard Keiffer at the Naval Research Laboratory is also specifically acknowledged for computing Figs. 7-19 and Jérôme Le Rousseau at the Colorado School of Mines for making Figs. 1-6.

REFERENCES

[1] L. Fishman, A.K. Gautesen and Z. Sun, "Uniform high-frequency approximations of the square root Helmholtz operator symbol," Wave Motion **26** (2), 127-161 (1997).

[2] L. Fishman, "One-way wave propagation methods in direct and inverse scalar wave propagation modeling," Radio Science **28** (5), 865-876 (1993).

[3] M.D. Collins and W.L. Siegmann, *Parabolic Wave Equations with Applications* (Springer-Verlag, New York, to appear in 2000).

[4] M.J.N. van Stralen, *Directional Decomposition of Electromagnetic and Acoustic Wave Fields: Applications in Integrated Optics, Exploration Seismics and Underwater Acoustics* (Delft University Press, Delft, the Netherlands, 1997).

[5] D. Lee and A.D. Pierce, "Parabolic equation development in recent decade," J. Comp. Acoust. **3** (2), 95-173 (1995).

[6] F.B. Jensen, W.A. Kuperman, M.B. Porter and H. Schmidt, *Computational Ocean Acoustics* (AIP Press, New York, 1994).

[7] F.D. Tappert, "The parabolic approximation method," in *Wave Propagation in Underwater Acoustics*, edited by J.B. Keller and J.S. Papadakis, Lecture Notes in Physics No. 70 (Springer-Verlag, New York 1977), pp. 224-287.

[8] L. Fishman, "Direct and inverse wave propagation in the frequency domain via the Weyl operator symbol calculus," in *Vibration Control, Analysis, and Identification: 1995 Design Engineering Technical Conf.*, edited by H.H. Cudney, DE Vol. **84-3** (ASME, New York, 1995), pp. 923-930.

[9] M.V. de Hoop and A.K. Gautesen, "Uniform asymptotic expansion of the generalized Bremmer series," SIAM J. Appl. Math., accepted for publication (1999).

[10] M.J.N. van Stralen, M.V. de Hoop and H. Blok, "Generalized Bremmer series with rational approximation for the scattering of waves in inhomogeneous media," J. Acoust. Soc. Am. **104** (4), 1943-1963 (1998).

[11] M.V. de Hoop, "Generalization of the Bremmer coupling series," J. Math. Phys. **37**, 3246-3282 (1996).

[12] L. Fishman, A.K. Gautesen and Z. Sun, "An exact, well-posed, one-way reformulation of the Helmholtz equation with application to direct and inverse wave propagation modeling," in *New Perspectives on Problems in Classical and Quantum Physics, Part II, Acoustic Propagation and Scattering, Electromagnetic Scattering*, edited by A.W. Sáenz and P.P. Delsanto (Gordon and Breach Science Publishers, Amsterdam, 1998), pp. 75-97.

[13] L. Fishman, "Exact solutions for reflection and Dirichlet-to-Neumann operator symbols in direct and inverse wave propagation modeling," in *Inverse Optics III*, edited by M.A. Fiddy (SPIE, Bellingham, 1994), pp. 16-27.

[14] G.B. Folland, *Harmonic Analysis in Phase Space* (Princeton University Press, Princeton, 1989).

[15] M.E. Taylor, *Pseudodifferential Operators* (Princeton University Press, Princeton, 1981).

[16] L. Hörmander, "The Weyl calculus of pseudo-differential operators," Comm. Pure Appl. Math. **32**, 359-442 (1979).

[17] L. Fishman and J.J. McCoy, "Derivation and application of extended parabolic wave theories. Part I. The factorized Helmholtz equation," J. Math. Phys. **25**, 285-296 (1984).

[18] L. Fishman and J.J. McCoy, "Derivation and application of extended parabolic wave theories. Part II. Path integral representations," J. Math. Phys. **25**, 297-308 (1984).

[19] L. Fishman, J.J. McCoy and S.C. Wales, "Factorization and path integration of the Helmholtz equation: numerical algorithms," J. Acoust. Soc. Am. **81**, 1355-1376 (1987).

[20] L. Fishman and S.C. Wales, "Phase space methods and path integration: the analysis and computation of scalar wave equations," J. Comp. Appl. Math. **20**, 219-238 (1987).

[21] L. Fishman and S.C. Wales, "A fast, filtered, Fourier-transform marching algorithm for wide-angle, one-way wave propagation," in *Computational Acoustics – Wave Propagation*, edited by D. Lee, R.L. Sternberg and M.H. Schultz (North-Holland, Amsterdam, 1988), pp. 369-385.

[22] L. Fishman, "Numerical solutions of the Helmholtz, Weyl composition equation in ocean seismo-acoustics," in *13th International Congress on Acoustics*, Vol. **5**, edited by P. Pravica (Sava Centar, Belgrade, 1989), pp. 149-152.

[23] L. Fishman, "Exact and operator rational approximate solutions of the Helmholtz, Weyl composition equation in underwater acoustics – The quadratic profile," J. Math. Phys. **33**, 1887-1914 (1992).

[24] C.L. Fefferman, "The uncertainty principle," Bull. Am. Math. Soc. **9** (2), 129-206 (1983).

[25] M.A. Shubin, *Pseudodifferential Operators and Spectral Theory* (Springer-Verlag, Berlin, 1987).

[26] C. Vassallo, *Optical Waveguide Concepts* (Elsevier Science Publishers B.V., Amsterdam, 1991).

[27] E. Merzbacher, *Quantum Mechanics* (John Wiley & Sons Inc., New York, 1961).

[28] E. Kreyszig, *Introductory Functional Analysis with Applications* (John Wiley & Sons Inc., New York, 1978).

[29] W. Magnus, F. Oberhettinger and R.P. Soni, *Formulas and Theorems for the Special Functions of Mathematical Physics* (Springer-Verlag, New York, 1966).

[30] H. Bremermann, *Distributions, Complex Variables, and Fourier Transforms* (Addison-Wesley, Reading, MA, 1965).

[31] R.R. Goldberg, *Methods of Real Analysis* (Blaisdell Publishing Company, Waltham, MA, 1964).

[32] E.C. Titchmarsh, *The Theory of Functions* (Oxford University Press, Oxford, 1939).

[33] E.D. Rainville, *Special Functions* (The Macmillan Company, New York, 1967).

[34] M. Abramowitz and I.A. Stegun, *Handbook of Mathematical Functions*, NBS Applied Mathematics Series 55 (U.S. Government Printing Office, Washington D.C., 1968).

[35] G.F. Carrier, M. Krook and C.E. Pearson, *Functions of a Complex Variable: Theory and Technique* (McGraw-Hill Book Company, New York, 1966).

[36] L.S. Schulman, *Techniques and Applications of Path Integration* (John Wiley & Sons Inc., New York, 1981).

[37] A. Erdélyi, W. Magnus, F. Oberhettinger and F.G. Tricomi, *Higher Transcendental Functions, Vol. 1* (McGraw-Hill Book Company, New York, 1953).

[38] A. Erdélyi, *Asymptotic Expansions* (Dover Publications Inc., New York, 1956).

[39] N. Bleistein and R.A. Handelsman, *Asymptotic Expansions of Integrals* (Dover Publications Inc., New York, 1986).

[40] S. Mallat, *A Wavelet Tour of Signal Processing* (Academic Press, San Diego, 1998).

[41] M.V. de Hoop, J.H. Le Rousseau and R.-S. Wu, "Generalization of the phase-screen approximation for the scattering of acoustic waves," Wave Motion, in print (1999).

[42] F.A. Milinazzo, C.A. Zala and G.H. Brooke, "Rational square-root approximations for parabolic equation algorithms," J. Acoust. Soc. Am. **101**, 760-766 (1997).

[43] The MATHWORKS Inc. MATLAB High-Performance Numerical Computation and Visualization Software, The MATHWORKS Inc., 1992.

[44] M.J.N. van Stralen, for a detailed discussion concerning the choice of α, send an e-mail to: m.vanstralen@plasma-optical-fibre.nl .

[45] W.H. Press, B.P. Flannery, S.A. Teukolsky and W.T. Vetterling, *Numerical Recipes* (Cambridge University Press, Cambridge, 1992).
[46] L.M. Brekhovskikh, *Waves in Layered Media* (Academic Press, San Diego, 1976).
[47] K. Gottfried, *Quantum Mechanics, Vol. 1: Fundamentals* (Benjamin, New York, 1966).
[48] B. Gaveau and L.S. Schulman, "Explicit time-dependent Schrödinger propagators," J. Phys. **A 19**, 1833-1846 (1986).
[49] L.D. Landau and E.M. Lifshitz, *Quantum Mechanics: Non-Relativistic Theory* (Pergamon Press, Oxford, 1965).
[50] R.E. Crandell, "Exact propagator for reflectionless potentials," J. Phys. **A 16**, 3005-3011 (1983).
[51] C. Grosche and F. Steiner, *Handbook of Feynman Path Integrals* (Springer-Verlag, New York, 1998).
[52] L. Fishman and J.J. McCoy, "Factorization, path integral representations, and the construction of direct and inverse wave propagation theories," IEEE Trans. Geosc. Rem. Sens. **GE-22**, 682-692 (1984).
[53] L. Fishman, "Path integral representations and the scalar Helmholtz equation," in *Path Integrals: Dubna '96*, JINR **E96-321**, edited by V.S. Yarunin and M.A. Smondyrev (Dubna, Russia, 1996), pp. 347-353.
[54] J. LaChapelle, "Path integral solution of the Dirichlet problem," Ann. Phys. **254** (2), 397-418 (1997).
[55] P. Cartier and C. DeWitt-Morette, "A new perspective on functional integration," J. Math. Phys. **36**, 2237-2312 (1995).
[56] A. Dynin, "A rigorous path integral construction in any dimension," Letters in Math. Phys. **44**, 317- 329 (1998).
[57] E.J. Heller and H.A. Yamani, "New L^2 approach to quantum scattering: Theory," Phys. Rev. **A 9** (3), 1201-1208 (1974).
[58] E.J. Heller and H.A. Yamani, "J-matrix method: Application to s-wave electron-hydrogen scattering," Phys. Rev. **A 9** (3), 1209-1214 (1974).
[59] H.A. Yamani and L. Fishman, "J-matrix method: Extensions to arbitrary angular momentum and to Coulomb scattering," J. Math. Phys. **16** (2), 410-420 (1975).
[60] H. Weinberg and R. Burridge, "Horizontal ray theory for ocean acoustics," J. Acoust. Soc. Am. **55**, 63 (1974).
[61] J.C. Claerbout, *Imaging the Earth's Interior* (Blackwell Scientific Publ., 1985).

Appendix A: Operation interchange and the Riesz/Young theorem

This appendix proves the identity

$$\int_0^\infty \mathrm{d}t\, t^{-1/2} \exp[(Y-1)t] \left[\sum_{n=N}^\infty \frac{1}{n!} \left(\frac{\mathrm{i}}{2}\right)^n \Psi_n(p,q)\, \exp(-2nt)\right] = \pi^{1/2} \sum_{n=N}^\infty \frac{1}{n!} \frac{1}{(2n+1-Y)^{1/2}} \left(\frac{\mathrm{i}}{2}\right)^n \Psi_n(p,q)\,, \quad \text{(A1)}$$

which was applied in establishing Eq.(28). The result in Eq.(A1) follows on establishing the validity of the interchange of integration and summation, which is a direct consequence of establishing that the power series

$$\mathcal{S}(\zeta) = \sum_{n=0}^\infty \frac{1}{n!} \left(\frac{\mathrm{i}}{2}\right)^n \Psi_n(p,q)\, \zeta^n\,, \quad \text{(A2)}$$

with $\zeta \in \mathbb{C}$ is uniformly convergent for $\zeta \in (0,1]$.

The power series in Eq.(A2) has a radius of convergence R_c equal to one, which follows directly from the derivation of the Mehler formula (33) or from the definition (31) of R_c and the previously referenced asymptotic estimates of the Hermite polynomials and the gamma function. Hence, the power series $\mathcal{S}(\zeta)$ is uniformly convergent (31) for $\zeta \in (0,1)$. Extension of uniform convergence to $\zeta = 1$ ($t = 0$), and the consequent completion of the proof, follow on establishing the convergence (31) of $\mathcal{S}(1)$.

The convergence of $\mathcal{S}(1)$ is an immediate consequence of the following theorem associated with M. Riesz and W.H. Young (32).

Theorem. If

$$f(\zeta) = \sum_{n=0}^\infty a_n \zeta^n\,, \quad \zeta \in \mathbb{C}\,,$$

is a power series with a finite radius of convergence (taken for convenience to be unity) and

$$\lim_{n\to\infty} a_n = 0\,,$$

then the series is convergent at every point of the unit circle where the function $f(\zeta)$ is regular.

For the series under consideration, the radius of convergence is one, and, further, the previously referenced asymptotic estimates of the Hermite polynomials and the gamma function establish that

$$a_n = \frac{1}{n!} \left(\frac{\mathrm{i}}{2}\right)^n \Psi_n(p,q) = \mathcal{O}(n^{-1/2}) \qquad \text{as } n \to \infty. \quad \text{(A3)}$$

Applying the Riesz/Young theorem, the convergence of $\mathcal{S}(1)$ is determined by the behavior of the function

$$f(\exp(-2t)) = 2^{-1/2} \exp(t)\, F(t)$$

evaluated at $t = 0$, where $F(\cdot)$ is defined in Eq.(29) (and is the generator in accordance with the Mehler formula (33)). Since $t = 0$ is a regular point of the function $F(\cdot)$, it follows that $\mathcal{S}(1)$ is convergent.

Appendix B: Alternative Helmholtz operator symbol integral representations

Following from Section 3, a number of alternative, equivalent integral representations can be derived for the Helmholtz operator symbols for the focusing quadratic profile case. Only two examples will be noted here. The first one, a counterpart

of Eq.(92),

$$\Omega^{\rm foc}_{\boldsymbol{B}^{-1}}(p,q) = \frac{1}{(2\varepsilon)^{1/2}\pi}\,\exp(-\chi)\int_{\mathcal{L}_p} {\rm d}s\, s^{-1}\exp(2s\,\chi)$$
$$\Big\{\zeta(1/2,(1-Y)/2,(1-s)/s)$$
$$-2\,[(1-s)/s]^L\zeta(1/2,L+(1-Y)/2,(1-s)/s)\Big\}\,,$$
$$Y \neq 1,3,5,\cdots\,, \qquad \text{(B1)}$$

where $\mathcal{L}_p$ is the contour in the complex s-plane associated with the inverse Laplace transform (35). This representation derives from the spectral (modal) summation representation in Eq.(56) and the inverse Laplace transform of the Laguerre polynomials (34) in combination with the appropriate representation of the Lerch transcendental function (37).

The second example is the representation,

$$\Omega^{\rm foc}_{\boldsymbol{B}^{-1}}(p,q) = -\exp\left(\tfrac{3}{4}\pi{\rm i}\right)\,\frac{2}{\varepsilon^{1/2}\pi}$$
$$\int_0^\infty {\rm d}\xi \frac{1}{(1/2)-(\widetilde{Y}/2)}$$
$$\times\sum_{n=0}^\infty \frac{(-\chi)^n}{((3/2)-(\widetilde{Y}/2))_n}$$
$${}_2F_1(n+1,(1/2)-(\widetilde{Y}/2);n+(3/2)-(\widetilde{Y}/2);-1)\,,$$
$$Y \neq 1,3,5,\cdots\,, \qquad \text{(B2)}$$

where $\widetilde{Y} = Y + {\rm i}\,\xi^2$ and ${}_2F_1(\cdot,\cdot;\cdot;\cdot)$ is the Gauss hypergeometric function discussed in Erdélyi *et al.* (37, chap.ii) (note the occurrence of Pochhammer's symbol). Equation (B2) follows from Eqs.(B17)-(B19) in Fishman (23) and utilizing properties of the gamma function. Representations such as Eq.(B2) provide another means to establish the extended analytic continuation results given in Eqs.(112)-(115). In addition, Eq.(B2), while expressed in a form which masks the underlying periodicity (so conveniently expressed by the Lerch transcendental function and the integration end points in Eq.(92)) in Gauss hypergeometric function integrals, is, nevertheless, a natural form for the exact operator symbol constructions in the hyperbolic profile case and the subsequent illustration of the canonical nature of the focusing quadratic profile.

In a similar manner, alternative integral representations, analogous to the ones constructed in Eqs.(B1) and (B2), can be derived for the exact, Helmholtz operator symbols corresponding to the additive, rational operator approximations presented in Section 7. For example, in conjunction with Eqs.(180)-(184),

$$\Omega_{[\beta\boldsymbol{I}+\gamma\boldsymbol{L}]^{-1}}(p,q) = -\frac{1}{\varepsilon\gamma}\,\frac{1}{(1/2)-(\widehat{Y}/2)}$$
$$\times\sum_{n=0}^\infty \frac{(-\chi)^n}{((3/2)-(\widehat{Y}/2))_n}$$
$${}_2F_1(n+1,(1/2)-(\widehat{Y}/2);\quad n+(3/2)-(\widehat{Y}/2);-1)\,,$$
$$\widehat{Y} \neq 1,3,5,\cdots\,. \qquad \text{(B3)}$$

Appendix C: Verification of Helmholtz operator symbol composition equations

Both the inverse square-root and square-root Helmholtz operator symbols, for the focusing quadratic profile in one transverse dimension, must satisfy the usual composition equations and be consistent with the appropriate, right-traveling- (outgoing-)wave radiation condition (1, 4, 23). The composition equations (cf. Eq.(23)) to be verified are

$$\frac{\bar{k}}{2\pi}\int_{\mathbb{R}^2}{\rm d}u{\rm d}s\; h^s_{\boldsymbol{B}^{-1}}(p-s,q)h^s_{\boldsymbol{B}^{-1}}(p,q-u)\,\exp(-{\rm i}\bar{k}\,su)$$
$$= h^s_{\boldsymbol{B}^{-2}}(p,q)\,, \qquad \text{(C1)}$$

and

$$\frac{\bar{k}}{2\pi}\int_{\mathbb{R}^2}{\rm d}u{\rm d}s\; h^s_{\boldsymbol{B}^{-1}}(p-s,q)h^s_{\boldsymbol{B}}(p,q-u)\,\exp(-{\rm i}\bar{k}\,su)$$
$$= h^s_{\boldsymbol{I}}(p,q) = 1\,, \qquad \text{(C2)}$$

and

$$\frac{\bar{k}}{2\pi}\int_{\mathbb{R}^2}{\rm d}u{\rm d}s\; h^s_{\boldsymbol{B}}(p-s,q)h^s_{\boldsymbol{B}}(p,q-u)\,\exp(-{\rm i}\bar{k}\,su)$$
$$= h^s_{\boldsymbol{B}^2}(p,q) = K_0^2 - \omega^2q^2 - p^2\,. \qquad \text{(C3)}$$

The calculations are briefly outlined in the standard (left) calculus where they are technically less cumbersome, however, the analogous results hold in the Weyl calculus. The verification outlines are illustrated for both the spectral (modal) summation and contour-integral operator symbol representations, given, respectively, by Eq.(21) and Eq.(103) for the inverse square-root Helmholtz operator symbol and, for the purposes of this appendix, extended to the square-root Helmholtz operator symbol through the composition relationship in Eq.(24).

For the verification of Eq.(C1) for the spectral (modal) summation operator symbol representation (21), substituting Eq.(21) into Eq.(C1), interchanging the order of the integrations and summations, applying the Hermite, Fourier transform result given in Eq.(20), and exploiting the Hermite orthogonality relationship (29),

$$\int_{-\infty}^\infty {\rm d}\zeta\,\exp(-\zeta^2)\,H_n(\zeta)\,H_m(\zeta) = \pi^{1/2}2^n n!\,\delta_{nm}\,, \qquad \text{(C4)}$$

lead to the final result (compare Eq.(21))

$$h^s_{\boldsymbol{B}^{-2}}(p,q)$$
$$= -\frac{2^{1/2}}{\varepsilon}\,\sum_{n=0}^\infty \frac{1}{n!}\,\frac{1}{(2n+1-Y)}\,\left(\frac{\rm i}{2}\right)^n\Psi_n(p,q)\,. \qquad \text{(C5)}$$

The expression (C5) is in agreement with the operator symbol calculations done in conjunction with the rational approximation operator symbol constructions in Section .

To establish Eq.(C1) for the contour-integral operator

symbol representation Eq.(103), it is convenient to first consider the case $Y < 1$. Choosing the contour $\mathcal{L} = \mathcal{C}'' = \Gamma_1'' + \Gamma_2'' + \Gamma_3''$, as illustrated in Fig. 6 for the defocusing quadratic profile analysis, then allows for Eq.(103) to be expressed as (compare Eq.(65))

$$h^s_{\boldsymbol{B}^{-1}}(p,q) = -\mathrm{i}\left(\frac{1}{\pi\varepsilon}\right)^{1/2} \int_0^\infty \mathrm{d}t\, t^{-1/2} \times \exp\left[Yt - \tfrac{1}{2}\chi\tanh(2t) + \mathrm{i}Z\left(\mathrm{sech}(2t) - 1\right)\right] \left(\mathrm{sech}(2t)\right)^{1/2}, \quad Y < 1\,. \tag{C6}$$

Substituting Eq.(C6) into Eq.(C1), interchanging the order of the integrations, evaluating two successive Gaussian integrals (in u and s), and applying standard hyperbolic function identities yield the result

$$h^s_{\boldsymbol{B}^{-2}}(p,q) = -\left(\frac{1}{\pi\varepsilon}\right) \int_0^\infty \mathrm{d}t \int_0^\infty \mathrm{d}t'\,(t\,t')^{-1/2} \times \exp\left[Y(t+t') - \tfrac{1}{2}\chi\tanh(2(t+t')) + \mathrm{i}Z\left(\mathrm{sech}(2(t+t')) - 1\right)\right] \left(\mathrm{sech}(2(t+t'))\right)^{1/2}, \; Y < 1\,. \tag{C7}$$

Exploiting the t t'-symmetry of the integrand in Eq.(C7) through the introduction of the new variables $u = t + s$ and $v = t - s$ reduces the double integral to a single integral of the form

$$h^s_{\boldsymbol{B}^{-2}}(p,q) = -\frac{1}{\varepsilon} \int_0^\infty \mathrm{d}u \exp\left[Yu - \tfrac{1}{2}\chi\tanh(2u) + \mathrm{i}Z\left(\mathrm{sech}(2u) - 1\right)\right] \left(\mathrm{sech}(2u)\right)^{1/2}, \quad Y < 1\,, \tag{C8}$$

or

$$h^s_{\boldsymbol{B}^{-2}}(p,q) = -\frac{1}{\varepsilon}\,\frac{1}{1-\exp(2\pi\mathrm{i}\,Y)} \int_{\mathcal{L}} \mathrm{d}\tau \exp\left[Y\tau - \tfrac{1}{2}\chi\tanh(2\tau) + \mathrm{i}Z\left(\mathrm{sech}(2\tau) - 1\right)\right] \left(\mathrm{sech}(2\tau)\right)^{1/2}, \quad Y \neq 0, 1, 2, \cdots\,. \tag{C9}$$

The final equality in Eq.(C9), establishing the full range of Y values, follows from analytic continuation arguments. The expression in Eq.(C9) is in agreement with the operator symbol calculations done in conjunction with the rational approximation operator symbol constructions in Section . The equivalence of the expressions in Eq.(C5) and Eq.(C9) follows from the Mehler formula (33), uniform convergence arguments (31) and the Riesz/Young theorem (32), and elementary integration.

Examining the composition equations (C2) and (C3), it is seen that the Fourier integrals involving the square-root Helmholtz operator symbol $h^s_{\boldsymbol{B}}(p,q)$ do not exist in the usual sense, but, rather, must be understood in the context of generalized functions (23, 30). This essentially means that the composition integral is given meaning through the analytic continuation in the parameter σ of the Lerch transcendental function appearing in Eqs.(103) and (24), for example (23, 30). Operationally, the implication is that the basic procedure used in going from Eq.(C6) to Eq.(C9) in the verification of composition equation (C1) can again formally be applied in evaluating composition equations (C2) and (C3) to derive the correct results. This was the method employed in establishing the corresponding composition equation results for the defocusing quadratic profile in Fishman (23). Substituting Eqs.(103) and (24) into Eq.(C2) and following the previously outlined procedure lead to the result

$$h^s_{\boldsymbol{I}}(p,q) = -\int_0^\infty \mathrm{d}u\, \frac{\mathrm{d}}{\mathrm{d}u}\left\{\exp\left[Yu - \tfrac{1}{2}\chi\tanh(2u) + \mathrm{i}Z\left(\mathrm{sech}(2u) - 1\right)\right] \left(\mathrm{sech}(2u)\right)^{1/2}\right\} = 1\,, \quad Y < 1\,. \tag{C10}$$

The analogous treatment of Eq.(C3) yields

$$h^s_{\boldsymbol{B}^2}(p,q) = -\varepsilon \int_0^\infty \mathrm{d}u\, \frac{\mathrm{d}}{\mathrm{d}u}\left\{\exp\left[Yu - \tfrac{1}{2}\chi\tanh(2u) + \mathrm{i}Z\left(\mathrm{sech}(2u) - 1\right)\right] \left(\mathrm{sech}(2u)\right)^{1/2} \times \left[Y - \chi\left(\mathrm{sech}(2u)\right)^2 - 2\mathrm{i}Z\,\mathrm{sech}(2u)\tanh(2u) - \tanh(2u)\right]\right\} = K_0^2 - \omega^2 q^2 - p^2\,, \quad Y < 1\,. \tag{C11}$$

Analytic continuation arguments extend the results in Eqs.(C10) and (C11) to the full range of Y values.

In addition to formally satisfying the composition equations (C1)-(C3), the Helmholtz operator symbols $h^s_{\boldsymbol{B}^{-1}}(p,q)$ and $h^s_{\boldsymbol{B}}(p,q)$ are consistent with the appropriate, right-traveling- (outgoing-)wave radiation condition by construction (1, 4, 23), with the correct evanescent behavior being apparent in Figs. 7-12 for $h^s_{\boldsymbol{B}}(p,q)$.